ELECTROMAGNETIC PROCESSES IN RELATIVISTIC HEAVY ION COLLISIONS

Carlos A. BERTULANI

Institut für Kernphysik, Kernforschungsanlage Jülich GmbH, D-5170 Jülich, Fed. Rep. Germany and Instituto de Física, Universidade Federal do Rio de Janeiro, 21944 Rio de Janeiro, Brazil

and

Gerhard BAUR

Institut für Kernphysik, Kernforschungsanlage Jülich GmbH, D-5170 Jülich, Fed. Rep. Germany

ELECTROMAGNETIC PROCESSES IN RELATIVISTIC HEAVY ION COLLISIONS

Carlos A. BERTULANI

Institut für Kernphysik, Kernforschungsanlage Jülich GmbH, D-5170 Jülich, Fed. Rep. Germany
and Instituto de Física, Universidade Federal do Rio de Janeiro, 21944 Rio de Janeiro, Brazil

and

Gerhard BAUR

Institut für Kernphysik, Kernforschungsanlage Jülich GmbH, D-5170 Jülich, Fed. Rep. Germany

Contents:

Abstract:

Here is presented a study of the processes generated by the electromagnetic interaction in relativistic nuclear, and atomic collisions. There is nowadays a vivid interest in this field due to the construction of relativistic heavy ion accelerators. Certainly, the most important purpose of these relativistic heavy ion machines is the study of nuclear matter under extreme conditions. In central nucleus–nucleus collisions one hopes to observe new forms of nuclear matter, like the quark–gluon plasma [Lu-84, Bay-86]. On the other hand, very strong electromagnetic fields for a very short time are present in distant collisions with no nuclear contact. Such fields can also lead to interesting effects, which are discussed here.

There have been many interesting theoretical and experimental developments on this subject, and new areas of research were opened. Of special interest is, e.g., the case of nuclear fragmentation. This is accomplished through the excitation of giant resonances or by direct break-up of the nuclei by means of their electromagnetic interaction. It is shown that this process can be used to study nuclear structure properties which are not accessible by means of the traditional electromagnetic excitation at nonrelativistic energies. The creation of particles is also of interest due to the large cross sections, specially in the case of electron–positron pair creation.

Although one can develop very elaborate and complicated calculations to explain the many processes originated in this way, the results can be understood in very simple terms because of our almost complete comprehension of the electromagnetic interaction. For those processes where the electromagnetic interaction plays the dominant role this is clearly a very useful tool for the investigation of the structures created by the strong interaction in the nuclei or hadrons.

1. Introduction

For a very long time electromagnetic processes in nonrelativistic nuclear collisions, like e.g. Coulomb excitation, has been a subject of considerable theoretical and also experimental interest. The basic assumption of these kinds of reactions is that the nuclei do not penetrate each other. When they penetrate the reactions are overwhelmingly due to the strong interaction, what complicates the analysis of these reactions in the relativistic regime where the two possibilities occur. But, since the photon exchange amplitude is singular at four-momentum transfer $q_\mu q_\mu = 0$, the virtual photon exchange makes a larger contribution to the amplitude for forward scattering angles than the exchange of strongly interacting particles. This allows one to separate the electromagnetic contribution for certain processes, and with certain experimental setups. Also, the passage of a relativistic charge provides a nuclear target with an electromagnetic pulse of short duration and enhanced due to the Lorentz contraction. Such a pulse can be sufficiently energetic to excite giant resonances in the nucleus, or to create particles ($e^- e^+$-pairs, pions, heavy leptons, etc.). The long range of the electromagnetic interaction leads to very large cross sections in some cases, which can be easily verified experimentally.

The simplest way to describe the reaction mechanism in relativistic electromagnetic collisions is provided by the equivalent photon method, which is originally due to Fermi [Fe-24] and later on developed by Weizsäcker [We-34] and Williams [Wi-34, Wi-35]. In the literature it is also commonly referred to as the Weizsäcker–Williams method. Let us present a resumé of the ideas involved in this method. A more complete description can be found in the excellent textbook of Jackson [Ja-75, p. 719] on classical electrodynamics.

We shall consider the target nucleus as fixed, neglecting its recoil, and we place the origin of our coordinate system in its centre of mass. In this way we analyse the effects of the electromagnetic field generated by the projectile on the target. This is a simple matter of convention, to simplify the notations, since the role of the target and of the projectile can be exchanged, i.e. we can consider the case of internal excitation of the projectile by the electromagnetic field of the target, and vice versa. The charges and mass numbers of the projectile and target are given by (Z_1, A_1) and (Z_2, A_2), respectively. The projectile is assumed to move in a straight line with velocity v and impact parameter b. When $v \simeq c$, where c is the velocity of light, the electromagnetic field generated by the projectile looks contracted in the direction perpendicular to its motion (see fig. 1.1a) and is given by
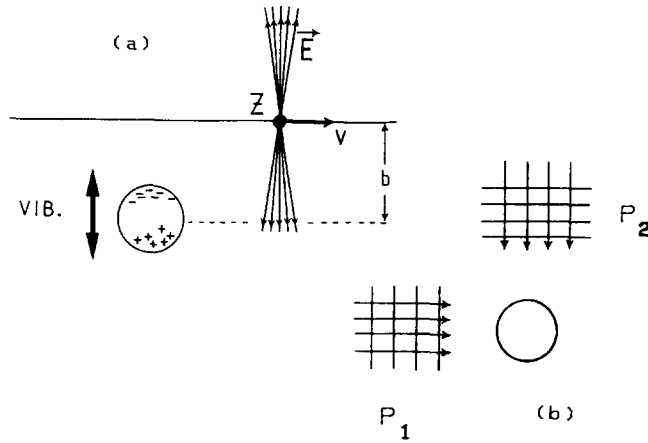
Fig. 1.1. (a) A relativistic charged projectile incident on a target with impact parameter larger than the strong interaction radius. A sketch of the electric field generated by it is also shown. One of the effects of this field is to induce collective vibrations of the nuclear charges. (b) Two pulses of plane wave of light which produce the same effect on the target as the electromagnetic field created by the projectile's motion.

$$E_z = -Z_1 e\gamma vt/[b^2 + \gamma^2 v^2 t^2]^{3/2} , \qquad\qquad\qquad (1.1a)$$

$$E_T = -Z_1 e\gamma b/[b^2 + \gamma^2 v^2 t^2]^{3/2} , \qquad\qquad\qquad (1.1b)$$

$$B_T = v/c \times E_T , \quad \text{and} \quad B_z = 0 , \qquad\qquad\qquad (1.1c)$$

where the z (T) indices denote the direction parallel (transverse) to the velocity of the projectile, and

$$\gamma = (1 - v^2/c^2)^{-1/2} , \qquad\qquad\qquad (1.2)$$

is the relativistic Lorentz factor.

When $\gamma \gg 1$, these fields will act during a very short time, of order

$$\Delta t \simeq b/\gamma c , \qquad\qquad\qquad (1.3)$$

and they are equivalent to two pulses of plane-polarized radiation incident on the target (see fig. 1.1b): one in the beam direction (P_1), and the other perpendicular to it (P_2). In the case of the pulse P_1 the equivalency is exact. Since the electric field in the z-direction is not accompanied by a corresponding magnetic field, the equivalency is not complete for pulse P_2, but this will not appreciably affect the dynamics of the problem since the effects of the field E_z are of minor relevance when $v \simeq c$. Therefore, we add a field $B_z = vE_z/c$ to eq. (1.1) in order to treat also P_2 as a plane-wave pulse of radiation. This analogy permits one to calculate the amount of energy incident on the target per unit area and per frequency interval as

$$I(\omega, b) = (c/4\pi)|E(\omega) \times B(\omega)| , \qquad\qquad\qquad (1.4)$$

where $E(\omega)$ and $B(\omega)$ are the Fourier transforms of the fields given by eq. (1.1).

Now, we associate the spectrum of the virtual radiation as obtained by means of eq. (1.4) to the one of a real pulse of light incident on the target. Then we can obtain the probability for a certain electromagnetic process in a relativistic nuclear collision to occur, in terms of the cross sections for the same process generated by an equivalent pulse of light, as

$$P(b) = \int I(\omega, b)\, \sigma_\gamma(\hbar\omega)\, \mathrm{d}(\hbar\omega) = \int N(\omega, b)\, \sigma_\gamma(\omega)\, \frac{\mathrm{d}\omega}{\omega} , \qquad (1.5)$$

where $\sigma_\gamma(\omega)$ is the photo cross-section for the photon energy $E_\gamma = \hbar\omega$, and the integral runs over all the frequency spectrum of the virtual radiation. The quantities $N(\omega, b)$ can be interpreted as the *number of equivalent photons* incident on the target per unit area. Performing a calculation of eq. (1.4) from eq. (1.1), and using the definition (1.5), we find

$$N(\omega, b) = \frac{Z_1^2 \alpha}{\pi^2} \left(\frac{\omega}{\gamma v}\right)^2 \left(\frac{c}{v}\right)^2 \left[K_1^2(x) + \frac{1}{\gamma^2}\, K_0^2(x) \right], \qquad (1.6)$$

where $x = \omega b/\gamma v$, $K_0(K_1)$ is the modified Bessel function of order zero (one), and $\alpha = e^2/\hbar c$ is the fine structure constant. In eq. (1.6) the first term inside parentheses comes from the contribution of the pulse P_1, whereas the second term comes from the contribution of the pulse P_2. One immediately sees that the contribution of pulse P_2 becomes negligible for $\gamma \gg 1$. The shape of the equivalent photon spectrum for a given impact parameter can be expressed in terms of the dimensionless function $\varphi(x) = x^2\, K_1^2(x)$, if we neglect the pulse P_2. In a crude approximation, $\varphi = 0$ for $x > 1$, and $\varphi = 1$ for $x \leq 1$, as can be seen from fig. 1.2. This implies that, in a collision with impact parameter b, the spectrum will contain equivalent photons with energies up to a maximum value of order

$$E_\gamma^{\mathrm{max}} = \gamma \hbar c/b , \qquad (1.7)$$

which we call by *adiabatic cutoff energy*. This means that in an electromagnetic collision of two nuclei the excitation of states with energies up to the above value can be reached. Although this result was
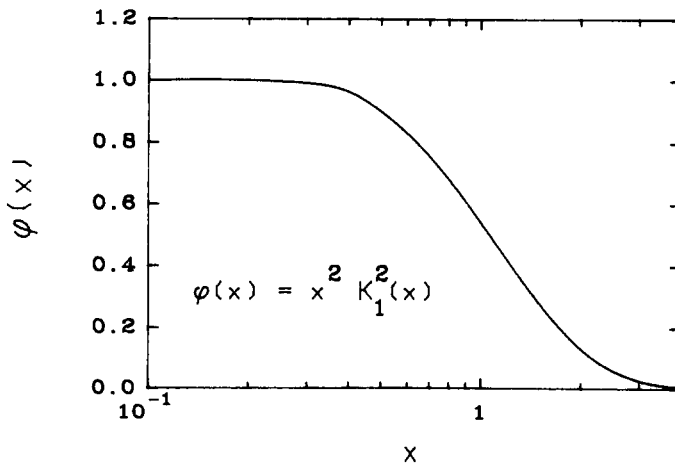

Fig. 1.2. The shape of the equivalent photon spectrum as a function of $x = \omega b/\gamma v$.

obtained classically, we can make a quantum analogy to it by observing that in a collision with interaction time given by eq. (1.3) only states satisfying the condition $T/\Delta t \gg 1$, where T is the period of the quantum states, will have an appreciable chance to be excited. Otherwise, the quantum system will respond adiabatically to the interaction. Later we shall see that quantum mechanical calculations confirm these expectations. In a collision with a typical impact parameter of $b = 10$ fm one can reach states with energy around $E_\gamma^{max} \simeq 20\gamma$ MeV. Among the many possibilities, we cite the following: for $E_\gamma \simeq 10$–20 MeV (already small values of γ), excitation of giant resonances, with subsequent nucleon emission; for $E_\gamma \simeq 20$–100 MeV, the quasideuteron effect which corresponds to a photon absorption of a correlated N–N pair in the nucleus; and for $E_\gamma > 100$ MeV, pion production through Δ-isobar excitation which has a maximum at $E_\gamma \simeq 200$ MeV. Also the production of lepton pairs (e^+e^-, $\mu^+\mu^-$, $\tau^+\tau^-$) are accessible with increasing value of γ.

The cross sections for electromagnetic processes in relativistic nuclear collisions are obtained by integrating eq. (1.5) from a minimum impact parameter, $b = R$, to $b = \infty$. The value of R depends on the process considered. In the case of internal nuclear excitation, i.e. Coulomb excitation, R will be equal to the sum of the two nuclear radii. We obtain

$$\sigma = \int_R^\infty 2\pi b\, P(b)\, \mathrm{d}b = \int n(\omega)\, \sigma_\gamma(\omega)\, \frac{\mathrm{d}\omega}{\omega} \,, \tag{1.8}$$

with

$$n(\omega) = \int_R^\infty 2\pi b\, N(\omega, b)\, \mathrm{d}b = \frac{2}{\pi}\, Z_1^2 \alpha \left(\frac{c}{v}\right)^2 \left[\xi K_0 K_1 - \frac{v^2 \xi^2}{2c^2}\, (K_1^2 - K_0^2) \right] \,, \tag{1.9}$$

where the modified Bessel functions are functions of the adiabaticity parameter

$$\xi = \omega R/\gamma v \,. \tag{1.10}$$

For $\gamma \gg 1$ (except for extreme low-energy frequencies, satisfying the relationship $\omega R/c \ll 1$) one can use the approximation

$$n(\omega) = \frac{1}{\pi}\, Z_1^2 \alpha \ln\left[\left(\frac{\delta}{\xi}\right)^2 + 1 \right] \simeq \frac{2}{\pi}\, Z_1^2 \alpha \ln\frac{\delta}{\xi} \,, \tag{1.11a}$$

where $\delta = 0.681, \ldots$ is a number related to the Euler's constant. This implies that the cross sections as given by eq. (1.8) will tend to increase logarithmically with the value of γ. Except for minor differences, this general behaviour will be found in the applications we shall study.

In the limit of very large frequencies, $\omega \gg \gamma v/R$, an adiabatic cutoff sets in and we have

$$n(\omega) = (Z_1^2 \alpha/2)\, e^{-2(\omega R/\gamma v)} \,. \tag{1.11b}$$

Although the above formulation of the electromagnetic collision of two fast nuclei was already

developed in the thirties with applications to many processes [see Ja-75], it was especially in the case of *relativistic heavy ion (RHI) collisions*, where these concepts were more useful. In some cases, the agreement of calculations based on the equivalent photon method and more exact quantum calculations are very good. This makes it a powerful tool for obtaining the values of probabilities and cross sections of a given electromagnetic process in RHI collisions with reasonable results, as compared to more complicated calculations.

We feel that a review of *electromagnetic processes in RHI collisions* is appropriate at this time. There is a fairly complete and coherent theoretical framework which describes such processes. Already well-established experimental work (mainly at BEVALAC) on Coulomb fragmentation has been analysed. There are new RHI accelerators being built (like SIS, Darmstadt, with energies in the GeV/A range), or already in operation (Brookhaven, with 15 GeV/A oxygen beams; CERN, with 60 and 200 GeV/A oxygen beams), or in the planning stage (relativistic heavy ion collider in the USA). New experiments related to electromagnetic processes are planned at these accelerators and many more could be envisaged. In view of these new possibilities, a review seems interesting for a large group of theoretical and experimental physicists at the present stage.

In section 2 we will present more elaborate semiclassical and quantum calculations of the probability amplitudes and cross sections for *relativistic Coulomb excitation*. There we shall see that, for not too high values of γ, there will be small deviations from the above results. We show that the equivalent photon spectrum can be decomposed in terms of a sum of different electric and magnetic multipolarities, which reproduces the limits (1.11) for $\gamma \gg 1$. The study of the contributions of the different multipolarities is specially important for Coulomb excitation.

In low-energy nuclear physics Coulomb excitation plays a key role in the study of collective low-lying states and multiple excitation has become a powerful tool to extract information about these states. In relativistic Coulomb collisions it is possible to excite high-lying states, like the giant E1 and E2 resonances, which mostly decay by particle emission. We will consider these processes in section 3 together with the possibilities for *multiple Coulomb excitation* of giant resonances which could lead to a disruption of the nuclei in fragments far from the stability line. In that section we also study the *direct dissociation of weakly bound nuclei* which is relevant for coincidence experiments. The different behaviour of the contributions of the electromagnetic and of the nuclear interaction to the differential and to the total cross sections is examined.

In section 4 the relativistic Coulomb excitation of hadrons in the field of a nucleus with large charge (*Primakoff effect*) will be studied on the same grounds. It is shown how useful this process can be in order to obtain information about the internal structure of these particles. The successful experimental study of the measurement of the lifetime of the Σ^0 particle is shown as a nice application of the theory of relativistic Coulomb excitation. Due to the enhancement of the cross sections with the charges of the ions, the production of particles in *two-photon processes* is also of great interest.

Although contributing little to the total emission of real photons (*Bremsstrahlung*) in RHI collisions, the Coulomb bremsstrahlung possesses have interesting features which will be studied in section 5.

The *ionization of atomic electrons* in RHI collisions has very large cross sections and is an extensively studied process, and we will show in section 6 the main theoretical aspects of it.

Section 7 is dedicated to the *production of lepton pairs* in RHI collisions. The consequences of the large cross sections for the production of electron–positron pairs are analysed. Of special interest for the development of relativistic heavy ion colliders is the case of electron–positron pair production with capture of the electron in an atomic orbit in the ions.

Conclusions and an outlook are given in section 8.

2. Theory of relativistic Coulomb excitation

Recently, new interest on the theory of relativistic Coulomb excitation has appeared. Among others, we cite the works of Fäldt, Pilkuhn, and collaborators [Fä-74, Jä-75]. In particular, Jäckle and Pilkuhn have deduced equivalent photon numbers for the lowest multipolarities with help of the *eikonal approximation*. A complete analytical evaluation of the contribution of all multipolarities was accomplished by Winther and Alder [Wi-79] in terms of a *semiclassical approach*. The relation between the electric-dipole excitation cross section obtained by Winther and Alder and the equivalent photon method was demonstrated by Hoffman and Baur [Ho-84]. Later on, it was shown by Goldberg [Go-84] how one can extend the equivalent photon method in order to calculate the equivalent photon numbers not only for the E1 but also for all other multipolarities of the virtual radiation. Bertulani and Baur [Ber-85, Ber-86a] have done calculations based on the plane wave Born approximation for the same process and made a comparison of all these different approaches.

In sections 2.1 and 2.2 we will show a resumé of the nice semiclassical calculations performed by Winther and Alder which contain the main ingredients of the process, and in sections 2.3 and 2.4 we will show the calculations of Bertulani and Baur in the plane wave Born approximation (PWBA) which are useful wherever quantum diffraction effects appear. In section 2.5 we will extract the equivalent photon numbers from the previous results which help us to obtain more insight into the theory by comparing it with the results from other formulations, which we will do in section 2.6. In section 2.7 we will follow the approach of Baur, Bertulani, and Rebel [Ba-86c] to account for *recoil corrections*, which are important for intermediate energy problems.

2.1. Excitation amplitude in the semiclassical approach

In the following we shall calculate the electromagnetic excitation amplitude of a target nucleus with mass and charge number A_2 and Z_2, respectively, by means of a relativistic projectile with velocity v, impact parameter b, and mass and charge number A_1 and Z_1. In fact, both nuclei will be excited and we can use all following results to calculate not only the target excitation amplitudes and cross sections, but also the projectile excitation ones, by exchanging the variables corresponding to the target and the projectile.

We shall consider the target nucleus as fixed, neglecting its recoil, and we place the origin of our coordinate system in its centre of mass. The target will be described by an eigenstate $|IM\rangle$, where I denotes its angular momentum and M the magnetic quantum number. In the semiclassical approach the projectile is assumed to move in a *straight-line* and will generate a time-dependent electromagnetic field which will excite the target. If the excitation is weak, we can calculate the excitation amplitude in the first order time-dependent perturbation theory as given by

$$a_{fi} = \frac{1}{i\hbar} \int_{-\infty}^{\infty} dt\, e^{i\omega t}\, \langle I_f M_f | V[r(t)] | I_i M_i \rangle \,, \tag{2.1.1}$$

where

$$\omega = (E_f - E_i)/\hbar \,, \tag{2.1.2}$$

and E_i (E_f) is the initial (final) excitation energy of the target. The interaction potential $V[r(t)]$ is given by[*]

$$V[r(t)] = \frac{1}{c} \int d^3 r \, A_\mu[r(t)] \, j_\mu(r) , \tag{2.1.3}$$

where $j_\mu \equiv (c\rho, \mathbf{j})$ is the internal target four-current and $A_\mu \equiv (1, \mathbf{v}/c)\Phi/c$, where $\Phi(r, t)$ is the Lienard–Wiechert potential [see e.g. Ja-75, p. 654],

$$\Phi(r, t) = \frac{Z_1 e \gamma}{[(x - b_x)^2 + (y - b_y)^2 + \gamma^2 (z - vt)^2]^{1/2}} \tag{2.1.4}$$

for a charged particle moving in a straight line with an impact parameter $b = \sqrt{b_x^2 + b_y^2}$. The z-axis is taken along the beam direction (see fig. 1.1). The Fourier components of the field (2.1.4) are

$$\Phi(r, \omega) = \int \Phi(r, t) \, e^{i\omega t} \, dt = \frac{2 Z_1 e}{v} \, e^{i(\omega/v)z} \, K_0\left(\frac{\omega q}{v}\right) , \tag{2.1.5}$$

where K_0 is the modified Bessel function of zero order and the quantity q is given by

$$q^2 = (1/\gamma^2)[(x - b_x)^2 + (y - b_y)^2] . \tag{2.1.6}$$

Now we expand $\Phi(r, \omega)$ in multipole components, i.e.

$$\Phi(r, \omega) = \sum_{lm} W_{lm}(r, \omega) \, Y_{lm}^*(\hat{r}) \tag{2.1.7}$$

with

$$W_{lm}(r, \omega) = \int d\Omega \, \Phi(r, \omega) \, Y_{lm}(\hat{r})$$

$$= \frac{2 Z_1 e}{v} \int_0^\pi e^{i(\omega/v)r \cos\theta} \, Y_{lm}(\theta, 0) \, d\cos\theta \int_0^{2\pi} e^{im\phi} \, K_0(\omega q/v) \, d\phi . \tag{2.1.8}$$

Since we are only treating the case in which the impact parameter b is larger than the nuclear radius, we can use the Graf addition theorem (see e.g. [Ab-64], p. 363, eq. (9.1.79))

$$K_0\left(\frac{\omega q}{v}\right) = \sum_{n=-\infty}^{\infty} e^{in\phi} \, K_n\left(\frac{\omega b}{\gamma v}\right) I_n\left(\frac{\omega}{\gamma v} \sqrt{r^2 - z^2}\right) . \tag{2.1.9}$$

Then the integral over ϕ in eq. (2.1.8) leads to

---

[*] Here we use the notation $A_\mu = (A_0, \mathbf{A})$, and the sum convention $A_\mu B_\mu = A_0 B_0 - \mathbf{A} \cdot \mathbf{B}$.

$$W_{lm}(r, \omega) = 4\pi \, \frac{Z_1 e}{v} \, K_m\left(\frac{\omega b}{\gamma v}\right) \int\limits_0^\pi \sin \theta \, \mathrm{d}\theta \, \mathrm{e}^{\mathrm{i}(\omega/v)r \cos \theta} \, Y_{lm}(\theta, 0) \, I_m\left(\frac{\omega r}{\gamma v} \sin \theta\right). \tag{2.1.10}$$

Writing $Y_{lm}(\theta, 0)$ in terms of the Gegenbauer polynomials $C_m^n(x)$ [see e.g. Ab-64, p. 771], and using the Gegenbauer integral (see e.g. [Gr-65], p. 832, eq. (7.333)) one finds for $m \geq 0$

$$W_{lm}(r, \omega) = \frac{Z_1 e}{v} \, \sqrt{16\pi(2l+1)} \left[\frac{(l-m)!}{(l+m)!}\right]^{1/2} (2m-1)!!\mathrm{i}^{l+m}$$

$$\times (c/\gamma v)^m \, K_m(\omega b/\gamma v) \, C_{l-m}^{m+1/2}(c/v) \, j_l(\kappa r) , \tag{2.1.11}$$

with

$$\kappa = \omega/c , \tag{2.1.12}$$

and $j_l(\kappa r)$ is the spherical Bessel function.

For $m < 0$ one finds

$$W_{l, -m}(r, \omega) = (-1)^m \, W_{lm}(r, \omega) . \tag{2.1.13}$$

Now we substitute eq. (2.1.3) in eq. (2.1.1) and utilise the multipole expansion (2.1.7) together with the result (2.1.11). Using the continuity equation for the charge and current density in nucleus 2, and the recursion relations for the Gegenbauer polynomials, one may write (2.1.1) in terms of the multipole matrix elements [see e.g. Al-75]

$$M(Elm) = \frac{(2l+1)!!}{\kappa^{l+1} c(l+1)} \int j(r) \cdot \nabla \times L[j_l(\kappa r) \, Y_{lm}(\hat{r})] \, \mathrm{d}^3 r , \tag{2.1.14a}$$

$$M(Mlm) = -\mathrm{i} \, \frac{(2l+1)!!}{\kappa^l c(l+1)} \int j(r) \cdot L[j_l(\kappa r) \, Y_{lm}(\hat{r})] \, \mathrm{d}^3 r \tag{2.1.14b}$$

for electric and magnetic excitations respectively.

The result may be written in the form

$$a_{fi} = -\mathrm{i} \, \frac{Z_1 e}{\gamma \hbar v} \sum_{\pi lm} (-1)^m \sqrt{2l+1} \kappa^l \, G_{\pi lm}\left(\frac{c}{v}\right) K_m\left(\frac{\omega b}{\gamma v}\right) \langle I_f M_f | M(\pi l, -m) | I_i M_i \rangle , \tag{2.1.15}$$

where $\pi = E$ for electric excitations, and $\pi = M$ for magnetic excitations. The functions $G_{\pi lm}$ can be expressed in terms of the associated Legendre polynomials and are given in explicit form in appendix A.

The amplitude (2.1.15) can be seen as a product of (i) a factor that only depends on the properties of the nuclear states involved through the matrix elements describing the electromagnetic decay of the state $|f\rangle$ to the state $|i\rangle$, (ii) a factor $K_m(x)$ that describes the degree of adiabaticity of the excitation and which vanishes exponentially as x becomes larger than unity, and (iii) a factor giving the strength of the field as a function of the velocity. Due to the conservation laws, m is the angular momentum

transfer from the relative motion to the internal degrees of freedom of the excited nuclei. That is,

$$m = M_i - M_f .$$ (2.1.16)

2.2. Cross sections

The square modulus of eq. (2.1.15) gives the probability amplitude of exciting the nucleus 2 from the initial state $|i\rangle$ to the final state $|f\rangle$. If the orientation of the initial state is not specified, the cross section for exciting the nuclear state of spin I_f in collisions with impact parameters larger than R is

$$\sigma_{i \to f} = 2\pi \int_R^\infty b \, db \, (2I_i + 1)^{-1} \sum_{M_i M_f} |a_{fi}|^2$$

$$= (Z_1 \alpha)^2 \sum_{\pi l m} \kappa^{2(l-1)} |G_{\pi l m}(c/v)|^2 \, g_m(\xi) \, B(\pi l, I_i \to I_f)/e^2 ,$$ (2.2.1)

where α is the fine-structure constant, ξ is given by eq. (1.10),

$$B(\pi l, I_i \to I_f) = \frac{1}{2I_i + 1} \sum_{M_i M_f} |\langle I_f M_f | M(\pi l m) | I_i M_i \rangle|^2$$ (2.2.2)

is the reduced transition probability, and g_m is given by

$$g_m(\xi) = g_{-m}(\xi) = 2\pi(\omega/\gamma v)^2 \int_R^\infty b \, db [K_m(\omega b/\gamma v)]^2$$

$$= \pi\xi^2 [K_{m+1}(\xi) K_{m-1}(\xi) - [K_m(\xi)]^2] .$$ (2.2.3)

In the limit $\xi \ll 1$, the functions $g_m(\xi)$ reduce to

$$g_m(\xi) = \begin{cases} \pi(m-1)[(m-2)!]^2 (2/\xi)^{2m-2} , & \text{for } m > 1 , \\ \pi \ln[(\delta/\xi)^2 + 1] , & \text{for } m = 1 , \\ \pi , & \text{for } m = 0 , \end{cases}$$ (2.2.4)

where $\delta = 0.681085 \ldots$.

We can obtain an estimate of the maximum angular deflection of the projectile due to Coulomb repulsion. It is given by (see [Ja-75, p. 643, eq. (13.89)])

$$\theta_C \simeq 2Z_1 Z_2 e^2 / RE ,$$ (2.2.5)

where E is the bombarding energy. For relativistic energies this quantity will be very small, justifying the use of straight lines for the projectile motion. For intermediate energy problems the recoil correction may be of importance and it amounts to small modifications in the above formulas, as we shall show in section 2.7.

2.3. Transition amplitude in the eikonal approximation

The scattering of highly energetic particles is, for most purposes, conveniently described by the so-called *eikonal approximation* [see e.g. Gl-59, Jo-74]. The transition amplitude in this approximation is given by

$$T_{fi} = \frac{ik}{2\pi} \int d^2b \, e^{iq_T \cdot b} \, \Gamma_\gamma(b) \,, \tag{2.3.1}$$

where $\hbar k$ is the momentum of the projectile's motion, q_T is the momentum transfer in the transverse direction, and $\Gamma_\gamma(b)$ is the profile function for the Coulomb scattering. We can use first order perturbation to calculate the profile function (in which case eq. (2.3.1) is formally equal to the first order Born approximation), and introduce a *cutoff* to account for the strong absorption. In this case we can write

$$\Gamma_\gamma(b, q_l) = \frac{\theta(b - R)}{2\pi i k} \int d^2q_T \, e^{-iq_T \cdot b} \, T_{Born}(q_T, q_l) \,, \tag{2.3.2}$$

where $\theta(b - R)$ is the step function, and

$$T_{Born} = \frac{1}{c} \int d^3r \, A_\mu(r) \, \langle I_f M_f | j_\mu(r) | I_i M_i \rangle \tag{2.3.3a}$$

with

$$A_\mu(r) = \frac{1}{c} \int d^3r' \, \frac{e^{i\kappa|r-r'|}}{|r-r'|} \, \langle k_f | J_\mu(r') | k_i \rangle \,, \tag{2.3.3b}$$

where $j_\mu \equiv (c\rho, j)$ is the target four-current and J_μ is the projectile one; $r(r')$ denotes the target (projectile) coordinate, and κ is given by eq. (2.1.12). The function $A_\mu(r)$ represents the four-potential created by the transition current of the projectile.

Inserting eqs. (2.3.3) and (2.3.2) in eq. (2.3.1), and performing the integration over b, we find that T_{fi} is also given by eq. (2.3.3a), only that eq. (2.3.3b) is changed by the introduction of a cut-off function in the r' integration, i.e.,

$$A_\mu(r) = \frac{1}{c} \int d^2\rho' \, \theta(\rho' - R) \int dz' \, \frac{e^{i\kappa|r-r'|}}{|r-r'|} \, \langle k_f | J_\mu(r') | k_i \rangle \,. \tag{2.3.4}$$

Describing the projectile by a plane wave $|k\rangle$, where k denotes its wave vector, and assuming that its velocity is not appreciably changed during the collision, we can put

$$\langle k_f | J_\mu(r') | k_i \rangle = Z_1 e v_\mu \, e^{iq \cdot r'} \,, \tag{2.3.5}$$

where

$$q = k_i - k_f \tag{2.3.6}$$

is the momentum transfer, and

$$v_\mu = (c, v) \,,$$

with v equal to the projectile's velocity. Choosing cylindrical coordinates for the projectile space integration and the z-axis in the incident beam direction, we obtain

$$e^{iq \cdot r'} = e^{iq_L z'} e^{iq_T \rho' \cos(\psi - \phi')} \,, \tag{2.3.7}$$

where ψ is the azimuthal scattering angle and q_L (q_T) is the longitudinal (transverse) momentum transfer to the projectile. For relativistic energies the polar scattering angle θ due to the electromagnetic interaction is very small and we can put

$$q_L = k_i - k_f \cos \theta \simeq k_i - k_f \simeq \omega/v \,, \tag{2.3.8a}$$

$$q_T = k_f \sin \theta \simeq (E/\hbar c)(v/c) \sin \theta \,, \tag{2.3.8b}$$

where we also assumed that the excitation energy $E_i - E_f = \hbar \omega$ is much smaller than the relative motion energy $E = E_i \simeq E_f$.

Using these approximations we can write

$$A_\mu(r) = Z_1 e(v_\mu/c) \int d^2\rho' \int dz' \, e^{i(\omega/v)z'} \, e^{iq_T \rho' \cos(\psi - \phi')} \frac{e^{i\kappa|r - r'|}}{|r - r'|} \,. \tag{2.3.9}$$

The z' integration can be performed by defining

$$d^2 = \rho^2 + \rho'^2 - 2\rho\rho' \cos(\phi - \phi') \,.$$

This leads to

$$\int_{-\infty}^{+\infty} dz' \, e^{i(\omega/v)z'} \frac{e^{i\kappa|r - r'|}}{|r - r'|} = 2e^{i(\omega/v)z} \, K_0\left(\frac{\omega d}{\gamma v}\right) \,. \tag{2.3.10}$$

Using the Graf addition theorem in order to separate the target and projectile coordinates, the ϕ' integration is easily obtained and $A_\mu(r)$ becomes

$$A_\mu = 4\pi Z_1 e(v_\mu/c) \, e^{i(\omega/v)z} \sum_{n = -\infty}^{\infty} i^n \, e^{-in\psi} \, e^{in\phi} \, J_n(\omega\rho/\gamma v) \, \chi_n(R) \,, \tag{2.3.11}$$

where

$$\chi_n(R) = \int\limits_{R}^{\infty} J_n(q_T \rho') \, K_n\left(\frac{\omega\rho'}{\gamma v}\right) \rho' \, d\rho'$$

$$= \frac{R}{[q_T^2 + (\omega/\gamma v)^2]} \left\{ \frac{\omega}{\gamma v} \, J_n(q_T R) \, K_{n+1}\left(\frac{\omega R}{\gamma v}\right) - q_T \, J_{n+1}(q_T R) \, K_n\left(\frac{\omega R}{\gamma v}\right) \right\}. \tag{2.3.12}$$

After these considerations, many steps of this calculation are exactly the same as in the semiclassical approach. Doing a multipole expansion of $A_\mu(r)$ we find

$$A_\mu = (4\pi)^{3/2} Z_1 e\left(\frac{v_\mu}{c}\right) \sum_{lm} i^l \sqrt{2l+1} \left[\frac{(l-m)!}{(l+m)!}\right]^{1/2} (2m-1)!! \left(\frac{c}{v\gamma}\right)^m$$

$$\times e^{-im\psi} \, \chi_m(R) \, C_{l-m}^{m+1/2}\left(\frac{c}{v}\right) j_l(\kappa r) \, Y_{lm}^*(\hat{r}) . \tag{2.3.13}$$

Now, inserting this relation into eq. (2.3.1), using the continuity equation for the nuclear current, and the recursion relations of the Gegenbauer polynomials, one can write T_{fi} in terms of the matrix elements of nuclear excitation:

$$T_{fi} = (2\pi Z_1 e/\gamma) \sum_{\pi l m} i^m \kappa^l \sqrt{2l+1} \, e^{-im\psi} \, \chi_m(R) \, G_{\pi l m}(c/v) \, \langle I_f M_f | M(\pi l, -m) | I_i M_i \rangle . \tag{2.3.14}$$

This expression is analogous to the one found in the semiclassical treatment, eq. (2.1.15). Again, we find a factorization into a kinematical part and a nuclear matrix element, which describes the electromagnetic transition of the state $|f\rangle$ to the state $|i\rangle$. Quite in contrast to the case of electron scattering [see e.g. FW-66], one does not obtain nuclear form factors which depend on q. The reason is the introduction of the cutoff due to the strong absorption (see eq. 2.3.2).

2.4. Differential cross section in the eikonal approximation

The differential cross section, for the case in which the orientation of the target is ignored, is given by

$$\frac{d\sigma}{d\Omega} = \left(\frac{E}{2\pi\hbar^2 c^2}\right)^2 \frac{1}{2I_i + 1} \sum_{M_i M_f} |T_{fi}|^2 . \tag{2.4.1}$$

From eq. (2.3.14), the Wigner–Eckart theorem and the orthogonality properties of the Clebsch–Gordan coefficients, one can show that

$$\frac{d\sigma}{d\Omega} = \left(\frac{Z_1 \alpha E}{\gamma \hbar c}\right)^2 \sum_{l,m} k^{2l} |G_{\pi l m}|^2 [\chi_m(R)]^2 \frac{B(\pi l)}{e^2} . \tag{2.4.2}$$

The dependence of the differential cross section on the scattering angle is given implicitly by the function $\chi_m(R)$. For forward scattering, $q_T = 0$, and we obtain

$$\frac{\chi_m(R, \theta = 0)}{R^2} = \delta_{m0} \frac{1}{\xi} K_1(\xi) , \tag{2.4.3}$$

where ξ is given by the eq. (1.10). This implies that

$$\frac{d\sigma}{d\Omega}(\theta = 0) = (Z_1\alpha)^2 \left(\frac{E}{\hbar\omega} \frac{v^2}{c^2}\right)^2 \xi^2 [K_1(\xi)]^2 \sum_l k^{2(l-1)} \left|G_{El0}\left(\frac{c}{v}\right)\right|^2 \frac{B(El)}{e^2} . \tag{2.4.4}$$

The quantity m is equal to the angular momentum transfer to the target in the direction of the incident beam, and eq. (2.4.3) shows that, for exact forward scattering, it is equal to zero. In this case there is no magnetic excitation of the target. This can be explained in terms of the symmetry properties of the scattering of spin-zero particles. The conservation of parity of the total system forbids the change of internal parity of the target by $(-1)^{l+1}$ in the case $m = 0$ [see e.g. Ja-59, eq. (43)]. Since magnetic excitations are accompanied by this change of parity, the forward scattering amplitude must vanish in this case.

For $\theta \neq 0$ one can use the integral (2.3.12) to obtain the dependence of the cross section on the scattering angle. It will be extremely forward-peaked with a diffraction angle of about

$$\theta_D \simeq \frac{1}{\Lambda} \quad \text{with} \quad \Lambda = \frac{Ev}{\hbar c^2} R . \tag{2.4.5}$$

The parameter Λ is equal to the ratio between the nuclear dimension R and the quantum wavelength of the relative motion energy. For relativistic heavy ion collisions this quantity is much greater than unity and θ_D will be very small. We can also compare the diffraction angle θ_D with the classically expected Coulomb deflection given by eq. (2.2.5). The ratio of these two quantities is

$$\theta_C / \theta_D \simeq (2/137) Z_1 Z_2 , \tag{2.4.6}$$

showing that only for small projectile and (or) target charge the diffraction effects will be comparable to the Coulomb deflection.

The total cross section is obtained by integrating (2.4.2) over the scattering angle θ. But, by means of (2.3.8b) we can transform the angular integration to one involving the momentum transfer q_T:

$$d\Omega = (\hbar c^2 / Ev)^2 q_T \, dq_T \, d\psi . \tag{2.4.7}$$

Accordingly, the integration in q_T must go from 0 to $Ev/\hbar c^2$. Nevertheless, expressions (2.3.8b) and (2.4.5) imply that already for $q_T \simeq 1/R \ll Ev/\hbar c^2$ the differential cross section is negligible. It then makes no difference if we take the integral in q_T until infinity. In this case we can use the closure relation of the Bessel functions

$$\int_0^\infty q_T J_m(q_T \rho') J_m(q_T \rho'') \, dq_T = \frac{1}{\rho'} \delta(\rho' - \rho'') \tag{2.4.8}$$

in order to obtain the total cross section

$$\sigma_{i \to f} = (Z_1 \alpha)^2 \sum_{\pi l m} k^{2(l-1)} g_m(\xi) |G_{\pi l m}(c/v)|^2 B(\pi l, I_i \to I_f)/e^2 , \tag{2.4.9}$$

which is equal to the Coulomb excitation cross section given by the semiclassical calculation. Also in the case where no absorption (cutoff radius) is assumed (for example, in atomic excitation processes), the cross sections in the PWBA and in the semiclassical formulations can be proven to be the same. For this general proof, see appendix B.

2.5. Equivalent photon numbers

According to the *equivalent photon method*, the excitation of the target nucleus can be described as the absorption of equivalent photons whose spectrum is determined by the Fourier transform of the time-dependent electromagnetic field generated by the projectile [see Ja-75]. The multipole expansion of the electromagnetic interaction as done in the last sections, permits us to deduce the equivalent photon spectrum for all multipolarities [see Ber-85].

Integrating (2.2.1) for all energy transfers $\varepsilon = \hbar\omega$ and summing over all possible final states of the target, we obtain

$$\sigma_C = \sum_f \int \sigma_{i \to f}(\varepsilon) \, \rho_f(\varepsilon) \, d\varepsilon , \tag{2.5.1}$$

where $\rho_f(\varepsilon)$ represents now the density of final states of the target, with energy $E_2^f = E_2^i + \varepsilon$. Inserting eq. (2.2.1) in eq. (2.5.1), we can rewrite it in the form

$$\sigma_C = \sum_l \int \{n_{El}(\omega) \, \sigma_\gamma^{El}(\omega) + n_{Ml}(\omega) \, \sigma_\gamma^{Ml}(\omega)\} \frac{d\omega}{\omega} , \tag{2.5.2}$$

where $\sigma_\gamma^{\pi l}$ are the photonuclear absorption cross sections for a given multipolarity πl:

$$\sigma_\gamma^{\pi l}(\omega) = \frac{(2\pi)^3(l+1)}{l[(2l+1)!!]^2} \sum_f \rho_f(\varepsilon) \, k^{2l-1} \, B(\pi l) . \tag{2.5.3a}$$

The total photonuclear cross section is a sum of all these multipolarities:

$$\sigma_\gamma = \sum_{\pi l} \sigma_\gamma^{\pi l}(\omega) . \tag{2.5.3b}$$

This allows us to obtain the *equivalent photon numbers* $n_{\pi l}(\omega)$ given by

$$n_{\pi l}(\omega) = Z_1^2 \alpha \frac{l[(2l+1)!!]^2}{(2\pi)^3(l+1)} \sum_m \left| G_{\pi l m}\left(\frac{c}{v}\right) \right|^2 g_m(\xi) . \tag{2.5.4}$$

Since all nuclear excitation dynamics is contained in the photoabsorption cross section, the equivalent photon numbers (2.5.4) do not depend on this process. They only depend on the way that the projectile moves. The equivalent photon method consists of using its kinematics to calculate the intensity of the equivalent photon spectrum, which for a straight-line-moving projectile must be the same as those of eq. (2.5.4).

It was shown by Hoffmann and Baur [Ho-84] that, for E1 excitations, the equivalent photon numbers obtained from the total cross section (2.2.1) are really equal to that calculated by Fermi, Weizsäcker, and Williams in the equivalent photon method [Fe-24, We-34, Wi-34 and Wi-35], which was presented in section 1. Nevertheless, while that method gives an expression for the equivalent photon numbers independent of the multipolarities, eq. (2.5.4) shows that this is not correct in general. Indeed, a merit of eq. (2.5.4) is that it gives an analytical expression to calculate the equivalent photon numbers for all multipolarities and radiation types.

Using the expressions of $G_{\pi lm}$ as given in appendix A, we can write explicitly

$$n_{E1}(\omega) = n_{E1, m=-1} + n_{E1, m=+1} + n_{E1, m=0} = \frac{2}{\pi} Z_1^2 \alpha \left(\frac{c}{v}\right)^2 \left[\xi K_0 K_1 - \frac{v^2 \xi^2}{2c^2} (K_1^2 - K_0^2)\right], \qquad (2.5.5a)$$

$$n_{M1}(\omega) = \left(\frac{v}{c}\right)^2 [n_{E1, m=-1} + n_{E1, m=+1}] = \frac{2}{\pi} Z_1^2 \alpha \left[\xi K_0 K_1 - \frac{\xi^2}{2} (K_1^2 - K_0^2)\right], \qquad (2.5.5b)$$

$$n_{E2}(\omega) = \frac{2}{\pi} Z_1^2 \alpha \left(\frac{c}{v}\right)^4 \left[2\left(1 - \frac{v^2}{c^2}\right)K_1^2 + \xi\left(2 - \frac{v^2}{c^2}\right)^2 K_0 K_1 - \frac{\xi^2 v^4}{2c^4} (K_1^2 - K_0^2)\right], \qquad (2.5.5c)$$

where all K's are functions of ξ as given by eq. (1.10).

In the limit $\gamma \gg 1$ simpler expressions can be obtained for the equivalent photon numbers. Using eq. (2.2.4) and the approximations given in the appendix A, we find that in the sum over m of eq. (2.5.4) the leading term for $\gamma \gg 1$ is the one with $m = 1$, which gives a logarithmic rise with γ, since for $m > 1$ there is no dependence on γ. In this case the equivalent photon numbers are equal to

$$n_{\pi l} = \frac{1}{\pi} Z_1^2 \alpha \ln\left[\left(\frac{\delta}{\xi}\right)^2 + 1\right] \simeq \frac{2}{\pi} Z_1^2 \alpha \ln\left(\frac{\delta}{\xi}\right), \qquad (2.5.6)$$

valid for all multipoles, which is exactly equal to eq. (1.11a). Since $\xi = \omega R/\gamma v \to 0$, we have a logarithmic rise of the cross section for all multipolarities with γ. The impinging projectile acts like a spectrum of plane wave photons with helicity $m = \pm 1$. Such a photon spectrum contains equally all multipolarities πl.

For $l > 1$ and a not too large value of γ, the $m = l$ term can still be substantial. For a comparison we retain only the terms $m = l$ in the sum (2.5.4), obtaining

$$n_{\pi l}(m = l \text{ contribution}) = Z_1^2 \alpha \frac{1}{2\pi} \frac{(2l)!}{(l+1)l(l-1)} (kR)^{2-2l}. \qquad (2.5.7)$$

For $kR \ll 1$, as is the case for low-lying excited levels, this term dominates over the $m = 1$ term (2.5.6), unless γ is extremely large. However, it must be kept in mind that in relativistic Coulomb collisions it is possible to excite states with $kR \simeq 1$, or as we shall see, even $kR > 1$ is possible. In this case the term $m = 1$ dominates, and the cross sections will always increase logarithmically with the beam energy.

In fig. 2.1 we show $n_{\pi l}$ (with Z_1 = unity) as given by eq. (2.5.5), as a function of $\omega R/c$. We see that $n_{E2} \gg n_{E1} \gg n_{M1}$ for small values of γ, in contrast to the limit $\gamma \gg 1$. The physical reason for these two different behaviours of the equivalent photon spectrum is the following. The electric field of a charged particle moving at low energies is approximately radial and the lines of force of the field are isotropically distributed, with their relative spacing increasing with the radial distance. When interacting with a target of finite dimension, the non-uniformity of the field inside the target is responsible for the
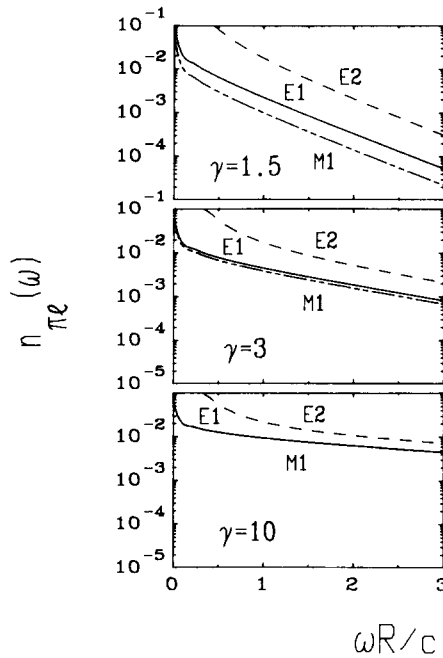
Fig. 2.1. Equivalent photon number per unit projectile charge, for E1, M1 and E2 radiation, and as a function of the ratio between R and the photon wavelength. γ is the ratio of the projectile energy to its rest energy.

large electric quadrupole interaction between them. The same lines of force of an ultrarelativistic ($\gamma \gg 1$) charged particle appear more parallel and compressed in the direction transverse to the particle's motion, due to the Lorentz contraction (see fig. 1.1a). As seen from the target, this field looks like a pulse of a plane wave. But plane waves contain all electric and magnetic multipolarities with the same weight. This is the cause for the equality between the equivalent photon numbers as $\gamma \to \infty$.

In the limit of large frequencies, $\omega \gg \gamma v / R$, an adiabatic cutoff sets in and $g_m(\xi) \to (\pi^2/2)\, e^{-2\xi}$. From eq. (2.5.4) one obtains that in this limit

$$n_{\pi l} \propto e^{-2\xi} .$$

(2.5.8)

This means that a useful approximation in many cases is to use the relation (2.5.6) for $\xi \leq 1$, and $n_{\pi l}(\omega) = 0$ for $\xi > 1$.

For general purposes, the utility of eq. (2.5.2) is twofold: (a) if one multipolarity is favoured in a certain reaction, then by measuring the total Coulomb reaction cross section one can get information about the respective photo-induced process; (b) if the experimental data on the photo-induced process are available, one can use eq. (2.5.2) to calculate the contribution of the electromagnetic interaction to the same process in a RHI collision.

2.6. Comparison with other methods

Also by means of the eikonal approximation, Jäckle and Pilkuhn [Jä-75] derived other expressions for n_{E1} and n_{M1}. In their calculations it was assumed that the projectile had a Yukawa charge distribution with length parameter $a = \sqrt{\langle r_1^2 \rangle}/6$, where $\sqrt{\langle r_1^2 \rangle}$ is the charge mean square radius of the

projectile. We can compare their expressions with the eq. (2.5.5) if we take in their results the projectile as a point particle $(a \to 0)$. This leads to

$$n_{E1}^{JP} = \frac{1}{\pi} Z_1^2 \alpha \left\{ \xi^2 [K_0 K_2 - K_1^2 - 2 K_0(\phi) [K_2 - K_0]] + \frac{\xi^2}{\gamma^2} (K_1^2 - K_0^2) + 4\phi K_0(\phi) K_1(\phi) \right\},$$

(2.6.1)

where the K's are the modified Bessel functions as a function of ξ given by eq. (1.10), except for the ones that are explicitly written as functions of $\phi = \omega R/v$. In the same limit, one can show that $n_{M1}^{JP} = n_{M1}$. But one cannot reduce eq. (2.6.1) to eq. (2.5.5a). However, for $\gamma \gg 1$ they will be equal (see fig. 2.2). But the consideration of a charge distribution for the projectile should not modify the final results, apart from influencing the value of the minimum impact parameter R. The Coulomb potential for a projectile, with a spherical distribution of charge in its rest frame is the same as that for a point particle with equal total charge. A Lorentz transformation to another inertial frame of reference obviously cannot modify this equality. All following results, such as cross sections or equivalent photon numbers, are therefore not changed by the introduction of a spherical charge distribution for the projectile. Therefore, the minor differences (E1 case) in the final results of Jäckle and Pilkuhn [Jä-75] and Bertulani and Baur [Ber-85] must be due to the small kinematic corrections used by the former authors.

Goldberg [Go-84] has also performed a calculation of the equivalent photon numbers by a direct multipole expansion of the electromagnetic field generated by the projectile. The final results are then obtained by performing, numerically, complicated integrals along the projectile trajectory. Actually, a merit of eq. (2.5.4) is that it gives an analytical expression to calculate the equivalent photon numbers for all different multipolarities and radiation types.
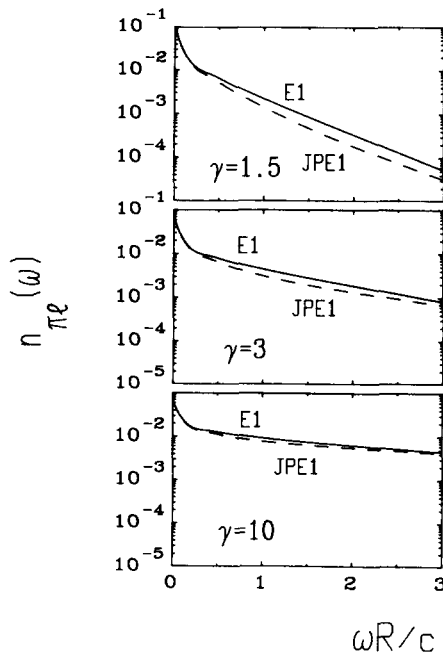

Fig. 2.2. Comparison of the equivalent photon number per unit charge with the Jäckle and Pilkuhn result (JPE1), for the electric-dipole radiation (see text).

For small-mass projectiles one can improve eq. (2.5.4), based on semiclassical ideas. In order to see how it works, we compare the final improved expressions with those obtained in the ultrarelativistic electron–nucleus scattering. But, besides the spin interactions, electron scattering is different from Coulomb excitation because the electrons can penetrate the nucleus and continue interacting only electromagnetically with it. Nevertheless, in the long-wavelength limit $q_e R \ll 1$, where q_e is the momentum transfer of the electron, the nuclear volume plays a minor role and the matrix elements contributing to the excitation in the near-forward scattering are just those appearing in the photo-excitation process, with $q_e \simeq k$ [Ei-70]. To disregard the nuclear volume means to put $R = 0$ in the expression (2.5.4). But in that case it goes to infinity. If we now evoke semiclassical ideas, we note that a normal procedure [see Ja-75] within the equivalent photon method is to use the quantum wavelength $\hbar/\gamma M v$ of the projectile, instead of the nuclear radius, as the minimum impact parameter when the projectile's mass M is small. This assumption is based on the uncertainty principle, which introduces a "smearing out" of the projectile's coordinates in a space interval of about its wavelength. By means of this recipe, we then replace eq. (1.10) by

$$\xi_e = \hbar\omega/\gamma^2 m_e v^2 , \tag{2.6.2}$$

where m_e is the electron rest mass. This quantity is generally much less than one, so that the expressions (2.5.5) become

$$n_{E1}^{electron} = \frac{2}{\pi} \alpha \ln \frac{\delta}{\xi_e} = n_{M1}^{electron} , \tag{2.6.3a}$$

$$n_{E2}^{electron} = \frac{2}{\pi} \alpha \left[\frac{1}{\gamma^2 \xi_e^2} + \ln \frac{\delta}{\xi_e} \right] . \tag{2.6.3b}$$

These are just the results that one derives from the equivalent photon numbers for electron scattering, first obtained by Thie, Mullin and Guth [Th-52], in the ultra-relativistic limit with small energy loss, where one can put $E_i \simeq E_f = \gamma m_e c^2 \gg m_e c^2$.

When the above conditions (forward scattering, long-wavelength approximation) are not matched, then this analogy is not valid at all. For example, electron scattering can generate longitudinal (E0) interactions with the nucleus, which are not accessible in Coulomb scattering.

Recently, Galletti, Kodama and Nemes [Ga-87] have studied the quantum and relativistic recoil effects in the theory of relativistic Coulomb excitation and found that relatively large transverse momentum transfers are allowed, which are not obtainable in the simple semiclassical or eikonal approaches described here. For the sake of simplicity, we shall not enter into the discussion of these effects, since they play minor roles in most of the cases we shall treat here. Instead of that, in the next section we will show how one can make a comparison of the previous results with Coulomb excitation at nonrelativistic energies in order to derive simple recoil corrections for the equivalent photon spectrum.

2.7. Effects of the Rutherford bending

In nonrelativistic Coulomb excitation the double differential cross section can also be expressed in the terms of equivalent photon numbers as

$$\frac{d^2\sigma}{d\Omega\, dE_\gamma} = \frac{1}{E_\gamma} \sum_{\pi l} \frac{dn_{\pi l}}{d\Omega}\, \sigma_\gamma^{\pi l}\,, \tag{2.7.1}$$

where

$$\frac{dn_{\pi l}}{d\Omega} = Z_1^2 \alpha\, \frac{l[(2l+1)!!]^2}{(2\pi)^3(l+1)}\, \zeta^{-2l+2} \left(\frac{c}{v}\right)^{2l} \frac{df_{\pi l}(\theta, \zeta)}{d\Omega} \tag{2.7.2}$$

are the equivalent photon numbers *per unit solid angle*. They are functions of the adiabaticity parameter

$$\zeta = E_\gamma a/\hbar v = \omega a/v\,, \tag{2.7.3}$$

where

$$a = Z_1 Z_2 e^2/m_0 v^2 \tag{2.7.4}$$

is half the distance of closest approach in a head-on collision and m_0 is the reduced mass of the ions. The functions $f_{\pi l}(\theta, \zeta)$ are given in terms of orbital integrals and can be found in a tabulated form in the textbook of Alder and Winther [Al-75] on Coulomb excitation. The first calculations of the functions $f_{\pi l}(\theta, \zeta)$ were performed by Ter-Martirosyan [Te-52], who found an analytical expression for the E1 multipolarity. Since this is the more important case, let us study it first.

Inserting the expression for $df_{E1}(\theta, \zeta)$ [see Al-75, p. 93] in eq. (2.7.2) we obtain

$$\frac{dn_{E1}}{d\Omega} = \frac{Z_1^2 \alpha}{4\pi^2} \left(\frac{c}{v}\right)^2 \varepsilon^4 \zeta^2\, e^{-\pi\zeta} \left\{ \frac{\varepsilon^2 - 1}{\varepsilon^2}\, [K_{i\zeta}(\varepsilon\zeta)]^2 + [K'_{i\zeta}(\varepsilon\zeta)]^2 \right\}, \tag{2.7.5}$$

where $\varepsilon = (\sin(\theta/2))^{-1}$ is the eccentricity parameter, and $K'_{i\zeta}(y)$ means the derivative of $K_{i\zeta}(y)$ with respect to the argument y.

For relativistic projectile energies the Rutherford trajectory can be substituted by a straight-line and, instead of the scattering angle θ, the concept of impact parameter b is used. The equivalent photon numbers in those cases is given by eq. (1.6), that is

$$\frac{dn_{E1}}{2\pi b\, db} = N(\omega, b) = \frac{Z_1^2 \alpha}{\pi^2} \left(\frac{\omega}{\gamma v}\right)^2 \left(\frac{c}{v}\right)^2 \left[K_1^2(x) + \frac{1}{\gamma^2} K_0^2(x) \right] \tag{2.7.6}$$

with $x = \omega b/\gamma v$. Since, for a Rutherford trajectory, the impact parameter is related to the scattering angle by the expression $b = a\, \mathrm{ctg}(\theta/2)$, we can rewrite the above equation as

$$\left(\frac{dn_{E1}}{d\Omega}\right)_{\mathrm{rel}} = \frac{Z_1^2 \alpha}{4\pi^2}\, \zeta^2 \varepsilon^4 \left(\frac{c}{\gamma v}\right)^2 \left[K_1^2(x) + \frac{1}{\gamma^2} K_0^2(x) \right]. \tag{2.7.7}$$

Of course, for relativistic energies $\theta \ll 1$ and $x = (\varepsilon\zeta/\gamma)\cos(\theta/2) \simeq \varepsilon\zeta/\gamma$.

For the nonrelativistic limit a small scattering angle is related to a large impact parameter trajectory $\varepsilon \simeq b/a \gg 1$. If we assume $\zeta \ll 1$, then by use of $K'_0 = -K_1$ we obtain from eq. (2.7.5)

$$\left(\frac{dn_{E1}}{d\Omega}\right)_{nonrel} = \frac{Z_1^2 \alpha}{4\pi^2} \, \varepsilon^2 \left(\frac{c}{v}\right)^2 x^2 [K_1^2(x) + K_0^2(x)] \,, \tag{2.7.8}$$

which is just eq. (2.7.7) for $\gamma \simeq 1$.

For not too large impact parameters, which still lead to small scattering angles the Rutherford bending of the trajectory is mainly reflected through the parameter ζ. In that case eq. (2.7.5) is approximately

$$\frac{dn_{E1}}{d\Omega} = \frac{Z_1^2 \alpha}{4\pi^2} \left(\frac{c}{v}\right)^2 \varepsilon^2 \, e^{-\pi\zeta} \, x^2 \{[K_{i\zeta}(x)]^2 + [K'_{i\zeta}(x)]^2\} \,. \tag{2.7.9}$$

Figure 2.3 displays the ratio $r(\zeta, x) = [$eq. (2.7.9)/eq. (2.7.8)$]$ which shows the effect of the Rutherford-bending to the straight-line calculation. This effect increases steadily with ζ.

In eq. (2.7.5) the Rutherford trajectory is accounted for properly in the calculations, but retardation effects in the interaction are ignored. The reverse is true in the calculations which lead to eq. (2.7.6). While one can safely use eq. (2.7.5) in nonrelativistic problems and eq. (2.7.6) in relativistic ones, the previous discussion has shown that none of them is suitable for intermediate energy problems, where both effects are present. But, by a direct look at eqs. (2.7.5) and (2.7.7), we see that the main effect of the Rutherford trajectory would be present in the imaginary indices (iζ) of the modified Bessel functions as well as in the factor $e^{-\pi\zeta}$. On the other hand, retardation effects imply in the appearance of the γ-factors in the eq. (2.7.7), thus suggesting that one can account simultaneously for both effects by defining the new variable

$$\eta = \zeta/\gamma = \omega a/\gamma v \,,$$

and setting

$$\frac{dn_{E1}}{d\Omega} = \frac{Z_1^2 \alpha}{4\pi^2} \left(\frac{c}{v}\right)^2 \varepsilon^4 \eta^2 \, e^{-\pi\eta} \left\{ \frac{1}{\gamma^2} \frac{\varepsilon^2 - 1}{\varepsilon^2} [K_{i\eta}(\varepsilon\eta)]^2 + [K'_{i\eta}(\varepsilon\eta)]^2 \right\} \,. \tag{2.7.10}$$
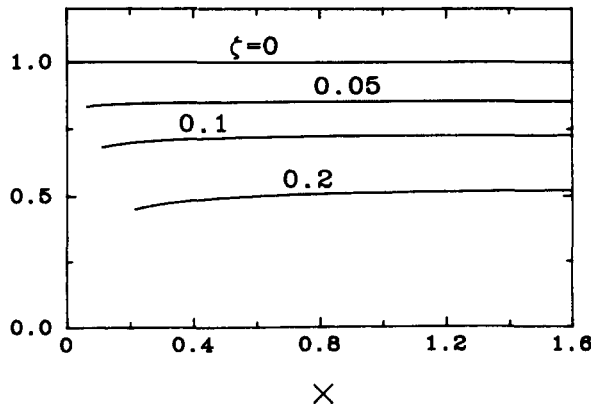

Fig. 2.3. Effect of Rutherford bending of the projectile motion for different values of the adiabacity parameter $\zeta = E_\gamma a / \hbar v$. The ratio of eq. (2.7.9) and eq. (2.7.8) is plotted as a function of $x = \varepsilon\zeta$ (for $\gamma \simeq 1$).

This equation reduces to eq. (2.7.5) for $\gamma \simeq 1$ and to eq. (2.7.7) for $\gamma \gg 1$, $\varepsilon \gg 1$ and should be a good improvement for the intermediate energy region.

According to eq. (2.7.1) the differential Coulomb excitation cross section for the E1 multipolarity integrated over angles is

$$\frac{d\sigma_{E1}}{dE_\gamma} = \frac{1}{E_\gamma}\, n_{E1}\sigma_\gamma^{E1}\,.$$ (2.7.11)

The equivalent photon number n_{E1} is obtained by an integration of eq. (2.7.10) over all angles corresponding to pure Coulomb trajectories. In terms of the eccentricity parameter, this integral can be expressed as

$$n_{E1} = \frac{2}{\pi}\, Z_1^2 \alpha \eta^2\, e^{-\pi\eta} \left(\frac{c}{v}\right)^2 \int_{\varepsilon_0}^{\infty} \varepsilon\, d\varepsilon \left\{ \frac{1}{\gamma^2}\, \frac{\varepsilon^2 - 1}{\varepsilon^2}\, [K_{i\eta}(\varepsilon\eta)]^2 + [K_{i\eta}'(\varepsilon\eta)]^2 \right\}.$$ (2.7.12)

The minimum value of the eccentricity parameter depends on whether the relative motion energy is smaller or greater than the Coulomb barrier energy E_B:

$$\varepsilon_0 = \begin{cases} 1\,, & \text{for } E \leqslant E_B\,, \\ \sqrt{1 + 4(E/E_B)^2(1 - E_B/E)}\,, & \text{for } E > E_B\,. \end{cases}$$ (2.7.13)

We see that when $E \gg E_B = Z_1 Z_2 e^2 / R$, then $\varepsilon_0 \simeq 2E/E_B = R/a$, where R is the sum of the two nuclear radii. The integration (2.7.12) can also be expressed in terms of the Bessel functions of imaginary or complex indices by means of the Lommel integral formulas [see e.g. Wa-58, p. 133]. This gives

$$n_{E1} = \frac{2}{\pi}\, Z_1^2 \alpha\, e^{-\pi\eta} \left(\frac{c}{v}\right)^2 \left\{ -x K_{i\eta} K_{i\eta}' \right.$$
$$\left. - \frac{1}{2}\left(\frac{v}{c}\right)^2 x^2 \left[K_{i\eta+1} K_{i\eta-1} - K_{i\eta}^2 + \frac{1}{\varepsilon_0}\left(K_{i\eta}\left(\frac{\partial K_\mu'}{\partial\mu}\right)_{\mu=i\eta} - K_{i\eta}'\left(\frac{\partial K_\mu}{\partial\mu}\right)_{\mu=i\eta}\right)\right]\right\},$$ (2.7.14)

where all K's are functions of $\xi = \varepsilon_0 \eta$. In the nonrelativistic limit $\beta = v/c \to 0$, $\varepsilon_0 \to 1$, and we obtain

$$n_{E1} = -\frac{2}{\pi}\, Z_1^2 \alpha \zeta\, e^{-\pi\zeta} \left(\frac{c}{v}\right)^2 K_{i\zeta}(\zeta)\, K_{i\zeta}'(\zeta)\,.$$ (2.7.15a)

In the relativistic limit $\beta \to 1$, $\varepsilon_0 \simeq R/a \to \infty$ and $\eta = \zeta/\gamma \to 0$, so that

$$n_{E1}(\omega) = \frac{2}{\pi}\, Z_1^2 \alpha \left(\frac{c}{v}\right)^2 \left[\xi K_0 K_1 - \frac{v^2\xi^2}{2c^2}\, (K_1^2 - K_0^2)\right],$$ (2.7.15b)

where the K's are functions of $\xi = \varepsilon_0 \eta \simeq \omega R/\gamma v$.

Of course, both expressions (2.7.15) agree with the known results of previous calculations (see eq. (2.5.5a) and ref. [Al-75, p. 96]). But, besides reproducing the nonrelativistic and the relativistic limits, eqs. (2.7.10) and (2.7.14) might be useful for intermediate energy problems.

Unfortunately, for the other multipolarities it is not possible to calculate the nonrelativistic functions $df_{\pi l}(\theta, \zeta)$ in an analytical form. But we can correct the equivalent photon numbers in the relativistic case to obtain approximate expressions for the angular distribution in intermediate energy problems, by making the same substitutions which lead to eq. (2.7.10) (disregarding the effects of the imaginary indices). We obtain

$$\frac{dn_{E2}}{d\Omega} = \frac{Z_1^2 \alpha}{4\pi^2} \left(\frac{c}{v}\right)^4 \varepsilon^2 e^{-\pi\eta} \left\{\frac{4}{\gamma^2} [K_1^2 + xK_0K_1 + x^2K_0^2] + x^2\left(2 - \frac{v^2}{c^2}\right)^2 K_1^2\right\}, \tag{2.7.16a}$$

with all K's as functions of $x = \eta\varepsilon$, and

$$\frac{dn_{M1}}{d\Omega} = \frac{Z_1^2 \alpha}{4\pi^2} \eta^2 \varepsilon^4 e^{-\pi\eta} K_1^2(x). \tag{2.7.16b}$$

In fig. 2.4 we plot the ratio between the exact nonrelativistic equivalent photon numbers, defined by eq. (2.7.2) in terms of the functions $df_{\pi l}(\theta, \zeta)$, and eqs. (2.7.16) for $\gamma \simeq 1$, that is

$$r_i(\theta, \zeta) = [\text{eq. (2.7.2)/eq. (2.7.16)}], \tag{2.7.17}$$

where $i = 1$ for the E2 case (solid line) and $i = 2$ for the M1 case (dashed line). We observe that for very forward angles, and $\gamma \simeq 1$, the expressions (2.7.16a, b) give the same values as the exact nonrelativistic calculations. Indeed, it can be shown that for very forward scattering angles all the functions $df_{\pi l}(\theta, \zeta)$ can be expressed in terms of the modified Bessel functions [see Al-66, p. 483, and also the appendix of Wi-79], which when inserted in eq. (2.7.2) will reproduce eq. (2.7.16) for $\gamma \simeq 1$. As the scattering angle increases, there will be deviations of eq. (2.7.16) from the exact values of eq. (2.7.2), specially for the M1 case which depends more strongly on the bending of the Rutherford trajectories. But, for $\zeta \ll 1$, the agreement between the two calculations is very good, which make expressions (2.7.16a, b) useful
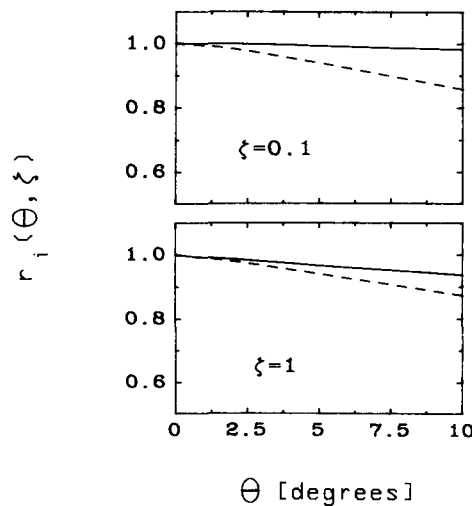

Fig. 2.4. Ratio of the exact nonrelativistic equivalent photon numbers given by eq. (2.7.2) and the approximate expressions (2.7.16), for $\gamma \simeq 1$, and for the E2 (solid curves) and M1 (dashed curves) multipolarities.

approximations for intermediate energy Coulomb excitation problems. For example, these ideas have been considered by Baur, Bertulani and Rebel [Ba-86c] for the study of Coulomb dissociation cross sections as a source of information on radiative capture processes of astrophysical interest. The integration of (2.7.16) over the scattering angle can be performed in the same way as in eq. (2.7.12).

We observe that, for $E \gg E_B$, a simpler recoil correction of the equivalent photon numbers as given by eqs. (2.5.5) is a rescaling of the minimum impact parameter of the form

$$R \rightarrow R + (\pi/2)a , \tag{2.7.18a}$$

where the factor $\pi/2$ can be obtained in a detailed analysis of the effects of the rescaling of the minimum impact parameter. Such a rescaling correction has indeed been observed by Winther and Alder [Wi-79] and later confirmed by the numerical calculations of Goldberg [Go-84]. For each impact parameter separately there will be a rescaling of the form (2.7.18a), i.e. for $\theta \ll 1$

$$x = \frac{\varepsilon \zeta}{\gamma} \cos(\theta/2) \rightarrow \frac{\omega}{\gamma v} \left(b + \frac{\pi}{2} a \right) . \tag{2.7.18b}$$

These corrections can be understood as following: the effects of the electromagnetic field are larger when the ions are closer together, but the closest distance will also be bigger than the initial impact parameter due to the Rutherford bending of the trajectory, and that is the reason for the rescaling (2.7.18b).

3. Electromagnetic fragmentation in RHI collisions

In the preceding section a complete description of the theory of relativistic Coulomb excitation was presented. In this section we shall apply this theory in the analysis of the Coulomb fragmentation of heavy ions in relativistic collisions. The first experimental hint for the possibility of existence of such processes was obtained in cosmic rays experiments by Balasubrahmanyan et al. [Ba-72]. They studied the absorption of carbon and oxygen nuclei in tungsten from 1 GeV/nucleon up to about 10 GeV/nucleon and obtained decreasing absorption lengths with increasing energies. Artru and Yodh [Art-72] were the first who suggested that Coulomb (electromagnetic) fragmentation could explain these phenomena, and made predictions about the Coulomb cross sections in the equivalent photon method. The first laboratory experiment which clearly confirmed the existence of an appreciable electromagnetic fragmentation in RHI collisions was reported by Heckman and Lindstrom [He-76]. Subsequently, electromagnetic fragmentation was observed by several other experiments [see e.g. We-79, Ol-81, Me-84, and Me-86]. A theoretical analysis of this process has been performed by Baur and Bertulani [Ber-86b, Ba-86a and Ba-86b].

In section 3.1 we will make an analysis of the experimental data of Mercier et al. [Me-84, Me-86], and introduce a harmonic vibrator model for the nuclei in order to obtain an illustrative way of describing the fragmentation problem. It is remarkable that classical, semiclassical and quantum descriptions of the process give approximately the same results. In particular, we show that, by using simple sum rules, the experimental data can be well explained. Of course, a more detailed consideration of the nuclear structure will be necessary in a more specific analysis of each reaction.

In section 3.2 we will study the consequences of a possible *multiple excitation* of giant resonances in the nuclei, and make some predictions based on the harmonic vibrator model.

In section 3.3 we will make a short analysis of the cross sections for *production of pions*.

The coincidence experiments for the *dissociation of weakly bound nuclei* are of great interest for the study of nuclear structure of, e.g., neutron-rich nuclei, and in section 3.4 we will make a study of the angular distributions of the fragments, and of the dependence of the cross sections on the reaction parameters.

3.1. Excitation of giant resonances

3.1.1. Coulomb and nuclear fragmentation in peripheral collisions

The passage of a particle with charge Z_1e, velocity v and impact parameter b (larger than the nuclear interaction radius) along a nucleus initially at rest will predominantly cause a momentum change of the charged constituents of the nucleus, i.e. the protons. This momentum is larger in the x-direction (perpendicular to the projectile's motion), and is given classically by [see e.g. Ja-75, p. 619]

$$\Delta p = 2Z_1Z_2e^2/bv . \tag{3.1.1}$$

From this we calculate the energy transferred to the nucleus as a whole as

$$\Delta E_A = \frac{(\Delta p)^2}{2m_A} = \frac{2(Z_1Z_2e^2)^2}{A_2 m_N b^2 v^2} , \tag{3.1.2}$$

where m_N is the nucleon mass. For very fast collisions we can assume the protons to move almost freely; the total amount of energy transferred to all protons being

$$\Delta E_Z = 2(Z_1e^2)^2 Z_2/m_N b^2 v^2 . \tag{3.1.3}$$

The difference gives the internal excitation energy of the nucleus

$$\Delta E_{int} = \Delta E_Z - \Delta E_A = \frac{2N_2Z_2}{A_2} \frac{(Z_1^2 e^2)^2}{m_N b^2 v^2} . \tag{3.1.4}$$

(This amounts to giving effective charges of Ne/A for protons and $(-Ze/A)$ for neutrons, respectively.) If the incident particle is also a nucleus, the same eq. (3.1.4) can be used for the determination of the internal excitation energy of it by exchanging the indices 1 and 2. As an example, we consider the case of relativistic $(v \simeq c)$ ^{238}U + ^{238}U collisions with $b = 15$ fm. We obtain

$$\Delta E_A \simeq 5 \text{ MeV} , \qquad \Delta E_Z \simeq 15 \text{ MeV} , \qquad \Delta E_{int} \simeq 10 \text{ MeV} .$$

This internal excitation energy corresponds to about the excitation energy of the giant dipole and quadrupole resonances in ^{238}U. From this simple classical estimate we can already deduce that there is a large probability for the excitation of giant resonances in peripheral RHI collisions. Since the giant resonances mainly decay by particle emission, this process will have an appreciable contribution to the fragmentation of the nuclei.

Indeed, among others, a group of experimentalists of the Lawrence Berkeley Laboratory and Iowa State University [Me-84, Me-86] have presented clear evidence of Coulomb fragmentation in RHI collisions. In those experiments one obtained the cross sections for *one-neutron removal* of ^{59}Co, ^{89}Y, and ^{197}Au targets due to the irradiation by relativistic beams of ^{1}H, ^{12}C, ^{20}Ne (2.1 GeV/nucleon), ^{40}Ar (1.8 GeV/nucleon) and ^{56}Fe (1.7 GeV/nucleon). From the data on fragmentation cross sections of the same targets by means of relativistic proton beams (for which Coulomb effects are negligible) they were able to deduce the nuclear contribution to the one-neutron removal cross sections by RHI beams. An example of their results is shown in fig. 3.1 which gives the cross section of one-neutron removal from ^{197}Au as a function of the atomic number of the incident projectile. One observes that the cross section increases with Z_2^2, which is a characteristic of Coulomb processes. A precise theoretical explanation of the experimental results is complicated by the presence of the nuclear contribution (shown in fig. 3.1 by the lower dashed curve) which can arise from a direct knockout of the neutrons or by means of a two-step process involving first the excitation of a giant resonance in the nuclei followed by the emission of one neutron. The nuclear contribution to this process is peaked at a certain impact parameter and falls down with increasing distances. It also falls down when the nuclei come closer together since other channels than the one-neutron removal process become more important [see e.g. Hü-81 or Hu-85]. In this way one can reasonably assume that the probability to remove one-neutron by means of the nuclear interaction in a RHI collision is given by a Gaussian function of the impact parameter b, such as

$$P(b) = \beta \exp\left[-\left(\frac{b-R}{\delta}\right)^2\right], \tag{3.1.5}$$

where 2δ is the thickness of the surface area contributing to that process and β is the maximum probability at an optimal impact parameter which, for simplicity, we set to the *touching distance* of the two nuclei
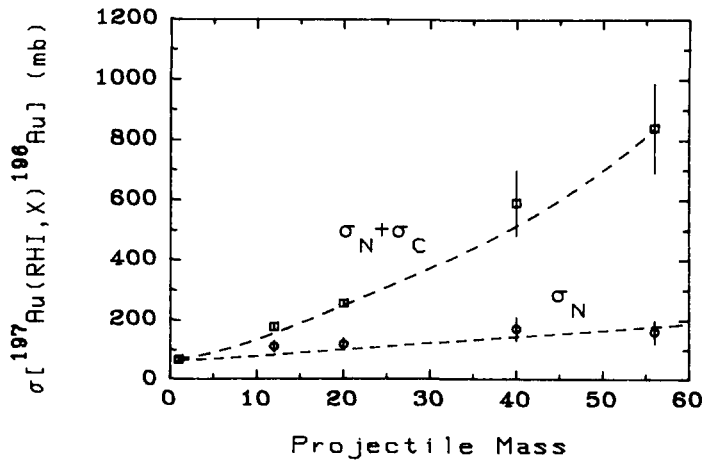
Fig. 3.1. One-neutron removal cross section of ^{197}Au by means of relativistic heavy ions as a function of the atomic number of the projectile. The squares are the total experimental cross sections. The circles represent the nuclear contribution to the cross section. The lower dashed curve is a fit of the form $a(1 + bA_1^{2/3})$, and the upper dashed curve is the sum of the experimental nuclear cross sections σ_N and the estimates σ_C based on the equivalent photon method.

$$R = R_1 + R_2 = 1.2 \times (A_1^{1/3} + A_2^{1/3}) \, \text{fm} .$$ (3.1.6)

Such a parametrization has also been found in theoretical calculations of fragmentation processes at nonrelativistic energies [see e.g. Ba-84a]. A justification of this surface peaked form can also be given in terms of a Glauber' model [see, e.g., Hü-81 and Hu-85]. The cross section will be

$$\sigma_{\text{N}} = 2\pi \int_0^\infty b \, P(b) \, \text{d}b \simeq 2(\pi)^{3/2} R\beta\delta .$$ (3.1.7)

In order to have an estimate of $\beta\delta$ we set the cross section given by eq. (3.1.7) to the experimental values determined by Mercier et al. [Me-86]. We find the values of $\beta\delta$ as given in table 3.1, which are collected in fig. 3.2 as a function of $A_1 + A_2$. From that one infers an average value of

$$\beta\delta \simeq (1.1 \pm 0.1) \, \text{fm} .$$ (3.1.8)

The question now arises about what the value of the maximum probability β should be. Clearly, there are other channels for fragmentation, like e.g. fission, two-nucleon removal, etc., in the peripheral collisions with small nuclear contact. Rasmussen, Canto and Qiu [Ra-86] have shown that there is an

Table 3.1
The thickness parameters $\beta\delta$, in fm, extracted from the experimental results of Mercier et al. [Me-86] for various projectiles and targets combinations used in these experiments

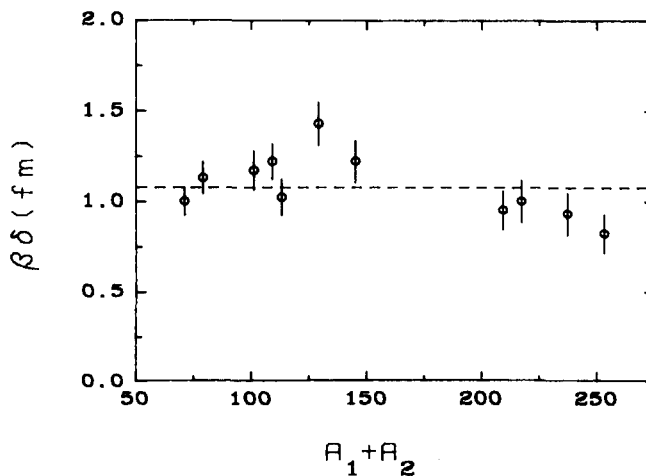| RHI	^{59}Co(RHI, X) ^{58}Co	^{89}Y(RHI, X) ^{88}Y	^{197}Au(RHI, X) ^{196}Au
^{12}C (2.1 GeV/nucleon)	1.00 ± 0.08	1.17 ± 0.11	0.95 ± 0.11
^{20}Ne (2.1 GeV/nucleon)	1.13 ± 0.09	1.22 ± 0.1	1.00 ± 0.12
^{40}Ar (1.8 GeV/nucleon)	—	1.43 ± 0.12	0.93 ± 0.12
^{56}Fe (1.7 GeV/nucleon)	1.02 ± 0.1	1.22 ± 0.12	0.82 ± 0.11

Fig. 3.2. Thickness $\beta\delta$ of the ring area contributing to the one-neutron removal cross section in peripheral RHI collisions as a function of the sum of the target and projectile mass number $A_1 + A_2$.

appreciable contribution to the fission channel in ^{238}U projectiles (1 GeV/nucleon) incident on nuclear emulsion. But, since the energy deposit in such collisions is small, the one-neutron removal process must be of greatest probability in most cases. If we use $\beta \approx 1$, we get $\delta \approx 1$ fm from eq. (3.1.8). This means that the nuclear contribution is restricted within a small range of impact parameters in comparison to a much wider interval for the Coulomb contribution to the same process. In spite of the smaller energy deposit by means of the Coulomb interaction in a RHI collision, its long range leads to total cross sections which can be even larger than the geometrical cross section.

The Coulomb contribution to the nuclear fragmentation in RHI collisions is a two-step process involving the excitation of the giant resonances followed by particle decay. The cross section for it can be calculated according to eq. (2.5.2). While, normally, the $\pi l = E1$ contribution to the sum (2.5.3b) is much larger than the others, the fact that $n_{E2} \gg n_{E1}$ for beam energies around 1 GeV/nucleon leads to an appreciable contribution (5–20%) of the quadrupole multipolarity to the total Coulomb cross section (2.5.2) at these energies. It is interesting to compare the experimental values of Mercier et al. [Me-86] with theoretical predictions based on eq. (2.5.2) and on sum rules for the photonuclear cross sections.

It is well known that heavy nuclei exhibit an electric dipole resonance at approximately

$$E_{GR}^{(1)} = 80/A^{1/3} \text{ MeV}$$ (3.1.9a)

and a quadrupole resonance at

$$E_{GR}^{(2)} = 62/A^{1/3} \text{ MeV} .$$ (3.1.9b)

To a good approximation we can take the factors $n_{E1}(\omega)$ and $n_{E2}(\omega)$ outside the integrals in eq. (2.5.2)

$$\sigma_C \simeq \frac{n_{E1}[E_{GR}^{(1)}]}{E_{GR}^{(1)}} \int \sigma_\gamma^{E1}(E_\gamma) \, dE_\gamma + n_{E2}[E_{GR}^{(2)}] \, E_{GR}^{(2)} \int \frac{\sigma_\gamma^{E2}(E_\gamma) \, dE_\gamma}{(E_\gamma)^2}$$ (3.1.10)

and make use of the Thomas–Reiche–Kuhn (TRK) sum rule for the electric dipole resonance [see e.g. Bo-75]

$$\int \sigma_\gamma^{E1}(E_\gamma) \, dE_\gamma \simeq 60NZ/A \text{ MeV mb} ,$$ (3.1.11a)

and the energy weighted sum rule for the electric quadrupole resonance

$$\int \sigma_\gamma^{E2}(E_\gamma)/(E_\gamma)^2 \, dE_\gamma \simeq 0.22 \, ZA^{2/3} \, \mu\text{b MeV}^{-1} .$$ (3.1.11b)

In addition to the E2 isoscalar resonance, there exists also an isovector E2 resonance at an even higher energy of about $E_{GR}^{E2} \simeq 120 \text{ MeV}/A^{1/3}$. Since it decays mainly by two-neutron emission, it will not contribute much to the one-neutron removal experiment discussed here.

Within these approximations the dependence of the Coulomb excitation cross sections σ_C on the energy of the projectile E_{lab} is due to the dependence of n_{E1} and n_{E2} on that parameter. As an example, in fig. 3.3 we plotted the Coulomb fragmentation cross section of ^{40}Ca projectiles incident on ^{238}U
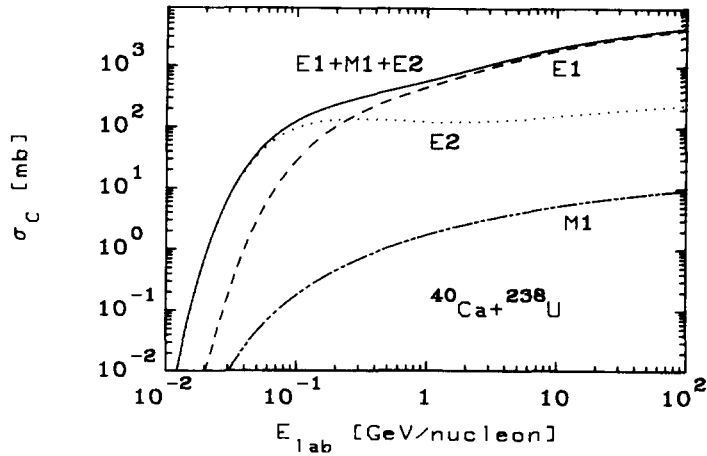
Fig. 3.3. Coulomb excitation cross section of giant resonances in ^{40}Ca projectiles hitting a ^{238}U target as a function of the laboratory energy per nucleon. The dashed line corresponds to the excitation of the giant electric dipole resonance, the dotted to the electric quadrupole, and the lower line to the magnetic dipole. The solid curve is the sum of these contributions.

targets as a function of the laboratory energy per nucleon. We use eq. (2.5.5) with the recoil correction $R \rightarrow R + \pi a/2$ (see section 2.7), which will only be important for $E_{lab}/A \lesssim 100$ MeV. We also used the fact that ^{40}Ca has a giant M1 resonance at $E_{GR}^{M1} \simeq 10.3$ MeV and a B-value of order $B(M1) \simeq 1 \ \mu_N^2$, to calculate the contribution of the M1-mode to the Coulomb fragmentation cross section. The lower curve corresponds to the M1 fragmentation mode, the dashed line to the E1 mode, and the dotted line to the E2 one. The solid line is the sum of the three contributions. We note that the Coulomb excitation cross section overcomes the geometrical cross section $\sigma_G = \pi(R_1 + R_2)^2$ for very high energies. One also observes that the E2 fragmentation mode is very important at intermediate energies (around some hundreds of MeV/nucleon) and even for very high energies it can account for approximately 10% of σ_C. Indeed, since for high energies $n_{E2} \simeq n_{E1}$, the cross section for the E2 excitation mode will be smaller than that for the E1 case by the relative strength of the two giant resonances $\sigma^{E2}/\sigma^{E1} \simeq Z\omega_1\omega_2 R^2/6Nc^2 \simeq 0.12$, where ω_1 (ω_2) are the frequencies of the giant dipole (quadrupole) resonance. The excitation of giant magnetic dipole resonances in RHI collisions is of less importance, since for low energies $n_{M1} \ll n_{E1}$ ($n_{M1} \simeq (v/c)^2 n_{E1}$), and for high energies, where $n_{M1} \simeq n_{E1}$, it will be smaller than the excitation of electric dipole resonances by the relative strength $\sigma^{M1}/\sigma^{E1} \simeq (\mu_N/eR)^2 = (\hbar/2m_N cR)^2 \ll 1$.

Table 3.2 shows the theoretical values based on eqs. (3.1.9–3.1.11) for the reactions studied by

Table 3.2

Theoretical electromagnetic excitation cross sections of E1 and E2 giant resonances for various projectile and target combinations. The incident projectile energy is given in parentheses and the cross sections are given in mb

RHI	^{59}Co(RHI, X) ^{58}Co		^{89}Y(RHI, X) ^{88}Y		^{197}Au(RHI, X) ^{196}Au	
	E1	E2	E1	E2	E1	E2
^{12}C (2.1 GeV/nucleon)	8.7	1.88	15.5	3.39	46.5	10.3
^{20}Ne (2.1 GeV/nucleon)	22.9	4.65	41.1	8.45	124	26.2
^{40}Ar (1.8 GeV/nucleon)	63.0	12.7	114	23.4	354	74.6
^{56}Fe (1.7 GeV/nucleon)	121	24.2	221	45	694	145

Mercier et al. One clearly sees the relevance of the E2 mode as compared to E1. From the ratio between the experimental data and the theoretical predictions,

$$r = \frac{\sigma_C^{exp}}{\sigma_C^{E1} + \sigma_C^{E2}} \equiv \frac{\sigma^{exp}}{\sigma_{SR}} ,$$

(3.1.12)

we obtain the values gathered in fig. 3.4 as a function of $A_1 + A_2$. On the average, $r \lesssim 1$, which is a reasonable result since σ_{SR} includes the total strength of the giant resonances which can decay not only by means of one-neutron emission. In principle, one could also use the experimental photonuclear cross sections $\sigma(\gamma, n)$ to do a more exact calculation of the one-neutron removal cross section by means of eq. (2.5.2) [see e.g. He-76]. However, the decomposition of $\sigma(\gamma, n)$ into E1 and E2 (or other) multipolarities is not exactly known.

The only empirical parameter entering in eq. (2.5.2) is the minimum impact parameter which we set to R as given by eq. (3.1.6). For impact parameters in the interval $R - \delta \leqslant b \leqslant R + \delta$ there is interference between the nuclear and the Coulomb interaction. By using $b_{min} = R - \delta$ in eq. (3.1.10) the theoretically estimated Coulomb cross sections increase by less than 10%. Because of our lack of knowledge of the nuclear and Coulomb interference effects, there exists even a greater uncertainty in the theoretical determination of the induced cross section in peripheral RHI collisions. The situation becomes simpler at higher energies and when both projectile and target are heavy nuclei, for which the Coulomb cross sections depend much less on the uncertainty in the minimum impact parameter. In that case the Coulomb interaction leads to much greater cross sections than the nuclear interaction and for practical purposes one can disregard the nuclear contributions in peripheral RHI collisions.

A semi-empirical *black sphere* expression for the reaction cross sections in RHI collisions, introduced by Bradt and Peters [Br-50], and extensively used in the literature, is

$$\sigma_R = \pi r_0^2 (A_1^{1/3} + A_2^{1/3} + \Delta)^2 ,$$

(3.1.13)

where $r_0 \simeq 1.2$ fm. The *overlap parameter* Δ is meant to represent the diffuseness and partial trans-
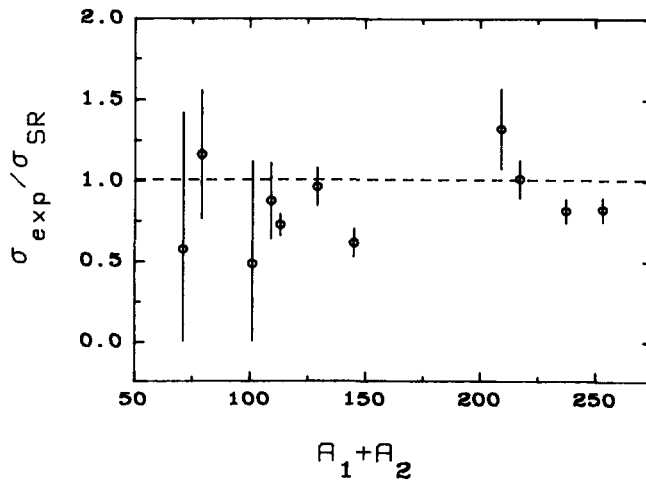

Fig. 3.4. The ratio of the experimentally determined Coulomb excitation cross section σ_{exp} and the theoretical σ_{SR} value, as derived from the sum rule model, as a function of the sum of the target and projectile mass numbers $A_1 + A_2$.

parency of the nuclear surfaces. Nevertheless, it has been already shown [see e.g. Gr-85] that the fit of expressions like eq. (3.1.13) with very high energy experiments are quite poor. This has also been the object of a theoretical analysis in ref. [Ber-86c]. The overprediction at low projectile and/or target masses is thought to be due to nuclear transparency effects and the underprediction at larger masses might be explained by the addition of Coulomb processes. In fact, since the Coulomb fragmentation cross sections increase approximately logarithmically with energy, there can be no parametrization of the reaction cross sections as implied by eq. (3.1.13) for sufficiently high energies.

As we have seen, there is a satisfactory agreement at the present stage between theory and experiment. The experiments are and will be going on at Brookhaven, CERN and SIS (Darmstadt). Many more accurate data will become available and perhaps need a further refined theoretical treatment. An interesting possibility of further experimental improvements is the Projectile Fragment Separator at SIS [Ge-87]. The production of relativistic radioactive beams (e.g. ^{19}Ne, a β^+ emitter) from a ^{20}Ne projectile, to be studied in Darmstadt can be useful for radiation biophysics [Ge-87].

Recently, Canto et al. [Ca-87] have analysed theoretically the so-called *clean fission* experiment of 0.2 TeV uranium beams on nuclear emulsion. The experiments have been performed by Friedlander et al. [Fr-83] and Jain et al. [Ja-84], which classified the reactions into *dirty* or *clean* fission, according to whether fission is or is not, respectively, accompanied by other tracks. It is, in principle, expected that the relativistic Coulomb excitation of the projectile would be of great relevance for the total reaction cross section for clean fission, which must be originated in the peripheral collisions. Nevertheless, they found that even with the inclusion of the nuclear contribution, the available theories are not able to explain the high values of the cross sections. A possible explanation is proposed by Galetti, Kodama and Nemes [Ga-87], who claim that a covariant study of the theory of Coulomb excitation, together with recoil effects can be a hint to explain not only the cross sections, but also the angular distribution of the fragments. We indicate the above references for a discussion of these experiments and theoretical problems.

3.1.2. Harmonic vibrator model

The internal excitation energy of a nucleus by means of a relativistic charged particle as given by eq. (3.1.4) does not take into account the binding energy of the nucleons. But we can account for it very easily if we use the *harmonic vibrator model* for the nucleus. The energy transferred to a harmonically bound particle, with charge e_i and mass M_i, by a relativistic particle with charge $Z_1 e$ is given by [see Ja-75, p. 623]

$$\Delta E_i(b) = 2Z_1^2 e^2 \left(\frac{e_i^2}{M_i} \right) \frac{1}{v^2 b^2} x^2 \left[K_1^2 + \frac{1}{\gamma^2} K_0^2 \right], \tag{3.1.14}$$

where the modified Bessel functions are functions of $x = \omega b / \gamma v$.

We now apply this result to the excitation of giant dipole resonances (GDR) in nuclei. In this case we assume that all nucleons vibrate with the same frequency $\omega = E_{GDR} \equiv E_{GR}^{(1)}$ and, to disregard the centre of mass motion, we use the effective charge of a nucleon as $(e_i)_{eff} = Ne/A$ for protons and $(e_i)_{eff} = -(Ze/A)$ for neutrons. Summing for all nucleons

$$\sum_i \left(\frac{e_i^2}{M_i} \right) = \frac{e^2}{m_N} \left[\sum_{i=1}^{Z} \left(\frac{N}{A} \right)^2 + \sum_{i=Z+1}^{A} \left(\frac{Z}{A} \right)^2 \right] = \frac{NZ}{A} \frac{e^2}{m_N}, \tag{3.1.15}$$

we obtain

$$\Delta E(b) = \sum_i \Delta E_i(b) = \frac{2[E_{GDR}]^2}{m_N c^2} \, \alpha^2 \, \frac{Z_1^2 N_2 Z_2}{A_2} \left(\frac{c}{v}\right)^4 \frac{1}{\gamma^2} \left[K_1^2 + \frac{1}{\gamma^2} \, K_0^2 \right].$$ (3.1.16)

One can easily verify that eq. (3.1.16) reduces to eq. (3.1.4) in the limit $x = \omega b/\gamma v \ll 1$, corresponding to the low-frequency limit. In this limit the interaction is so sudden that the binding energy of the nucleons is unimportant and they can be considered as free.

One can also interpret $\Delta E(b)/E_{GDR}$ as the probability $\Phi(b)$ of exciting a GDR in a collision with impact parameter b, i.e.,

$$\Phi(b) = \frac{2E_{GDR}}{m_N c^2} \, \alpha^2 \, \frac{Z_1^2 N_2 Z_2}{A_2} \left(\frac{c}{v}\right)^4 \frac{1}{\gamma^2} \left[K_1^2 + \frac{1}{\gamma^2} \, K_0^2 \right].$$ (3.1.17)

By taking $E_{GDR} = 80 \, \text{MeV}/A^{1/3}$, we obtain

$$\Phi(b) = a_0^2 + a_1^2 + a_{-1}^2,$$ (3.1.18a)

where

$$a_0 = 0.41\alpha \, \frac{Z_1 \sqrt{N_2 Z_2}}{A_2^{2/3}} \left(\frac{c}{\gamma v}\right)^2 K_0(x)$$ (3.1.18b)

and

$$a_1 = 0.29\alpha \, \frac{Z_1 \sqrt{N_2 Z_2}}{A_2^{2/3}} \left(\frac{c}{v}\right)^2 \frac{1}{\gamma} \, K_1(x).$$ (3.1.18c)

We can also calculate these excitation amplitudes by using the eq. (2.1.15) and the TRK sum rule to evaluate the matrix elements for the excitation of GDR states [see Ber-86b, Ba-86a, Ba-86b]. The result
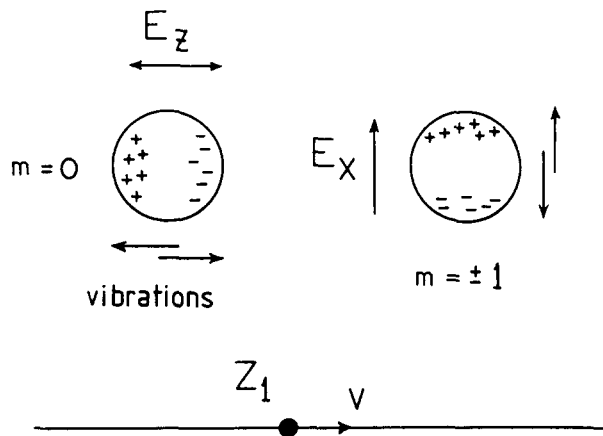

Fig. 3.5. Proton and neutron vibrations induced by the passage of a relativistic heavy ion.

will be exactly the same as that obtained above by means of a purely classical derivation. This indicates that $a_m = |a_{fi}^m|$ is the probability of exciting a nucleus by transferring to it an amount $m\hbar$ of angular momentum in the beam direction. Classically the amplitude a_0 corresponds to the action of the electric field E_z (see fig. 3.5) which generates vibrations along the beam direction. These vibrations correspond to an angular momentum perpendicular to the beam direction, i.e. $m = 0$. The field E_x will generate $m = \pm 1$ vibrations and the excitation probability, by symmetry, must be equally distributed between $m = -1$ and $m = +1$. Since E_x dominates for $\gamma \gg 1$, the target (or the projectile) will gain essentially internal vibrations perpendicular to the beam direction in that limit.

3.1.3. Angular distribution of the fragments

From the dynamics of the electromagnetic excitation process, the angular distribution of the fragments can be directly calculated. For the sake of simplicity of presentation, we illustrate the essential points for spinless projectiles and fragments. We consider the projectile fragmentation process $A \rightarrow B + C$ in the system of reference of the projectile. The transition from the projectile's ground state

$$\psi_i = (1/r) \, f(r) \, Y_{00}(\hat{r}) \, , \tag{3.1.19}$$

described by a $B + C$ cluster wave function, to the final state, characterised by the relative momentum k_f, given by the wave function

$$\psi_f = \frac{1}{r} \sum_{lm} Y_{lm}^*(\hat{r}) \, Y_{lm}(\hat{k}_f) \, g_l(r, k_f) \, , \tag{3.1.20}$$

is determined by the excitation amplitude

$$a_{fi} = \frac{2Z_2 e^2}{\hbar b v} \, x \left[K_1(x) \, D_{fi}^x + \frac{i}{\gamma} \, K_0(x) \, D_{fi}^z \right] , \tag{3.1.21}$$

where the K's are functions of $x = \omega b / \gamma v$. The x- and z-components of the nuclear dipole matrix elements are denoted by D_{fi}^x and D_{fi}^z, respectively. As usual, these matrix elements can be separated into a geometrical part determined entirely by the angular momentum quantum numbers and an overall strength factor, which gives the $B(E1)$-value (in the simplified model given here it is determined by the radial dipole matrix element $R(k_f) = \int dr \, g_{l=1}(r, k_f) \, r \, f(r)$). One finds for a_{fi}

$$a_{fi} = \frac{2Z_2 e^2}{\hbar b v} \, x \left[(-\sin\theta \cos\phi) \, K_1(x) + \frac{i}{\gamma} \cos\theta \, K_0(x) \right] \frac{R(k_f)}{\sqrt{4\pi}} \, , \tag{3.1.22}$$

where θ and ϕ denote the polar angles of $\hat{k}_f$. As we saw before, the $m = \pm 1$ excitations are proportional to first term, the $m = 0$ one to the second term. For $\omega b / \gamma v \ll 1$ this leads to a very strong alignment of the final fragment state, as has already been seen above (cf. fig. 3.5). Because of the phase difference there is no interference of the $m = \pm 1$ and $m = 0$ excitations for the angular distributions. Averaging over the azimuthal angle ϕ, one obtains

$$|a_{fi}|^2 = \frac{Z_2^2 \alpha^2}{\pi} \left(\frac{\omega}{c}\right)^2 \left(\frac{c}{v}\right)^4 [R(k_f)]^2 \left[K_1^2(x) \sin^2\theta + \frac{1}{\gamma^2} \, K_0^2(x) \cos^2\theta \right] , \tag{3.1.23}$$

i.e., for $\omega b \gamma v \ll 1$, as will usually be the case, there is a strong tendency of emission perpendicular to the beam axis.

Let us compare the momentum of the fragment obtained from the decay of the excited resonance state to the momentum obtained from the Coulomb repulsion of the whole projectile during the collision. The momentum due to the Coulomb repulsion is perpendicular to the beam and is given by eq. (3.1.1). The momentum due to the decay of the resonant state is given by

$$\Delta p_{\rm d} = \sqrt{2m_0 \, \Delta E_{\rm d}} \, ,$$

where $\Delta E_{\rm d}$ is the decay energy and m_0 is the reduced mass of $B + C$. As seen above, the main component of $\Delta p_{\rm d}$ is also perpendicular to the beam axis. As an example, for $Z_2 = 92$, $Z_1 = 8$, $b = 15$ fm, and $v \simeq c$, we obtain from eq. (3.1.1) $\Delta p \simeq 150$ MeV/c for the momentum due to the Coulomb repulsion of the projectile. If we assume a decay energy of $\Delta E_{\rm d} \simeq 10$ MeV (i.e. excitation energy above the threshold for $A \rightarrow B + C$) and a reduced mass $m_0 \simeq 1$ GeV (which is about the reduced mass in the case of one-nucleon emission), then $\Delta p_{\rm d} \simeq 140$ MeV/c. Compared to the incident momentum

$$p_{\rm lab} \simeq E_{\rm lab}/c \simeq (\gamma - 1)A \text{ GeV}/c$$

the above quantities are only a small percent of it. This means that a study of the angular distribution of the fragments can only be achieved in very high precision measurements [see Br-85 and Em-87]. It is also proposed [Fi-87] to study γ- and particle decay of GDR of target nuclei in peripheral collisions at SIS.

3.2. Multiphonon excitation of giant dipole resonances

3.2.1. Failure of first order perturbation theory

Quantum-mechanically, the relation (3.1.17) is the result of a *first order perturbation theory*. In principle this is a good approximation since, roughly speaking, the Coulomb interaction time in a RHI collision is so short that one expects that at most one virtual photon can be exchanged. In the time-dependent perturbation theory this means that the excitation amplitudes must be much smaller than one to justify the use of a first order perturbation method. In fig. 3.6 we plot the values of a_0 and a_1, as given by eqs. (3.1.18b) and (3.1.18c), for the excitation of ^{16}O in the reaction ^{16}O + ^{208}Pb, and of ^{238}U in the reaction ^{238}U + ^{238}U, as a function of the laboratory energy per nucleon and in the case at which they could be as large as possible, namely, when the impact parameter b is equal to the sum of the two nuclear radii $R = R_1 + R_2$. We observe that in both cases a_0 decreases with increasing laboratory energy while a_1 reaches a constant value. This occurs because a_0 is equivalent to the excitation generated by a pulse of light in the direction perpendicular to the ion beam while a_1 is equivalent to the excitation due to another pulse in the beam direction (see section 1 and fig. 1.1). For high energies the first pulse becomes negligible and only the second one is important [see Ja-75, p. 719]. One also notes that the Coulomb excitation (mainly a_1) of light systems like ^{16}O by heavy ions has a small amplitude, while the same is not true for a heavy system like ^{238}U. We took the smallest possible impact parameter; for larger impact parameters the excitation amplitudes will diminish. Nevertheless, a study of the role of *multiple excitation* in RHI collisions is worthwhile, since the first order effects are so large. The possibility of multiple excitation in RHI collisions would also be of great experimental interest.
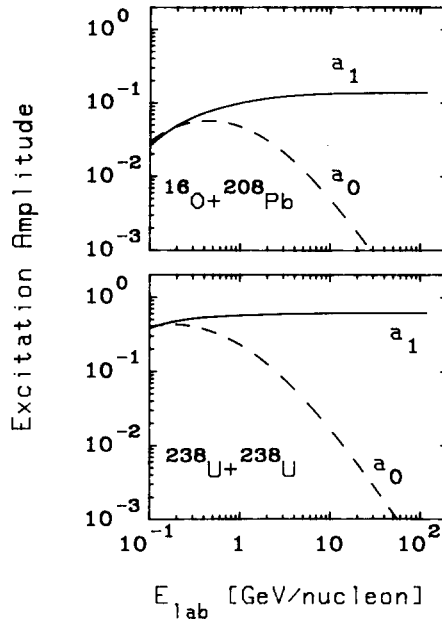
Fig. 3.6. Amplitudes for excitation of the giant electric dipole resonance in ^{16}O and ^{238}U relativistic projectiles hitting ^{208}Pb and ^{238}U targets, respectively, as a function of the laboratory energy per nucleon. The amplitude $a_{0(1)} = |a_{if}|_{m=0(1)}$ corresponds to an angular momentum transfer of zero (one) unit in the direction parallel to the beam from the relative motion of the target.

The problem of multiple excitation can be put in a tractable form if we use the simple harmonic vibrator model for the collective dipole oscillations in the nuclei. In the exact theory of multiple excitations of a quantum harmonic oscillator [see e.g. Me-70] one obtains a Poisson distribution for the excitation probability of a N-phonon state

$$P_N = \frac{1}{N!} \, \Phi^N \, e^{-\Phi} \, . \tag{3.2.1}$$

In our case, $\Phi(b)$ is given by eq. (3.1.17). This result can also be interpreted classically. The probability P_N to excite an oscillator by an energy amount $N\hbar\omega$ is equivalent to the probability to excite N uncoupled oscillators from a given ensemble, each by an energy amount $\hbar\omega$. In the limit that this ensemble possesses an infinite number of oscillators, P_N will be given by a Poisson distribution of the probability to excite only one oscillator [see e.g. Al-66, p. 269]. In the equivalent photon method one can use eq. (1.6), and assume that the probability for a nucleus to absorb N photons from the equivalent photon spectrum is given statistically by a Poisson distribution. This procedure will also give exactly the expression (3.2.1) with $\Phi(b)$ given by eq. (3.1.17), as mentioned by Braun-Munzinger et al. [Br-85].

One interesting feature is that, for the mean excitation energy, we obtain

$$\overline{\Delta E(b)} = \sum_N N\hbar\omega \, P_N(b) = \hbar\omega \, \Phi(b) \, . \tag{3.2.2}$$

This means that the energy transfer, calculated in first order perturbation theory, gives the correct

average value, even in the case where first order excitation calculations are not justified (e.g., if $\Phi(b) \gtrsim 1$). This is a special property of the harmonic oscillator model.

3.2.2. Ultrarelativistic limit

As quoted above, in the high energy limit $\gamma \gg 1$, $a_0 \ll a_{\pm 1}$, and a good approximation, as long as $b \lesssim \gamma c/\omega$, is

$$a_{\pm 1} = 0.29\alpha \, \frac{Z_1 \sqrt{N_2 Z_2}}{A_2^{2/3}} \, \frac{c}{\omega b} \, , \qquad a_0 = 0 \, , \tag{3.2.3}$$

and (3.2.1) becomes

$$P_N(b) \simeq \frac{1}{N!} \left(\frac{S}{b^2} \right)^N e^{-S/b^2} \, , \tag{3.2.4a}$$

where

$$S = 5.45 \times 10^{-5} \, \frac{Z_1^2 N_2 Z_2}{A_2^{2/3}} \, \text{fm}^2 \, . \tag{3.2.4b}$$

The total cross section is obtained by integrating over the impact parameter, starting from a minimum impact parameter $b_{\min} = R$, where the nuclear absorption sets in:

$$\sigma_C^{(N)} = 2\pi \int\limits_R^\infty b \, P_N(b) \, \mathrm{d}b \, . \tag{3.2.5}$$

If we use the approximation (3.2.4), then for $N = 1$ it is necessary to introduce the adiabatic cutoff radius $b_{\max} \simeq \gamma c/\omega$ (see eq. 1.7) in order to have a convergent integral. For $N \geq 2$ the excitation probability decreases fast enough to ensure convergence. We obtain

$$\sigma_C^{(N=1)} \simeq 2\pi S \ln(\gamma c/\omega R) \, , \tag{3.2.6a}$$

and

$$\sigma_C^{(N \geq 2)} \simeq \frac{\pi S}{N(N-1)} \left[1 - e^{-u} \sum_{k=0}^{N-2} \frac{u^k}{k!} \right] \simeq \frac{\pi S u^{N-1}}{N!(N-1)} \, , \tag{3.2.6b}$$

where $u = S/R^2$, and the last approximation is valid for $u \ll 1$, which is generally the case for light ions.

With these values, the maximum possible cross section $\sigma_C^{(N)}$ can be immediately calculated. The cross sections for the excitation of relativistic ^{16}O, ^{32}S and ^{238}U projectiles in the collision with ^{238}U targets are given in table 3.3. We also show in fig. 3.7 the N-phonon Coulomb fragmentation cross sections of ^{16}O projectiles incident on ^{238}U as a function of the laboratory energy per nucleon. The solid lines correspond to the use of eqs. (3.1.17), (3.1.18) and (3.2.1), and the dashed lines correspond to the approximations (3.2.6). As is expected from the increase of S with the mass, N-phonon states are excited with larger cross sections with increasing mass. On the other hand, the amplitude of the

Table 3.3
Ultrarelativistic limit of the total cross sections for
N-phonon GDR excitation of ^{16}O, ^{32}S and ^{238}U pro-
jectiles with ^{238}U as the target nucleus

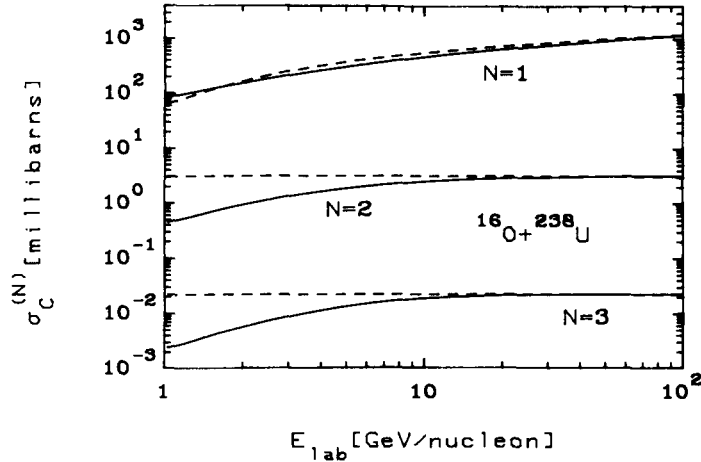|	^{16}O	^{32}S	^{238}U
$N = 2$	3.1 mb	17 mb	1.28 b
$N = 3$	22 μb	0.25 mb	0.14 b
$N = 4$	0.16 μb	4 μb	15 mb

Fig. 3.7. Total cross sections for the excitation of N-phonon GDR states in ^{16}O projectiles hitting ^{238}U targets as a function of the incident energy E_{lab}. The exact results are given by a continuous line; the dashed lines correspond to the approximations (3.2.6).

collective motion of all protons against all neutrons are larger for light nuclei than for heavier ones. This can be readily seen from the simple model adopted for the GDR. The dipole operator is given by

$$\hat{D} = \sum_{i=1}^{A} (\hat{\rho}_i - \hat{R}_{cm}) = (NZ/A)\hat{\rho} ,$$ (3.2.7)

where $\hat{R}_{cm}$ is the centre of mass and

$$\hat{\rho} = \frac{1}{Z} \sum_{i=1}^{Z} \hat{\rho}_i - \frac{1}{N} \sum_{i=Z+1}^{A} \hat{\rho}_i ,$$ (3.2.8)

is the difference between the centre of mass of all protons with respect to all neutrons. Assuming that the TRK sum rule is exhausted by the GDR, one obtains

$$D^2 \equiv |\langle \Psi_{GDR} | \hat{D} | \Psi_0 \rangle|^2 = \frac{NZ}{A} \left(\frac{\hbar^2}{2m_N} \right) \frac{1}{E_{GDR}} = 0.26 \frac{NZ}{A^{2/3}} \text{ fm}^2 .$$ (3.2.9)

In terms of the collective coordinate ρ, one has

$$\rho = (A/NZ)D = 0.51(A^{2/3}/\sqrt{NZ}) \text{ fm} .$$ (3.2.10)

It decreases like $A^{-1/3}$ with A. Thus neutrons and protons are more effectively separated in low-mass nuclei. However, the excitation cross sections are smaller. The average p–n separating distance over a period of vibration in a N-phonon state is $\rho^{(N)} = \sqrt{2N+1}\rho$. For ^{16}O one finds an average p–n separating distance in a GDR of about $\rho^{(1)} \simeq 0.7$ fm. It would be interesting to know about the response of the nuclear system to a $N \geq 2$ phonon state. For $N = 4$ we would obtain an average p–n separating distance of $\rho^{(4)} \simeq 1.2$ fm in ^{16}O, which is a quite high value, since this is an averaged quantity. Indeed, the excitation energy of such a state would be $E^{(N=4)} = 4E_{GDR} \simeq 127$ MeV which is exactly the energy necessary to separate all protons from all neutrons in ^{16}O. In the simple harmonic model, the maximum separating distance of the p–n vibrations, i.e. the amplitude of the vibration, is given by $d = \sqrt{2}\rho$, which implies that in a $N = 4$ state the protons and neutrons would separate beyond the range of the nuclear forces. Since the cross sections for the excitation of this state by means of the electromagnetic interaction in a RHI collision with a heavy target are of orders of millibarns this process could be of great importance for producing neutron-rich fragments.

The usual GDR is a one-phonon state of angular momentum l (assuming a spin zero nuclear ground state $|0\rangle$)

$$|1,1\mu\rangle = c_\mu^+|0\rangle , \qquad (3.2.11)$$

where c_μ^+ denotes the creation operator for a GDR phonon with angular momentum projection μ. The operators c_μ^+ and c_μ satisfy the usual boson commutation relations. The two-phonon states $|2,IM\rangle$, coupled to good angular momentum I, M with $I = 0$ and 2, are given explicitly by (see e.g. [Al-75, p. 197])

$$|2,IM\rangle = (1/\sqrt{2}) \sum_{\mu\mu'} \langle 1\mu 1\mu'|IM\rangle c_\mu^+ c_{\mu'}^+|0\rangle . \qquad (3.2.12)$$

These states are explicitly given by

$$|2,00\rangle = (1/\sqrt{6})(2c_1^+ c_{-1}^+ - c_0^+ c_0^+)|0\rangle = \sqrt{2/3}|1,0,1\rangle - (1/\sqrt{3})|0,2,0\rangle , \qquad (3.2.13a)$$

$$|2,20\rangle = (1/\sqrt{3})(c_0^+ c_0^+ + c_1^+ c_{-1}^+)|0\rangle = \sqrt{2/3}|0,2,0\rangle + (1/\sqrt{3})|1,0,1\rangle , \qquad (3.2.13b)$$

$$|2,21\rangle = c_1^+ c_0^+|0\rangle = |0,1,1\rangle , \qquad (3.2.13c)$$

$$|2,22\rangle = (1/\sqrt{2})c_1^+ c_1^+|0\rangle = |0,0,2\rangle , \qquad (3.2.13d)$$

and similarly for $M = -1$ and -2. Here we have introduced the uncoupled normalized states $|n_{-1}, n_0, n_1\rangle$, where n_μ denotes the number of phonons with angular momentum projection μ. Since for $\gamma \gg 1$ the $m = \pm 1$ excitation amplitude completely dominates over the $m = 0$ excitation, we can put $a_0 \simeq 0$, and $a_{\pm 1} = \chi$, to obtain the excitation probability $P_{n_{-1}n_0n_1}$ of the uncoupled states $|n_{-1}, n_0, n_1\rangle$ as

$$P_{101} = \chi^4 e^{-2\chi^2} , \qquad P_{002} = P_{200} = \tfrac{1}{2}\chi^4 e^{-2\chi^2} . \qquad (3.2.14a)$$

The other combinations give only a negligible contribution. From eq. (3.2.13) we obtain for the excitation probability $P_{2,IM}$ of the angular momentum coupled states $|2,IM\rangle$

$$P_{2,22} = P_{2,2-2} = \tfrac{1}{2}\chi^4 e^{-2\chi^2}, \qquad P_{2,21} = P_{2,2-1} = 0,$$

$$P_{2,20} = \tfrac{1}{3}\chi^4 e^{-2\chi^2}, \qquad P_{2,00} = \tfrac{2}{3}\chi^4 e^{-2\chi^2}.$$

(3.2.14b)

The total $N = 2$ excitation probability adds of course up to the value $P_{N=2}$ which has already been obtained above (eq. (3.2.1) with $2\chi^2 = \Phi$). From eqs. (3.2.14a) and (3.2.14b) we conclude that the ratio of excitation of 0^+ and 2^+ states is 1:2.

The possible signatures of the $N \geq 2$ phonon states remain a speculation, specially what the specific decay widths and decay channels will be, like the probability of formation of *polyneutrons* and other *exotic* phenomena. For more details about the possible experimental identification of these states, see the proposals of Braun-Munzinger et al. [Br-85] and of Emling et al. [Em-87]. The study of polyneutrons at SIS is proposed by Hilscher et al. [Hi-87]. Yet it is interesting and necessary to discuss the influence of damping of the GDR motion on the excitation process in more general terms.

3.2.3. The influence of damping: a dissipative quantum vibrator

The giant dipole state is a very short-lived state. Being high in the continuum, it couples strongly to other more complicated states and eventually decays, mainly statistically by particle (neutron) emission. A typical width of $\Gamma = 5$ MeV corresponds to a lifetime of $\tau_{\text{decay}} \simeq 10^{-22}$. The width of the N-phonon ($N \geq 2$) GDR states can be expected to be even larger. In a situation where the lifetime of a state is comparable or even smaller than the collision time, an essential modification of the usual description of Coulomb excitation has to be introduced. This was accomplished by Weidenmüller and Winther [We-71]. The nuclear states are divided into bound and continuum states, direct excitation of continuum states as well as continuum–continuum coupling is neglected. In this case, the usual coupled equations for the time dependent amplitudes $C_N(t)$ read

$$i\hbar \frac{dC_N(t)}{dt} = \sum_M \langle N|V(t)|M\rangle \, e^{i(E_N - E_M)t/\hbar} \, C_M(t) + \int_{-\infty}^{\infty} dt' \, K_N(t - t') \, C_N(t'),$$

(3.2.15)

where the function K_N takes the coupling to the more complicated channels into account (in our example, the N-phonon states are identified with the bound states of the nucleus; all the complicated decay channels of these states correspond to the continuum, which is assumed to be excited only via the GDR-doorway states). This function is given in terms of the width $\Gamma_N(E)$ by

$$K_N(t - t') = -\frac{i}{4\pi} \int_{-\infty}^{\infty} d\omega \, e^{i\omega(t - t')} \, \Gamma_N(\omega + E_N/\hbar).$$

(3.2.16)

For $\Gamma_N = $ constant, one obtains $K_N(t - t') = -i(\Gamma_N/2) \, \delta(t - t')$ and the coupled equations (3.2.15) become

$$i\hbar \, dC_N(t)/dt = \sum_M \langle N|V(t)|M\rangle \, e^{i(E_N - E_M)t/\hbar} \, C_M(t) - i(\Gamma_N/2) \, C_N(t).$$

(3.2.17)

Since $V(t)$ is very well known for the Coulomb interaction and the nuclear states $|N\rangle$ are assumed to be solutions of the harmonic oscillator with energies $E_N = N\hbar\omega$, the excitation amplitudes $C_N(t)$ can be

calculated from eq. (3.2.17) and the initial condition $C_N(-\infty) = \delta_{N0}$. For that aim, more about the values of the widths Γ_N should be known. Up to now we only know that $\Gamma_0 = 0$ and $\Gamma_1 = \Gamma_{GDR}$. The solution for $\Gamma_N = 0$ ($N = 0, 1, 2, \ldots$) was given in the preceding section.

As a consequence of having $\Gamma_N \neq 0$, the total probability $P_{tot} = \Sigma |C_N(t)|^2$ is no longer conserved because a flux is now put into the decay channels. Multiplying eq. (3.2.17) by C_N^* and its complex conjugate by $C_N(t)$ and subtracting the results, we obtain for the change of the occupation probability $\tilde{P}_N(t) = |C_N(t)|^2$,

$$\frac{d\tilde{P}_N(t)}{dt} = \frac{2}{\hbar} \, \text{Im}\left\{\sum_M \langle N|V(t)|M\rangle \, e^{i(E_N - E_M)t/\hbar} \, C_N C_M^*\right\} - \frac{\Gamma_N}{\hbar} \, \tilde{P}_N(t) \, . \tag{3.2.18}$$

The first part of the RHS of eq. (3.2.18) describes the redistribution of the flux among the N channels during the collision. If only this term were present, we would have conservation of the total probability $P_{tot}(t) = \Sigma_N \tilde{P}_N(t)$, since $V(t)$ is Hermitian. This term leads to a change of the occupation probability given by

$$G_N(t) = \frac{2}{\hbar} \, \text{Im}\left\{\sum_M \langle N|V(t)|M\rangle \, e^{i(E_N - E_M)t/\hbar} \, C_M(t) \, C^*_N(t)\right\} \, . \tag{3.2.19}$$

The non-Hermitian part of the interaction leads to a loss out of channel N, given by

$$L_N(t) = (\Gamma_N/\hbar) \, \tilde{P}_N(t) \, , \tag{3.2.20}$$

i.e., we have the balance equation

$$d\tilde{P}_N(t)/dt = G_N(t) - L_N(t) \, . \tag{3.2.21}$$

This equation can also be written as the integral equation

$$\tilde{P}_N(t) = \int_{-\infty}^{t} e^{-\Gamma_N(t-t')/\hbar} \, G_N(t') \, dt' + \delta_{N0} \, , \tag{3.2.22}$$

where we used the initial condition $\tilde{P}_N(-\infty) = \delta_{N0}$. A further insight into eq. (3.2.21) can be obtained by summing it over all states:

$$\sum_N \frac{d\tilde{P}_N(t)}{dt} = \sum_N L_N(t) \, . \tag{3.2.23}$$

Defining the flux function

$$F_N(t) = \int_{-\infty}^{t} L_N(t') \, dt' = \frac{\Gamma_N}{\hbar} \int_{-\infty}^{t} \tilde{P}_N(t') \, dt' \, , \tag{3.2.24}$$

the integration of eq. (3.2.23) can be written as

$$1 = \sum_N \tilde{P}_N(t) + \sum_N F_N(t) \, . \tag{3.2.25}$$

Due to the exponential decay of the states with $N \geqslant 1$, we have for $t \to \infty$ the limit $\tilde{P}_N(\infty) = \delta_{N0} \tilde{P}_0(\infty)$ and

$$1 = \tilde{P}_0(\infty) + \sum_N F_N(\infty) \, . \tag{3.2.26}$$

This means that for $t \to \infty$ there is a probability to find the system in the ground state given by $\tilde{P}_0(\infty)$ and a probability that it has been excited and decayed through the channel N which is given by $F_N(\infty)$. If the widths Γ_N are known, eq. (3.2.17) can be solved and from eq. (3.2.24) the contribution to the fragmentation through the channel N can be deduced.

An approximate solution can be found in the case of linearly increasing widths with increasing energy, i.e. $\Gamma_N = N\Gamma$. An explanation for this possibility in terms of N-particle–N-hole excitations was given by Baur and Bertulani [Ba-86e]. Following the classical interpretation leading to the Poisson distribution as discussed in section 3.2.1, the excitation probability of the state $|N\rangle$ is equal to the excitation probability of N uncoupled oscillators, each having a decay width of Γ. Instead of eq. (3.1.16), the energy transferred to a damped oscillator will be given by [see Ja-75, eq. (13.24)]

$$\Delta\tilde{E}(b) = \frac{2\hbar\Gamma}{\pi m_N c^2} \alpha^2 \frac{Z_1^2 N_2 Z_2}{A_2} \left(\frac{c}{v}\right)^4 \frac{1}{\gamma^2}$$

$$\times \left\{ \int_0^\infty \frac{\Omega^4 K_1^2(\Omega b/\gamma v) \, d\Omega}{(\Omega^2 - \omega^2)^2 + \Omega^2 \Gamma^2/4\hbar^2} + \frac{1}{\gamma^2} \int_0^\infty \frac{\Omega^4 K_0^2(\Omega b/\gamma v) \, d\Omega}{(\Omega^2 - \omega^2)^2 + \Omega^2 \Gamma^2/4\hbar^2} \right\} \tag{3.2.27}$$

$$= \frac{2 E_{GDR}^2}{m_N c^2} \alpha^2 \frac{Z_1^2 N_2 Z_2}{A_2} \left(\frac{c}{v}\right)^4 \frac{1}{\gamma^2} \left[g_1(x,\eta) K_1^2(x) + \frac{1}{\gamma^2} g_0(x,\eta) K_0^2(x) \right],$$

where

$$g_m(x,\eta) = \frac{\eta^2}{\pi K_m^2(x)} \int_0^\infty \frac{y^4 K_m^2(\eta x y) \, dy}{(y^2 - 1/\eta^2)^2 + y^2/4} \, , \tag{3.2.28}$$

with $x = \omega b/\gamma v$ and $\eta = \Gamma/\hbar\omega \equiv \Gamma/E_{GDR}$. In terms of $g_m(x,\eta)$ the excitation probability in first order is, as in eq. (3.1.18), given by

$$\tilde{\Phi}(b) = \tilde{a}_0^2 + \tilde{a}_1^2 + \tilde{a}_{-1}^2 \, , \tag{3.2.29a}$$

with

$$\tilde{a}_0^2 = \frac{2 E_{GDR}}{m_N c^2} \alpha^2 \frac{Z_1^2 N_2 Z_2}{A_2} \left(\frac{c}{\gamma v}\right)^4 g_0(x,\eta) K_0^2(x) \, , \tag{3.2.29b}$$

and

$$\tilde{a}_1^2 = \frac{E_{GDR}}{m_N c^2} \, \alpha^2 \, \frac{Z_1^2 N_2 Z_2}{A_2} \left(\frac{c}{v}\right)^4 \frac{1}{\gamma^2} \, g_1(x, \eta) \, K_1^2(x) .$$ (3.2.29c)

The functions $g_m(x, \eta)$ are plotted in fig. 3.8 for $\eta = 0.1$ and $\eta = 0.3$. When $\eta \to 0$, then $g_m \to 1$ and we obtain the same results as given by eq. (3.1.18). For $\eta \neq 0$, then we observe that g_0 will have the greater influence, specially for $x \ll 1$. Since, as we saw in section 3.1.2, $a_0 \ll a_1$ in the limit of high energies of collision, we expect that in this limit the influence of the widths of the states in the cross sections calculated in section 3.2.2 will be very small. Inserting eq. (3.2.29) in the eqs. (3.2.1) and (3.2.5) we find the results given in table 3.4 for the reaction $^{16}O + ^{238}U$ as a function of the laboratory energy. One observes that the inclusion of the widths of the states modifies appreciably the previous calculations only for low energies and for large N. In the limit $\gamma \gg 1$, the interaction is very sudden and the widths of the states have practically no influence on the excitation process. In that limit the theoretical results of section 3.1 are of enough accuracy for application in RHI collisions. However, if the widths of the states are too large, then this approach is unrealistic and, moreover, the experimental detection of those states will be very difficult.

As a final remark, we observe that here the interesting possibilities are not studied, which arise in the channelling of relativistic heavy ions in crystals. Due to the periodicity of the crystal lattice this may lead to resonance effects which influence the cross sections and which may be of use for the production of monochromatic beams of highly energetic neutrons. An analysis of these effects is given by Pivovarov et al. [Pi-80, Pi-83, and references therein].
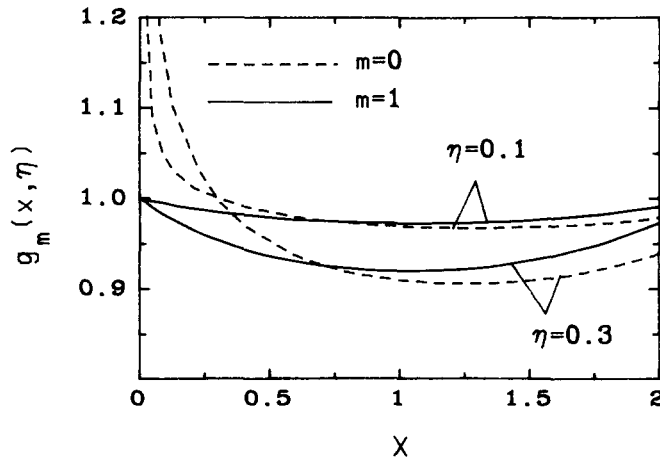
Fig. 3.8. The dimensionless functions $g_m(x, \eta)$ as defined by eq. (3.2.28). In the limit of zero widths, $\eta = \Gamma/E_{GDR} \to 0$, we have $g_m(x, \eta) \to 1$.

Table 3.4

Cross sections for N-phonon Coulomb excitation of ^{16}O in the reaction $^{16}O + ^{238}U$. The values corresponding to $\tilde{\sigma}_c^{(N)}(\sigma_c^{(N)})$ take (do not take) into account the widths of the states (see text)

E_{lab} (GeV/nucleon)	$\tilde{\sigma}_c^{(1)}$	$\sigma_c^{(1)}$	$\tilde{\sigma}_c^{(2)}$	$\sigma_c^{(2)}$	$\tilde{\sigma}_c^{(3)}$	$\sigma_c^{(3)}$
0.5	36 mb	34 mb	0.13 mb	0.12 mb	0.5 μb	0.43 μb
2	0.14 b	0.13 b	0.81 mb	0.67 mb	4.9 μb	3.9 μb
10	0.43 b	0.41 b	2.4 mb	2.2 mb	18 μb	16 μb
100	1.0 b	1.0 b	3.1 mb	3.1 mb	23 μb	22 μb

3.3. Production of pions

Another very interesting subject is that concerning *pion-production* in RHI collisions. The pions produced are supposed to be a source of information of the violent hadronic processes occurring in the central collisions. As implied by the relation (1.7) more and more equivalent photons become available for energies $E_\gamma \geq 140$ MeV corresponding to the photonuclear pion threshold, as one goes to higher beam energies. Above this energy the total photonuclear cross section is dominated by pion production and can be approximated by

$$\sigma_{\gamma X} = A_{\text{eff}}(\omega)\left[\frac{Z}{A}\,\sigma_{\gamma,\text{proton}}(\omega) + \frac{N}{A}\,\sigma_{\gamma,\text{neutron}}(\omega)\right].$$ (3.3.1)

Experimentally it is found that A_{eff} is approximately independent of ω, and shows a pronounced shadowing effect $A_{\text{eff}} \simeq A^\alpha$, with $\alpha = 0.6-0.9$. We assume, for simplicity,

$$\sigma_{\gamma,\text{proton}} \simeq \sigma_{\gamma,\text{neutron}} \equiv \sigma_{\gamma p},$$ (3.3.2)

and take $\alpha = 0.7$. Then, pion production in RHI collisions through the electromagnetic interaction can be approximately written as

$$\sigma(XY \to \pi XY) \simeq \int\limits_{0.14\,\text{GeV}}^{\infty} n_1(E_\gamma)\, A_2^{0.7}\, \sigma_{\gamma p}(E_\gamma)\, \frac{\mathrm{d}E_\gamma}{E_\gamma} + \int\limits_{0.14\,\text{GeV}}^{\infty} n_2(E_\gamma)\, A_1^{0.7}\, \sigma_{\gamma p}(E_\gamma)\, \frac{\mathrm{d}E_\gamma}{E_\gamma},$$ (3.3.3)

where n_1 corresponds to the equivalent photon spectrum generated by the nucleus X and that will cause the production of pions by the interaction with nucleus Y, and n_2 corresponds to the inverse case. We use $\pi l = M1$ since the pions are mostly produced through the nucleonic excitation to a Δ-state, which we assume to be of magnetic dipole origin. But the exact treatment of the multipolarity in this process is unimportant, since for the relevant equivalent photon energies which lead to pion production, the equivalent photon numbers are all approximately given by eq. (2.5.6). We used the experimental data of Armstrong et al. [Ar-72] for $\sigma_{\gamma p}$. The results of the integrations in eq. (3.3.3) is shown in fig. 3.9 for
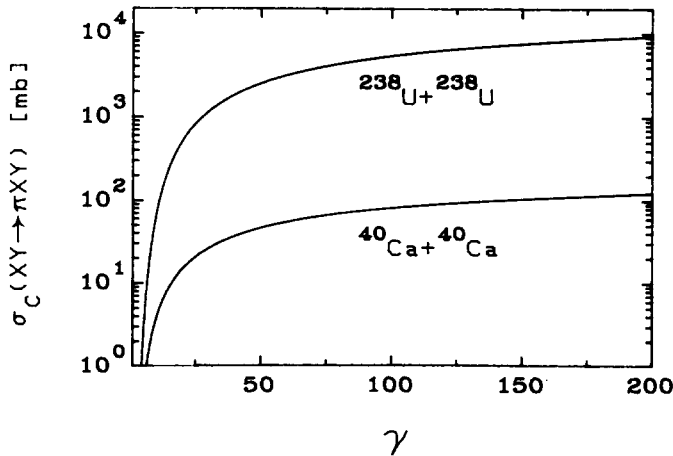

Fig. 3.9. Coulomb production cross sections of pions in the reactions ^{40}Ca + ^{40}Ca and ^{238}U + ^{238}U as a function of the relativistic Lorentz factor γ.

the reactions ^{40}Ca + ^{40}Ca and ^{238}U + ^{238}U as a function of γ (roughly $E_{lab}/A_1 \simeq \gamma$ GeV, for $\gamma \gg 1$). There is a steep increase of the cross sections until a stage where they increase approximately proportional to $(A_1 Z_2^2 + A_2 Z_1^2) \ln \gamma$. The cross sections at this stage are quite large and for very heavy systems like ^{238}U + ^{238}U it even can compete with those arising from hadronic interactions. The main difference is that, while in a given Coulomb collision $(b > R_1 + R_2)$ the pion multiplicity can be at most one, in a central collision a large amount of pions can be produced.

3.4. Dissociation of light ions in coincidence experiments

3.4.1. Breakup of weakly bound nuclei in high-energy collisions

The coincidence experiments for *breakup of loosely bound nuclei* in high-energy collisions can also give precious information about the structure of these nuclei and about the related photonuclear reactions. For instance, the cross sections for radiative capture of α-particles, deuterons and protons by light nuclei at very low relative energies are of particular importance for the understanding of the nucleosynthesis of chemical elements and for determining the relative elemental abundances in stellar burning processes at various astrophysical sites [see e.g. Fo-84, Ro-78]. However, the direct experimental determination of the cross sections at astrophysically relevant energies under laboratory conditions is rather difficult or even precluded, mainly as the Coulomb barrier strongly supresses the cross sections for the reactions of interest. For example, the ^{3}He(^{4}He, γ) ^{7}Be reaction, which at solar temperatures affects the solar neutrino flux and bears strongly on the solar neutrino problem [see e.g. Ka-84, Os-82, Os-84], is experimentally studied [Os-82, Os-84, Na-69] down to c.m. energies $E_{CM} = 165$ keV, while the cross section is actually needed at $E_{CM} = 1$–20 keV. A similar situation is found for the ^{12}C(α, γ) ^{16}O reaction [Ke-82, La-85] which is important for the stellar helium-burning process and where the values of the low-energy cross section (at $E_{CM} \simeq 0.3$ MeV corresponding to temperatures of 2×10^8 K) are actually a matter of controversial discussion presently. In cases of nonresonant direct capture reactions the energy dependence is dominated by the Coulomb barrier penetration, which is usually factored out by defining the astrophysical S-factor

$$S(E_{CM}) = E_{CM} \sigma_{capt} \, e^{2\pi\zeta} , \tag{3.4.1}$$

where

$$\zeta = Z_1 Z_2 e^2 / \hbar v_{CM} \tag{3.4.2}$$

is the usual Sommerfeld parameter. This S-factor shows a smooth energy dependence and seems to be adequate for an extrapolation of the measured values to astrophysically relevant energy ranges. But in most cases of interest the extrapolation covers several orders of magnitude and is particularly suspect if resonances and subthreshold resonances are expected to be present in the considered reaction [see Ro-78]. In addition, the extrapolation needs often considerable theoretical support and bias, and despite strong efforts to understand nuclear reactions on theoretical grounds, it appears to be generally impossible to predict the astrophysically interesting cross sections with sufficient accuracy.

In view of this situation, all dedicated efforts which are able to explore additional experimental information on the quantities determining low-energy nuclear reaction cross sections are of considerable interest. Recently the investigation of continuum stripping processes has been discussed [Ba-84a, b,

Ba-85, Ba-86f] as a possible method to overcome the problem arising from the Coulomb barrier. However, the method involves a theoretical reaction model which might cast some doubts on the results.

Baur, Bertulani and Rebel [Re-85, Ba-86c and Ba-86d] have proposed a different approach for the investigation of the electromagnetic transitions between a bound state of two nuclear particles and continuum states at small relative energies. The proposal suggests to use the nuclear Coulomb field as a source of the photodisintegration processes. In fact, instead of studying directly the radiative capture process

$$b + c \rightarrow a + \gamma,$$ (3.4.3)

one may consider the time reversed process (a being in the ground state)

$$\gamma + a \rightarrow b + c.$$ (3.4.4)

The corresponding cross sections are related by the detailed balance theorem

$$\sigma(b + c \rightarrow a + \gamma) = \frac{2(2j_a + 1)}{(2j_b + 1)(2j_c + 1)} \frac{k_\gamma^2}{k_{CM}^2} \sigma(a + \gamma \rightarrow b + c).$$ (3.4.5)

The wave number in the (b + c) channel is

$$k_{CM}^2 = 2\mu_{bc} E_{CM}/\hbar^2,$$ (3.4.6)

with μ_{bc} the reduced mass, while the photon wave number is given by

$$k_\gamma = \frac{E_\gamma}{\hbar c} = \frac{E_{CM} + Q}{\hbar c}$$ (3.4.7)

(neglecting a small recoil correction) in terms of the Q-value of the capture reaction (3.4.3). Except for the extreme case very close to threshold ($k_{CM} \rightarrow 0$), we have $k_\gamma \ll k_{CM}$, so that the phase space favours the disintegration cross section as compared with the radiative capture. However, direct measurements of the photodisintegration near the breakup threshold do hardly provide experimental advantages and seem presently impracticable [Re-85]. On the other hand, the copious source of equivalent photons acting on a fast charged nuclear projectile when passing the Coulomb field of a (large-Z) nucleus offers a more promising way to study the photodisintegration process as Coulomb dissociation. As an example we cite the reactions

$$^7Be + {}^{208}Pb \rightarrow \alpha + {}^3He + {}^{208}Pb - 1.58\,MeV,$$

$$^{16}O + {}^{208}Pb \rightarrow \alpha + {}^{12}C + {}^{208}Pb - 7.58\,MeV.$$
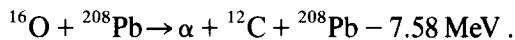
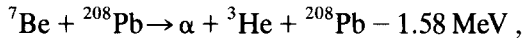Figure 3.10 indicates schematically the dissociation reactions due to the Coulomb and to the nuclear interaction.

At sufficiently high projectile energy the two fragments b and c emerge with rather high energies (around the beam-velocity energies) which facilitates the detection of these particles. At the same time, the choice of adequate kinematical conditions for coincidence measurements allows one to study rather
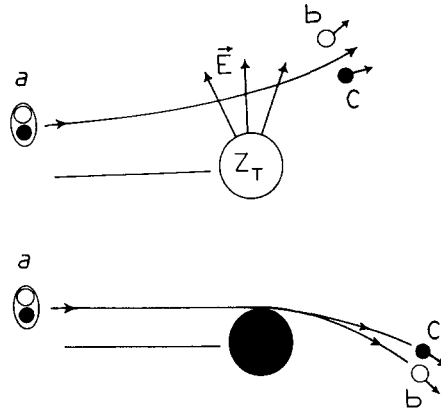
Fig. 3.10. Top: Coulomb dissociation a→b + c in the field of a target nucleus (Z_T). Bottom: dissociation due to the nuclear interaction on the target surface.

low relative energies E_{CM} of b and c and to ensure that the target nucleus stays in the ground state (elastic breakup). By repeating the experiment for different projectile energies and different angular measurements, and by using eq. (2.7.1) one can extract the values of the photonuclear cross sections for each multipolarity which contributes to the breakup. A more detailed analysis of the experimental conditions for such experiments is shown in refs. [Ba-86c, Ba-86d, and Re-86]. The most favourable theoretical and experimental conditions seem to be practicable for energies around 50 MeV/nucleon.

Another interesting possibility is the study of the nuclear matter distribution of extremely neutron-rich nuclei like, e.g., ^{11}Li. Some high-energy experiments [Ta-85a, Ta-85b, HK-87] for the breakup of such nuclei are beginning to be available, and seem to be a very promising field of study of such nuclei. Nevertheless, these experiments up to now have been *inclusive* ones, i.e., only one fragment is observed. Therefore, a summation has to be done over all unobserved channels, leading to a partial loss of information about the process. More useful would be the *exclusive* experiments, where the dissociation process of the projectile is separated from the background of other reactions by means of the coincidence detection of the two outgoing fragments together with a simultaneous measurement of their energies. Perhaps, one could also determine the momentum transfer in these reactions by a measurement of the recoil energy of the target nucleus. Although these experiments are much harder to perform in high-energy collisions, they certainly seem to be realisable and there are some experimental proposals in this direction [see, e.g., Re-87, Ge-87, and Br-85].

Next, we shall use some simple assumptions about the structure of the weakly bound nuclei composed of *two clusters*, disregarding some more specific details, for the sake of simplicity. We use the *diffraction dissociation* theory to account for the nuclear interaction. This theoretical approach has been introduced by Akhiezer and Sitenko [Ak-57], Glauber [Gl-55], and Feinberg [Fe-55], to describe the dissociation of high-energetic deuterons. Also important in this context are the so-called *stripping reactions* in which one of the clusters of the projectile suffers a strong inelastic collision with the target while the other is diffracted inelastically [Gl-55]. The cross sections for the stripping reactions depend much more on the exact knowledge of the nuclear structure and can be only approximately calculated [Fä-70a, Fä-70b]. The following study is complementary to several works on the fragmentation of relativistic particles. We refer, for example, to the works of Hüfner and Nemes [Hü-81], Fäldt [Fä-70a], and of Evlanov and Sokolov [Ev-86a, Ev-86b].

3.4.2. Amplitudes for diffraction and Coulomb dissociation

The amplitude for the dissociation of the incident projectile on a target nucleus, assumed to stay in its ground state, in the eikonal approximation is

$$f_d(\boldsymbol{q}, \boldsymbol{Q}) = \frac{ik}{2\pi} \int d^2b \, e^{i\boldsymbol{Q}\cdot\boldsymbol{b}} \, \Gamma_d(\boldsymbol{b}) \,, \qquad (3.4.8)$$

where k is the centre of mass momentum of the projectile, Q is the momentum change in the scattering ($Q = 2k \sin(\theta/2) \simeq k\theta$, where θ is the scattering angle of the centre of mass), q is the relative motion momentum of the outgoing fragments, and k_1 and k_2 are the momenta of the corresponding clusters with masses m_1 and m_2, respectively. In non-relativistic collisions $q = (m_2 k_1 - m_1 k_2)/(m_1 + m_2)$, while for high-energetic collisions q can be determined by the invariant mass of the two fragments. $\Gamma_d(b)$ is the profile function for the dissociation. In the approximations we will use, it contains contributions from diffraction dissociation on the target surface, and from Coulomb dissociation for impact parameters b larger than the sum of the nuclear interaction radii. Assuming a sharp boundary target, it can be written as $\Gamma_d(b) = \Gamma_N(b) + \Gamma_C(b)$, where $\Gamma_N(b)$ vanishes for $b > R$ and $\Gamma_C(b)$ vanishes for $b < R$. Therefore, we obtain

$$f_d(\boldsymbol{q}, \boldsymbol{Q}) = f_N(\boldsymbol{q}, \boldsymbol{Q}) + f_C(\boldsymbol{q}, \boldsymbol{Q}) \,. \qquad (3.4.9)$$

The total dissociation cross section is given by

$$d\sigma = |f_d(\boldsymbol{q}, \boldsymbol{Q})|^2 \, d\Omega \, d^3q/(2\pi)^3 \,, \qquad (3.4.10a)$$

where

$$d\Omega \simeq (2\pi/k^2) Q \, dQ \qquad (3.4.10b)$$

for high-energy collisions.

The relative motion of the clusters within the projectile is described by the wave function

$$\psi_i(r) = \sqrt{\eta/2\pi} \, e^{-\eta r}/r \,, \qquad (3.4.11)$$

where $\eta = \sqrt{2\mu\varepsilon/\hbar^2}$ is determined by the separation energy ε of the clusters $(1+2)$ and μ is the reduced mass of the system $(1+2)$. The relative motion of the clusters released after the disintegration of the projectile is described by the wavefunction

$$\psi_i(r) = e^{i\boldsymbol{q}\cdot\boldsymbol{r}} + \frac{1}{iq - \eta} \frac{e^{-iqr}}{r} \,. \qquad (3.4.12)$$

These wavefunctions correspond to the assumption of zero-range nuclear forces between the clusters in the projectile. They are very useful because most of the following calculations can be performed analytically. An extension to the use of more realistic wavefunctions is straight-forward. They form a complete set of orthonormal functions satisfying the relation

$$\psi_i(r)\,\psi_i^*(r') + \frac{1}{(2\pi)^3} \int \psi_f(r)\psi_f^*(r')\,\mathrm{d}^3q = \delta(r - r')\,.$$

The use of the above wavefunctions presupposes a simple model, where the Coulomb repulsion between the clusters are not taken into account (as would be important in systems like $\alpha + {}^3\mathrm{He}, \mathrm{d} + \mathrm{p}, \ldots$). The Coulomb repulsion between the clusters must lose its importance for high relative motion after their dissociation.

By using the energy and momentum conservation laws, we can also express eq. (3.4.10a) in terms of coincidence cross sections which are of interest in inclusive experiments. One finds

$$\frac{\mathrm{d}^3\sigma}{\mathrm{d}\Omega_1\,\mathrm{d}\Omega_2\,\mathrm{d}E_2} = \frac{\mu}{(2\pi)^3\hbar^2}\,\frac{k_1 k_2}{k}\,|f_\mathrm{d}(q, Q)|^2\,, \tag{3.4.13}$$

where Ω_1 and Ω_2 are the solid angles of emission of the two fragments, and E_2 is the energy of one of them. But, since the theoretical analysis is more transparent by using the variables q and Q, we shall keep them, and use eq. (3.4.10) in what follows.

The amplitudes for diffraction dissociation of deuterons by a *black nucleus* were calculated by Akhiezer and Sitenko [Ak-57]. The extension to the dissociation of other weakly bound nuclei gives

$$f_\mathrm{N}(q, Q) = \mathrm{i}kR\left\{\frac{J_1(QR)}{Q}\,[F(-\beta_2 Q, q) + F(\beta_1 Q, q)]\right.$$

$$\left. - \frac{\mathrm{i}kR^2}{2\pi} \int \mathrm{d}^2Q'\,\frac{J_1(Q'R)}{Q'}\,\frac{J_1(|Q - Q'|R)}{|Q - Q'|}\,F(\beta_1 Q - Q', q)\right\}\,, \tag{3.4.14}$$

where $\beta_1 = m_2/(m_1 + m_2)$, $\beta_2 = m_1/(m_1 + m_2)$, $R = 1.2A_\mathrm{T}^{1/3}$ fm is the radius of the target nucleus, and

$$F(Q, q) = \int \mathrm{d}^3r\,\psi_f^*(r)\,\mathrm{e}^{\mathrm{i}Q\cdot r}\,\psi_i(r) = \sqrt{8\pi\eta}\left\{\frac{1}{\eta^2 + (Q - q)^2} + \frac{1}{2Q(\mathrm{i}\eta - q)}\,\ln\left[\frac{q + Q + \mathrm{i}\eta}{q - Q + \mathrm{i}\eta}\right]\right\}\,. \tag{3.4.15}$$

The first term in eq. (3.4.14) corresponds to the *impulse approximation*, i.e., the independent scattering of separate clusters by the target. The second term corresponds to the simultaneous scattering of the clusters, also called by *eclipse term*. In order to describe the differential cross sections, we shall keep the impulse approximation, which gives reasonable results for small scattering angles. But, in order to obtain the total diffraction cross sections we have to include this term, since it decreases more slowly with increasing Q, and becomes the dominant contribution to the scattering amplitude (3.4.14) for larger values of Q.

The amplitude for Coulomb dissociation is given by eq. (2.3.14), which we shall multiply by a factor in order to have the same normalization for f_C and f_N. We shall restrict ourselves to the electric dipole and to the electric quadrupole modes, which are the most important ones. We obtain

$$f_\mathrm{C}(q, Q) = \mathrm{i}Z_1\alpha\left(\frac{c}{\gamma v}\right)k \sum_{lm} \mathrm{i}^m\left(\frac{\omega}{c}\right)^l \sqrt{2l + 1}\,\chi_m(R)\,G_{Elm}\left(\frac{c}{v}\right)M(El, m)\,, \tag{3.4.16}$$

where

$$\hbar\omega = \varepsilon + E_q = (\hbar^2/2\mu)(\eta^2 + q^2) \qquad (3.4.17)$$

is the sum of the absolute value of the binding energy and the kinetic energy of the relative motion of the separated clusters. The functions G_{Elm} are tabulated in the appendix A, and $\chi_m(R)$ is given by eq. (2.3.12) with $q_T = Q$.

The functions $M(Elm)$ are given by eqs. (2.1.14). Since the energy transferred to the dissociation of clusters $(1 + 2)$ is rather small, we can use the so-called *long-wavelength approximation*, and obtain

$$M(Elm) = \sum_{k=1,2} Z_k e \int \psi_f^*(r)\, r_k^l\, Y_{lm}(\hat{n}_k)\, \psi_i(r)\, \mathrm{d}^3 r , \qquad (3.4.18)$$

where $r_1 = \beta_1 r$, $r_2 = -\beta_2 r$ and $\hat{n}_2 = -\hat{n}_1$ are the position and direction of orientation of the clusters 1 and 2 in the centre of mass of the projectile, and Z_k are their respective charges. Inserting the wavefunctions (3.4.11) and (3.4.12) in (3.4.18), expanding it in multipoles, and using the integral

$$\int_0^\infty e^{-\eta r}\, r^{l+1}\, j_l(qr)\, \mathrm{d}r = \frac{l!(2q)^l}{(\eta^2 + q^2)^{l+1}} ,$$

we obtain

$$M(Elm) = e\sqrt{2\pi\eta}\,(-\mathrm{i})^l l!\, 2^{l+1}[Z_1\beta_1^l + (-1)^l Z_2\beta_2^l]\, \frac{q^l}{(\eta^2 + q^2)^{l+1}}\, Y_{lm}(\hat{q}) . \qquad (3.4.19)$$

We observe that for $\beta_1 Z_1 = \beta_2 Z_2$ there will exist no electric dipole contribution to the Coulomb dissociation. This is a well-known result and can be readily understood: in this case the electric dipole field pushes the two clusters with the same acceleration in the same direction, and does not lead to their separation. In such situations the E2 multipolarity will be the most effective one for dissociating the projectile. This result is a direct consequence of the assumption of a cluster-like structure for the projectile. For more complicated nuclear wavefunctions a deviation from this result is to be expected. For example, in the reaction $\gamma + {}^{16}\mathrm{O} \rightarrow \alpha + {}^{12}\mathrm{C}$ one indeed finds experimentally an appreciable suppression of the E1 multipolarity, but not completely. In fact, it is found that both multipolarities play important roles in such reaction [see, e.g., Re-85].

As an application of the formulas above, we plot in figure 3.11 the differential cross section $\mathrm{d}^4\sigma/\mathrm{d}^3 q\,\mathrm{d}Q$ for the dissociation of the simplest cluster-like nucleus, i.e., the deuteron, incident on ${}^{208}\mathrm{Pb}$ with energy $E_d = 200\,\mathrm{MeV}$. We take $q = \eta$, $Q = 1/R$ and $\theta = 90°$, corresponding to the emission of the fragments perpendicular to the beam, in the reference frame of the projectile. ϕ_q is the angle between Q and the component of q perpendicular to the incident beam. We observe that the Coulomb contribution, C, is approximately proportional to $\cos\phi_q$. The nuclear contribution, N, and the interference, CN, between them, are also shown. The interference tends to be destructive, oscillating around zero with approximately the same amplitude. This is a common trend, valid for all values of q and Q, as can be easily checked by using the formulas developed above.

Next, we shall integrate eq. (3.4.10) over the angular distribution Ω_q of the relative motion between the fragments. We obtain the differential cross section $\mathrm{d}^2\sigma/\mathrm{d}q\,\mathrm{d}Q$, which can be related to $\mathrm{d}^2\sigma/\mathrm{d}E_q\,\mathrm{d}\Omega$, where E_q is the energy of the relative motion of the final fragments and Ω is the solid angle of
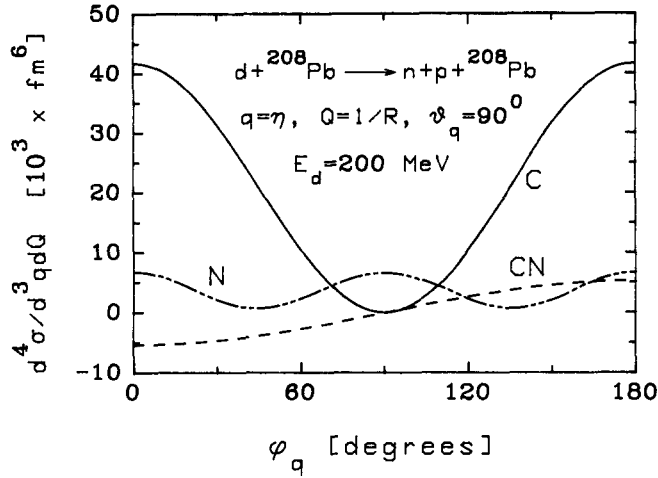
Fig. 3.11. The differential cross section $d^4\sigma/d^3q\,dQ$ for the dissociation of the deuteron, incident on ^{208}Pb with energy $E_d = 200$ MeV. We used $q = \eta$, $Q = 1/R$ and $\theta = 90°$. ϕ_q is the angle between Q and the component of q perpendicular to the incident beam.

scattering of their centre of mass. By using the impulse approximation, and eq. (3.4.15), we find for the nuclear contribution, after performing some simple integrals,

$$\frac{d^2\sigma_N}{dq\,dQ} = 8q^2R^2\,\frac{\eta}{Q}\,J_1^2(QR)\left\{\frac{1}{[\eta^2 + (q + \beta_1Q)^2][\eta^2 + (q - \beta_1Q)^2]}\right.$$

$$+ \frac{1}{[\eta^2 + (q + \beta_2Q)^2][\eta^2 + (q - \beta_2Q)^2]}$$

$$+ \frac{M}{2qQ(\eta^2 + q^2 + \beta_1\beta_2Q^2)} + \frac{M}{4qQ^2(q^2 + \eta^2)}\left(\eta N - \frac{q}{2}\,M\right)$$

$$\left. + \frac{1}{4Q^2(q^2 + \eta^2)}\left(\frac{M^2}{4} + N^2\right)\right\},$$ (3.4.20a)

where

$$M = \frac{1}{\beta_1}\ln\left[\frac{\eta^2 + (q + \beta_1Q)^2}{\eta^2 + (q - \beta_1Q)^2}\right] + \frac{1}{\beta_2}\ln\left[\frac{\eta^2 + (q + \beta_2Q)^2}{\eta^2 + (q - \beta_2Q)^2}\right],$$ (3.4.20b)

and

$$N = \frac{1}{\beta_1}\arctan\left(\frac{2\beta_1\eta Q}{\beta_1^2Q^2 - q^2 - \eta^2}\right) + \frac{1}{\beta_2}\arctan\left(\frac{2\beta_2\eta Q}{\beta_2^2Q^2 - q^2 - \eta^2}\right).$$ (3.4.20c)

The Coulomb contribution is easily obtained from the orthonormality of the spherical harmonics and one finds after inserting eqs. (3.4.16–3.4.19) in eq. (3.4.10a), integrating over Ω_q, and summing over m,

$$\frac{d^2\sigma_C}{dq\,dQ} = \frac{d^2\sigma_{E1}}{dq\,dQ} + \frac{d^2\sigma_{E2}}{dq\,dQ} ,$$
(3.4.21a)

where

$$\frac{d^2\sigma_{E1}}{dq\,dQ} = 128\,\frac{Z_T^2\alpha^2}{\gamma^2}\left(\frac{c}{v}\right)^4 (\beta_1 Z_1 - \beta_2 Z_2)^2 \eta QR^4\left[\chi_1^2 + \frac{\chi_2^2}{\gamma^2}\right]\frac{(q^2\omega/c)^2}{(\eta^2 + q^2)^4} ,$$
(3.4.21b)

and

$$\frac{d^2\sigma_{E2}}{dq\,dQ} = \frac{512}{15}\,\frac{Z_T^2\alpha^2}{\gamma^2}\left(\frac{c}{v}\right)^6 (\beta_1^2 Z_1 + \beta_2^2 Z_2)^2 \eta QR^4\left[\frac{\chi_2^2}{\gamma^2} + \left(2 - \frac{v^2}{c^2}\right)^2\chi_1^2 + \frac{3\chi_0^2}{\gamma^2}\right]\frac{q^2(q\omega/c)^4}{(\eta^2 + q^2)^6} .$$
(3.4.21c)

The E1–E2 interference is lost after the integration over Ω_q. However, in coincidence experiments, where $d^4\sigma/d^2q\,dQ$ is measured, the E1–E2 interference is important.

The interference term between Coulomb and nuclear amplitudes can be found by computing numerically the integral in the expression

$$\frac{d^2\sigma_{CN}}{dq\,dQ} = \frac{q^2 Q}{(2\pi)^2 k^2}\int (f_c^* f_N + f_n^* f_c)\,d\Omega_q .$$
(3.4.22)

In fig. 3.12 we plot $d^2\sigma/dq\,dQ$ for the reaction $d + {}^{208}Pb \rightarrow n + p + {}^{208}Pb$, at deuteron energy $E_d = 200$ MeV, for $q = \eta$, and as a function of QR. The Coulomb, C, the nuclear, N, and the interference, CN, contributions are shown separately. One observes that the Coulomb contribution is peaked at low values of Q. Actually, it peaks around $Q_C^{max} \simeq \omega/\gamma v$, so that for increasing beam energies the peak moves to lower values of Q, i.e., to more forward angles, and will also increase in height. This

Fig. 3.12. The double differential cross section $d^2\sigma/dq\,dQ$ for the dissociation of the deuteron, incident on ${}^{208}Pb$, with energy $E_d = 200$ MeV, for $q = \eta$, and as a function of QR. The curves labelled by C, N and CN correspond to the Coulomb, nuclear, and Coulomb–nuclear interference contributions, respectively.
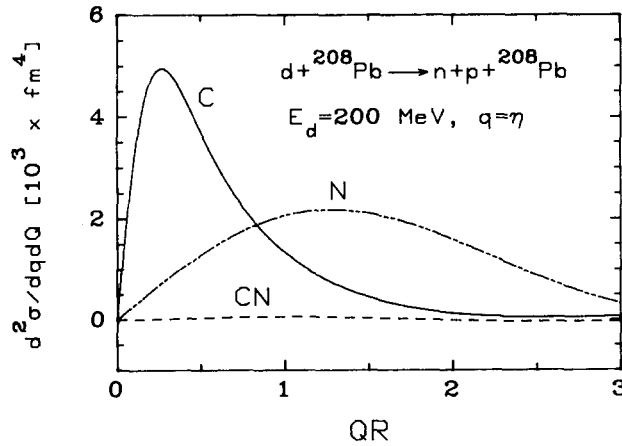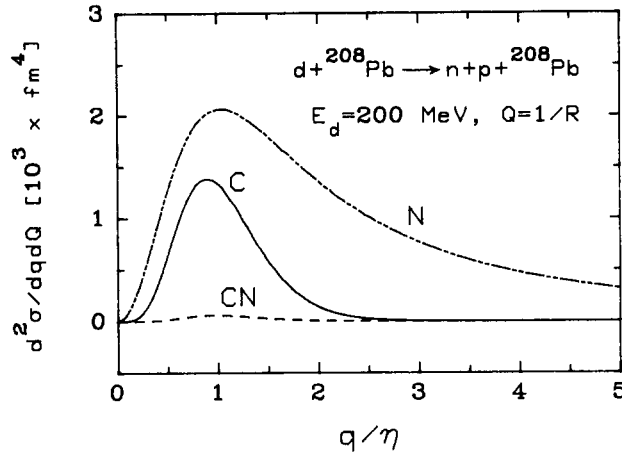
Fig. 3.13. The double differential cross section $d^2\sigma/dq\,dQ$ for the dissociation of the deuteron, incident on ^{208}Pb, with energy $E_d = 200$ MeV, for $Q = 1/R$, and as a function of q/η. The curves labelled by C, N and CN correspond to the Coulomb, nuclear, and Coulomb–nuclear interference contributions, respectively.

is in contrast with the nuclear contribution, which within our approach will always extend to large values of Q, being peaked around $Q_N^{max} \simeq 1/R$. This behaviour may help to separate the nuclear and Coulomb dissociation from the measurement of the scattering angle of the centre of mass of the two-cluster system in intermediate energy collisions. Unfortunately, with increasing energy both nuclear and Coulomb dissociation will lead to very forward angular distributions, with $\theta^{max} \simeq 1/kR \ll 1$, what makes the experimental measurements very difficult to proceed. For $Z_1 Z_2 \alpha \gtrsim 1$, the effects of Coulomb repulsion between the projectile and the target will considerably change the Q-dependence of the Coulomb dissociation amplitude. A study of these effects based on semiclassical calculations has been performed in section 2. In the present context, it implies the use of Coulomb distorted waves, instead of plane waves, in the calculation leading to the amplitude (3.4.16). Nevertheless, the relative behaviour between the Coulomb and nuclear angular distributions remains qualitatively the same.

In fig. 3.13 we plot $d^2\sigma/dq\,dQ$ for the same reaction as above, as a function of q/η and for $Q = 1/R$. As a general trend, for fixed Q, the Coulomb dissociation is more pronounced for $q \simeq \eta$, decreasing very fast for large values of q, while the nuclear dissociation peaks for $q \simeq Q$ and decreases slowly with increasing values of q. In both figs. 3.12 and 3.13 we see that the Coulomb plus nuclear interference are very small, being some orders of magnitude smaller than the nuclear or the Coulomb contribution.

3.4.3. Cross sections for the dissociation of weakly bound nuclei

Inserting eq. (3.4.14) in eq. (3.4.10) and using the orthonormality conditions of the wavefunctions, the integration over q can be easily performed in the impulse approximation. One gets

$$\frac{d\sigma_N}{dQ} = \frac{2\pi R^2}{Q} J_1^2(QR) \left\{ \int d^3r\, |\psi_i(r)|^2 |e^{i\beta_1 Q \cdot r} + e^{-i\beta_2 Q \cdot r}|^2 - \left| \int d^3r |\psi_i(r)|^2 [e^{i\beta_1 Q \cdot r} + e^{-i\beta_2 Q \cdot r}] \right|^2 \right\},$$

which gives

$$\frac{d\sigma_N}{dQ} = \frac{4\pi R^2}{Q} J_1^2(QR) \left\{ 1 + \frac{2\eta}{Q} \arctan\left(\frac{q}{2\eta}\right) - \frac{2\eta^2}{Q^2} \left[\frac{1}{\beta_1} \arctan\left(\frac{\beta_1 Q}{2\eta}\right) + \frac{1}{\beta_2} \arctan\left(\frac{\beta_2 Q}{2\eta}\right) \right] \right\}. \tag{3.4.23}$$

Using eq. (3.4.23) we find that for $\eta \to \infty$, corresponding to infinite binding energy of the clusters, $d\sigma_N/dQ \to 0$. For $\eta \to 0$, corresponding to very loosely bound nuclei,

$$\frac{d\sigma_N}{dQ} \to \frac{4\pi R^2}{Q} J_1^2(QR),$$

which means that in this case the total nuclear dissociation cross section will be just the sum of the elastic diffraction cross section for each cluster separately. Both limits is what one expects from the simple arguments of the diffraction dissociation theory. But, for large values of Q the impulse approximation is not more reasonable: the second term of eq. (3.4.14) will increase in importance for $Q \gtrsim \eta$. Therefore, to obtain the contribution of the diffraction dissociation to the total dissociation cross section, one has to integrate eq. (3.4.10) numerically by using eqs. (3.4.14) and (3.4.15).

By using the integral

$$\int \chi_m^2 Q \, dQ = R^2 \int_1^\infty x \, K_m^2\left(\frac{\omega R}{\gamma v} x\right) dx = \frac{R^2}{2} \left[K_{m+1}(\xi) \, K_{m-1}(\xi) - K_m^2(\xi)\right], \qquad (3.4.24)$$

where $\xi = \omega R/\gamma v$, we find for the Coulomb dissociation

$$\frac{d\sigma_C}{dq} = \frac{d\sigma_{E1}}{dq} + \frac{d\sigma_{E2}}{dq}, \qquad (3.4.25a)$$

with

$$\frac{d\sigma_{E1}}{dq} = 128 Z_T^2 \alpha^2 \left(\frac{c}{v}\right)^2 (\beta_1 Z_1 - \beta_2 Z_2)^2 \frac{\eta q^4}{(\eta^2 + q^2)^4} \left[\xi K_0 K_1 - \frac{v^2 \xi^2}{2c^2} (K_1^2 - K_0^2)\right], \qquad (3.4.25b)$$

and

$$\frac{d\sigma_{E2}}{dq} = \frac{512}{15} Z_T^2 \alpha^2 \left(\frac{c}{v}\right)^4 (\beta_1^2 Z_1 + \beta_2^2 Z_2)^2 \frac{\eta q^6 (\omega/c)^2}{(\eta^2 + q^2)^6}$$

$$\times \left[\frac{2}{\gamma^2} K_1^2 + \left(2 - \frac{v^2}{c^2}\right)^2 \xi K_0 K_1 - \frac{\xi^2 v^4}{2c^4} (K_1^2 - K_0^2)\right]. \qquad (3.4.25c)$$

The total Coulomb dissociation cross section $\sigma_C = \sigma_{E1} + \sigma_{E2}$ can be obtained by a numerical integration of eq. (3.4.25).

In fig. 3.14 we show the Coulomb and nuclear dissociation cross sections for the reaction $^7\text{Be} + {}^{208}\text{Pb} \to \alpha + {}^3\text{He} + {}^{208}\text{Pb}$ as a function of the laboratory energy per nucleon of the ^7Be projectile. In the calculation of the Coulomb dissociation cross sections we use $R + \pi Z_1 Z_2 e^2 / m_{\text{Be}} v^2 \gamma$, instead of R, as the minimum impact parameter, to account for the Rutherford bending corrections (see section 2.7) at energies E_{lab} per nucleon $\lesssim 100$ MeV. We observe that the E1 contribution is larger than the E2, and also than the nuclear dissociation. In such a case the study of the experimental data is simplified, since one can disregard the nuclear dissociation and assume all being due to the Coulomb dissociation, which is more accurately described.
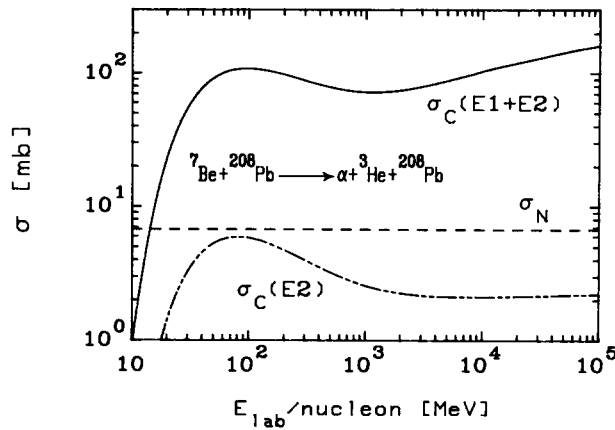
Fig. 3.14. Dissociation cross sections for the reaction $^7Be + {}^{208}Pb \rightarrow \alpha + {}^3He + {}^{208}Pb$ as a function of the laboratory energy per nucleon of the ^{7}Be-projectile. σ_N represents the nuclear diffraction dissociation, $\sigma_C(E2)$ the contribution of the electric quadrupole multipolarity to the Coulomb dissociation, and $\sigma_C(E1 + E2)$ is the sum of the electric dipole and of the electric quadrupole contributions.

In fig. 3.15 we plot the values for the dissociation cross section in the reaction $^6Li + {}^{208}Pb \rightarrow \alpha + d + {}^{208}Pb$. In this case, and within the simple cluster model, the E1 component of the Coulomb dissociation vanishes and only the next component, E2, will be effective in order to dissociate the nucleus. This makes the Coulomb cross section smaller than the nuclear one and the separation between these two contributions has to be measured on the basis of the angular distributions, as discussed in the last sections.

One observes in figs. 3.14 and 3.15 that the Coulomb cross sections increase with energy up to a maximum around approximately 100 MeV per nucleon, afterwards it decreases a little and then begins to increase with energy again, approximately proportional to $\ln(E_{lab}/A)$, for very high energies. This behaviour was also found in the cross sections for the excitation of giant resonances, as for example in fig. 3.3. The reason for that lies in the fact that the effects of Rutherford bending and of Lorentz contraction compete in the region of some hundreds of MeV per nucleon. With increasing energy, the nuclei come closer together, where the fields are stronger, which increases the probability that they will
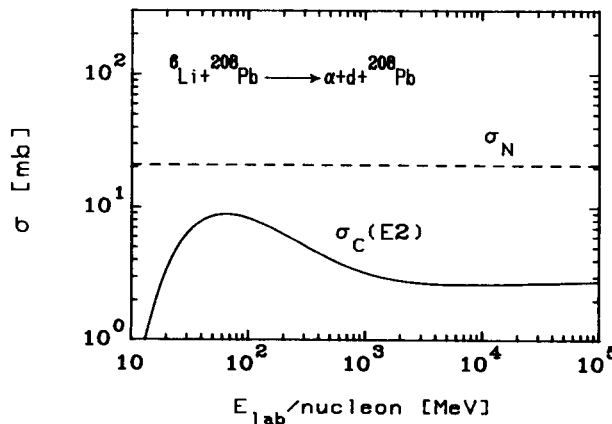

Fig. 3.15. Same as fig. 3.14, but for the dissociation reaction $^6Li + {}^{208}Pb \rightarrow \alpha + d + {}^{208}Pb$.

get Coulomb excited. That is the reason why the cross sections increase with energy for $E_{lab} \lesssim$ 100 MeV/nucleon. Above these energies the trajectories are approximately straight lines, and since the collision time decreases with energy, the momentum transferred from the electromagnetic field to the internal degrees of freedom of the nuclei diminishes. That is the reason for the decreasing of the cross sections for $E_{lab} \gtrsim 100$ MeV/nucleon. But this effect will not continue for too high energies because the electromagnetic field becomes contracted and stronger by a factor equal to the Lorentz parameter, γ, i.e., $E \simeq \gamma Z e^2 / b$. Since the momentum transfer is proportional to the product of the strength of the electromagnetic field and the collision time, which is approximately $\Delta t \simeq b/\gamma c$, it will be constant, independent of the beam energy. These simple arguments work, for impact parameters up to a maximum value given by the adiabatic cutoff $b \simeq \gamma c/\omega$, where $\hbar\omega$ is the excitation energy. That is the reason for the logarithmic increase of the cross sections for relativistic energies.

One interesting application of the fragmentation of cluster-like nuclei is the possibility of deducing information on the neutron skin of neutron-rich nuclei. For example, the reaction $^{11}Li + X \rightarrow {}^9Li$ could give information about the possible stability of the *di-neutron* system in the presence of a nuclear core. It has been suggested [Ha-87, Mi-72] that the force between two neutrons, itself too weak to form a bound system, under the influence of another nucleus can lead to a bound state of two particles: a di-neutron system and a nuclear core. The binding energy of the two neutrons in ^9Li is about 190 ± 110 keV. Assuming that ^{11}Li possesses the above mentioned cluster-like structure we find the values $\sigma_C \simeq 2.4$–12 b for the Coulomb dissociation cross section in the energy range $E_q = 80$–300 keV, respectively, in the reaction $^{11}Li + {}^{208}Pb \rightarrow 2n + {}^9Li + {}^{208}Pb$ at ^{11}Li-energies of 0.8 GeV/nucleon. For the diffraction dissociation one finds $\sigma_N \simeq 210$–662 mb. Recently, the reaction $^{11}Li \rightarrow {}^9Li$ at this energy, on lead targets, has been performed at the LBL BEVALAC by Tanihata et al. [Ta-85a, Ta-85b, Ko-87]. They found the total cross section of about 9.5 barns. One important contribution to this cross section is the stripping of the neutrons from the ^{11}Li-nucleus. It is about the same order of magnitude as the Coulomb dissociation and depends much more on the assumptions about the neutron excess on the surface of that nucleus. Therefore, the knowledge of the Coulomb dissociation cross sections and of the experimental values for the inclusive reactions are of great importance for the study of the tail of the nuclear matter distribution. By using several targets and beam energies, one can separate the Coulomb and stripping contributions (diffraction dissociation is of little importance in this case) in these reactions due to their different dependence on the nuclear parameters.

Precise coincidence experiments for the dissociation reaction of weakly bound nuclei at high bombarding energies are only at a beginning. As discussed above, such exclusive experiments would give valuable information on photodisintegration reactions, or indirectly, of radiative capture reactions of astrophysical interest, and also about the distribution of the nuclear density in the nuclear surface. At high energies both electromagnetic and the nuclear interaction between projectile and target will be important. Far from being a drawback, this can be of utility to extract complementary information about these different reaction mechanisms in the peripheral collisions. A decomposition of these mechanisms from the analysis of the angular distribution of the fragments, or from the dependence of the cross sections on the energy, charge, and mass parameters, is possible in accurate measurements. In the case of electromagnetic dissociation this decomposition can tell us about the relevance of each multipolarity in the dissociation reaction.

We have done very simple assumptions regarding the structure of the nuclei, and pointed out the main theoretical considerations for more complicated calculations. More specific structure effects, like, e.g., resonances, are expected to appear on a background parametrized by the above equations. The availability of experimental data in the near future will certainly raise interest on the detailed investigation of such effects. More details of the above calculations can be found in ref. [Ber-87c].

4. Coulomb production (Primakoff effect)

In section 4.1 we will show a beautiful example of the application of the theory of relativistic Coulomb excitation. It consists in the excitation of composite particles (e.g. baryons, mesons) in the Coulomb field of a target nucleus. The original idea was set in by Primakoff [Pr-51] who calculated the cross section for photo-production of π^0 in nuclear electric fields and suggested the measurement of it as a way to determine the mean lifetime of the π^0 particle. As an example of this technique we shall specially study the case of the measurement of the lifetime of the Σ^0 particle. A direct measurement of it in a bubble chamber is hopeless with the experimental technique available nowadays since the Σ^0 decay is electromagnetic, and the lifetime is of order of 10^{-19} s which produces a too short track to measure directly. Besides, the width of the decay is of order of 10 keV, much smaller than the resolution presently attainable. An indirect method is nonetheless possible by measuring the cross sections for the inverse process: electromagnetic production of Σ^0's in the field of a heavy nucleus. This process is commonly referred to as *Coulomb production* or as *Primakoff effect* [see Dr-62 and Po-61].

In section 4.2 we study the production of a neutral particle by means of the *two-photon* mechanism in RHI. There we also make a comparison with the similar process in electron–electron or electron–positron colliders.

4.1. Study of particle properties with relativistic Coulomb excitation

4.1.1. Coulomb excitation of a hadron: an example of application

In an experiment at CERN by Dydak et al. [Dy-77], a highly relativistic ($E_{\text{lab}} \simeq 20$ GeV) Λ beam was scattered on a nuclear target, where Σ^0 hyperons were produced at forward angles in the nuclear Coulomb field:

$$\Lambda + Z \rightarrow \Sigma^0 + Z .\tag{4.1.1}$$

The Σ^0 were detected through their decay $\Sigma^0 \rightarrow \Lambda\gamma$, which is by far the dominant decay mode of the Σ^0 particle. The cross section for the Σ^0 *Coulomb production* can be expressed in terms of the magnetic transition moment $\mu_{\Lambda\Sigma^0}$ or the Σ^0 lifetime. This is especially interesting since it allows for a test of the $SU(3)_{\text{flavour}}$ properties of the strong and electromagnetic interactions. Ignoring the strong violations of $SU(3)$, the unitary symmetry scheme introduced by Gell–Mann proposes that the elementary particles may be represented as tensors in a generalised isospin space (eightfold way), and that the strong interactions are invariant under unitarity transformations in this space. The electromagnetic current will also have definite and nontrivial transformation properties under $SU(3)$ and this makes it possible to derive a number of useful consequences of the symmetry for electromagnetic interactions of hadrons. In fact, Coleman and Glashow [Co-61] deduced in this way values of all the Λ, Σ, and Ξ magnetic moments, including the $\Lambda \rightarrow \Sigma^0$ transition magnetic moment which determines the rate of Σ^0 decay into $\Lambda + \gamma$, from the neutron and proton magnetic moments. They obtained the value

$$\mu_{\Lambda\Sigma^0} = (\sqrt{3}/2)\mu_{\text{n}} = -1.65\mu_{\text{N}} ,\tag{4.1.2}$$

where μ_{n} is the neutron magnetic moment and $\mu_{\text{N}} = e\hbar/2m_{\text{n}}c$ is the nuclear magneton. One can also make use of quark models for the baryons to obtain $\mu_{\Lambda\Sigma^0}$. In the simple model of Lipkin [Li-81], one assumes that the baryons are s-wave states of quarks, antisymmetric in colour and symmetric in spin, space and flavour. The wave functions for Σ^0 and Λ are

$$|\Sigma^0\rangle = \sqrt{2/3}|u\uparrow d\uparrow s\downarrow\rangle - \sqrt{1/6}|(u\uparrow d\downarrow + u\downarrow d\uparrow)s\uparrow\rangle \, ,$$

$$|\Lambda\rangle = \sqrt{1/2}|(u\uparrow d\downarrow - u\downarrow d\uparrow)s\uparrow\rangle \, ,$$

(4.1.3)

where $u\uparrow$, for example, is the wavefunction for a spin-up u quark. The $\Lambda\Sigma^0$ transition moment in terms of the quark wavefunctions is given by

$$\mu_{\Lambda\Sigma^0} = \sum_i \langle \Sigma^0|\hat{\mu}_i|\Lambda\rangle = \sqrt{1/3}(\mu_d - \mu_u) \, ,$$

(4.1.4a)

where $\hat{\mu}$ is the magnetic dipole operator. By using the same quark models for the neutron and proton we can express the result above in terms of the magnetic dipole moments of the proton and the neutron;

$$\mu_{\Lambda\Sigma^0} = (\sqrt{3}/5)(\mu_n - \mu_p) = -1.63\mu_N \, ,$$

(4.1.4b)

which differs very little from the value (4.1.2).

The $\Lambda\Sigma^0$-conversion cross section in the field of a nucleus was calculated by Dreitlein and Primakoff [Dr-62] and by Pomeranchuk and Shmushkevich [Po-61]. In these calculations, nuclear form factor and absorption are taken into account in a rather complicated method. We shall show that their final results can be obtained with the help of the much simpler Coulomb excitation approach of section 2.4, where the nuclear absorption is included from the outset, and no nuclear form factors enter any longer.

According to eq. (2.4.2), the angular distribution for the process (4.1.1) can be expressed in terms of the $B(M1)$ value of the $\Lambda\to\Sigma^0$ transition as

$$\frac{d\sigma}{d\Omega} = \frac{16\pi}{9} \, q_\Lambda^2\left(\frac{Z\alpha\omega}{\gamma v}\right)^2 [\chi_1(R)]^2 \, \frac{B(M1)}{e^2} \, ,$$

(4.1.5)

where $p_\Lambda = \hbar q_\Lambda$ is the momentum of the incident Λ beam, and $\hbar\omega$ is the energy of the virtual photon absorbed by the Λ in its rest frame:

$$\hbar\omega = (m_{\Sigma^0}^2 - m_\Lambda^2)c^2/2m_{\Sigma^0} \, .$$

(4.1.6)

The $B(M1)$ value is related to the transition magnetic moment $\mu_{\Lambda\Sigma^0}$ and to the lifetime τ_{Σ^0} by

$$B(M1) = \frac{9\mu_{\Lambda\Sigma^0}^2}{4\pi} = \frac{9\hbar}{16\pi(\omega/c)^3\tau_{\Sigma^0}} \, .$$

(4.1.7)

From this relation and eq. (4.1.4b), we find $\tau_{\Sigma^0} = 7 \times 10^{-20}$ s.

The angular distribution is given by quantal diffraction effects through the function (see eq. 2.3.12)

$$\chi_1(R) = \int_R^\infty x \, J_1(q_T x) \, K_1(q_\ell x) \, dx = \frac{R^2}{\eta^2 + \xi^2} \, [\xi \, J_1(\eta) \, K_2(\xi) - \eta \, J_2(\eta) \, K_1(\xi)] \, ,$$

(4.1.8)

where

$$\eta = q_T R = q_\Lambda R \sin\vartheta \, , \quad \text{and} \quad \xi = q_\ell R = \omega R/\gamma v \, .$$

(4.1.9)

The momenta q_T and q_ℓ are, respectively, the transversal and the longitudinal momentum transfer in the laboratory frame of reference.

By means of eqs. (4.1.6) and (4.1.8), we can rewrite eq. (4.1.5) as

$$\frac{d\sigma}{d\eta} = \frac{32\pi^2}{9} (Za\xi R)^2 \frac{B(M1)}{e^2} \frac{df(\eta, \xi)}{d\eta}.$$

(4.1.10)

The function

$$df(\xi, \eta)/d\eta = \eta[\chi_1(R)/R^2]^2$$

(4.1.11)

is plotted in fig. 4.1 for $\xi = 0.1$, 0.2, 0.5, and 1. The values are normalised so that $df/d\eta = 1$ for $\eta = 1$. To obtain the real values one must multiply $df/d\eta$ by the corresponding factors for each ξ. Since for relativistic collisions $q_\Lambda R \gg 1$, the peaks of the angular distribution will occur for $\eta \simeq \xi$, which means a maximum scattering angle $\vartheta_{max} \simeq \xi/q_\Lambda R \ll 1$, so that the cross section will be strongly forward peaked. Nonetheless, for exact forward scattering ($\vartheta = 0$) the angular distribution vanishes. This is a characteristic of all magnetic multipole excitations in relativistic Coulomb collisions, as was shown in section 2.4. Inserting eq. (4.1.7) in eq. (4.1.10), and approximating eq. (4.1.8) for small scattering angles, we obtain

$$\frac{d\sigma}{d\vartheta} = \frac{8Z^2\alpha\hbar^3 m_{\Sigma^0}^3}{(m_{\Sigma^0}^2 - m_\Lambda^2)^3 c^4} \frac{\vartheta^2}{[\vartheta^2 + (\omega/\gamma c q_\Lambda)^2]^2} \frac{1}{\tau_{\Sigma^0}},$$

(4.1.12)

which agrees with the result obtained by Dreitlein and Primakoff [Dr-62, eq. (35a)], apart from irrelevant additive factors. While those authors obtained this result in a more complicated approach, we observe that it can be reached in a very simple and transparent way as shown above.

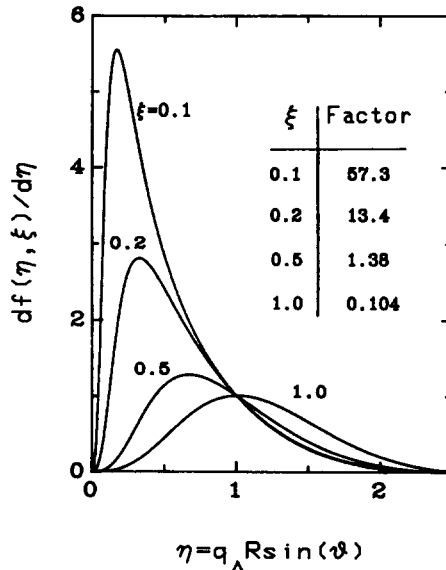| ξ	Factor
0.1	57.3
0.2	13.4
0.5	1.38
1.0	0.104

$\eta = q_\Lambda R \sin(\vartheta)$

Fig. 4.1. Angular distribution of the inelastically scattered particles after a magnetic dipole excitation. The values are normalized so that $df/d\eta = 1$ for $\eta = 1$. To obtain the absolute values one must multiply $df/d\eta$ by the corresponding factors shown in the table for each ξ.

The total cross section is obtained by integrating (4.1.10) over η;

$$\sigma_{\Lambda\Sigma^0} = 8\pi(Z\alpha)^2[\xi K_0 K_1 - \tfrac{1}{2}\xi^2(K_1^2 - K_0^2)]\mu_{\Lambda\Sigma^0}^2/e^2 ,$$

(4.1.13)

where the K's are functions of ξ. For $\xi \ll 1$ we have

$$\sigma_{\Lambda\Sigma^0} = 8\pi(Z\alpha)^2 \frac{\mu_{\Lambda\Sigma^0}^2}{e^2} \ln \frac{\delta}{\xi} = \frac{16\pi^2 Z^2 \alpha\hbar^3 m_{\Sigma^0}^3}{(m_{\Sigma^0}^2 - m_\Lambda^2)^3 c^4 \tau_{\Sigma^0}} \ln \frac{\delta}{\xi} ,$$

(4.1.14)

where $\delta = 0.681...$

The only parameter which enters into this calculation is the nuclear absorption radius, which we assume to be $R = 1.2 \times A^{1/3}$ fm.

4.1.2. Comparison with experiment

The first measurements of the lifetime of the Σ^0 particle were done by Dydak et al. [Dy-77], which measured the cross sections for the process (4.1.1) with a Λ-beam with laboratory energy of $\simeq 20$ GeV. They used ^{238}U and ^{58}Ni as targets, and their results are shown in fig. 4.2. The solid line represents the use of eq. (4.1.13), together with the value of $\mu_{\Lambda\Sigma^0}$ given by eq. (4.1.2). From these figures one can see that the above theory is in agreement with the analysis of Dydak et al. They obtained the value $\tau_{\Lambda\Sigma^0} = (5.8 \pm 1.3) \times 10^{-20}$ s, which agrees with the theoretical predictions.

The essential reason for overcoming the large excitation energy $m_{\Sigma^0} - m_\Lambda = 76.86$ MeV/c^2 is the high
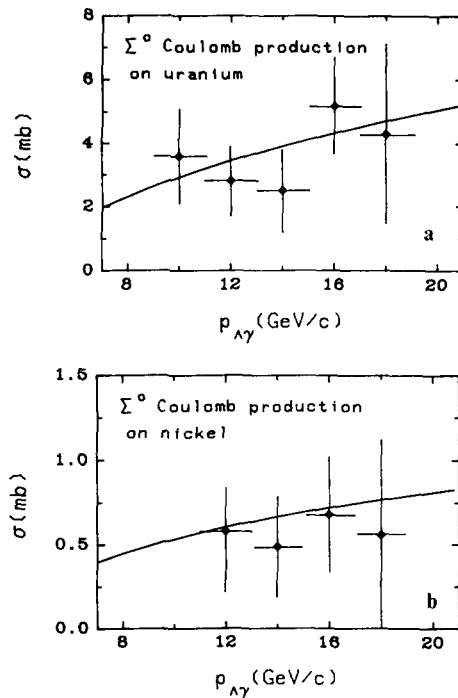

Fig. 4.2. Total cross section of the Coulomb production $\sigma(\Lambda \to \Sigma^0)$ as a function of the momentum of the $\Lambda\gamma$-pair from the decay of Σ^0, for (a) a uranium target and (b) a nickel target. The full line corresponds to eq. (4.1.13) with $\tau_{\Sigma^0} = 0.7 \times 10^{-19}$ s.

value of γ. For $\gamma \simeq 20$, as was the case in this experiment, the distance d where the adiabacity parameter $\xi = \omega d/\gamma v$ becomes equal to 1 is given by $d \simeq 50\,\mathrm{fm}$; i.e. the area which contributes to the electromagnetic excitation cross section is much larger than the nuclear geometric cross section.

This experiment has been recently [Pe-85, Pe-86] redone at Fermilab with a Λ beam of $p_\Lambda \simeq 200\,\mathrm{GeV}/A$ incident on nuclear targets with $Z = 4$, 50 and 82. These experiments show the expected logarithmic increase of the electromagnetic cross section with energy. In table 4.1 we make a comparison of their experimental data with the result obtained by using eq. (4.1.14). The agreement is quite good, within the experimental errors. This is more clearly seen in fig. 4.3 where we show the ratio between the experimental and the theoretical values.

One could also think in obtaining information on the different contributions of the M1 and of the E2 excitation of a nucleon to a Δ-resonance by measuring the total Coulomb cross section for this process in the collisions of nucleons and high-Z nuclei at relativistic energies, in the same way as was done in the experiment of Dydak et al. The differential cross section for the E2 excitation can be calculated by eq. (2.4.2), also analytically, and has a very different behaviour as compared to the M1 case. But the experimental detection of this process would be very difficult due to the background of contributions from strong interactions.

There are also other examples, where the Primakoff effect is used to study the interaction of photons with unstable particles. Quite recently [Ant-87], the vertex $\gamma \to 3\pi$ has been investigated in the reaction of pion pair production by pions in the nuclear Coulomb field

$$\pi^- + Z \to \pi^- + \pi^0 + Z$$
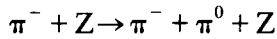
in the region of low-invariant-mass of the $\pi^-\pi^0$ system. A highly relativistic 40 GeV pion beam has been used. This is interesting in the context of the so-called Chiral anomalies.

In a similar experiment the polarisability of the π^- has been measured [Ant-83, Ant-85]. The Compton effect on a pion was studied in the reaction
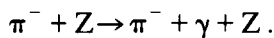
$$\pi^- + Z \to \pi^- + \gamma + Z.$$

Table 4.1
Cross sections for Coulomb production of Σ^0 on several targets by means of Λ particles with incident energy $E_{\mathrm{lab}} \simeq 200\,\mathrm{GeV}$. The experimental data are from ref. [Pe-86]

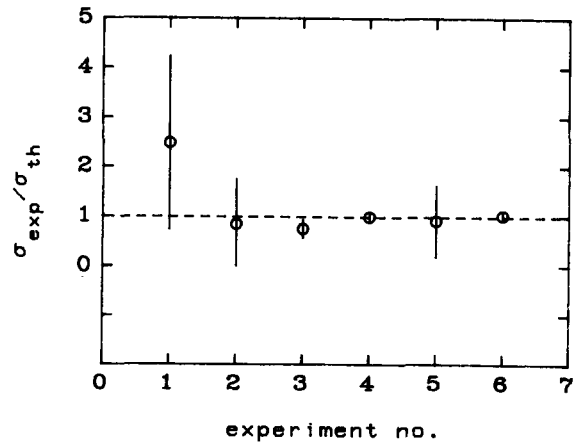| Experiment no.	Target Z	$\sigma_{\Lambda\Sigma^0}^{\mathrm{exp}}$ (mb)	$\sigma_{\Lambda\Sigma^0}^{\mathrm{th}}$ (mb)
1	4	0.068 ± 0.048	0.0274
2	4	0.023 ± 0.025	0.0274
3	50	2.65 ± 0.64	3.51
4	50	3.48 ± 0.36	3.51
5	82	8.17 ± 6.45	8.99
6	82	9.22 ± 0.82	8.99

Fig. 4.3. Ratio of the experimental data on Σ^0 production in the reaction $\Lambda + Z \to \Sigma^0 + Z$ and the theoretical calculation based on eq. (4.1.14) (see table 4.1).

From this the cross section for the elastic π^- photon scattering was deduced; this in turn, could be related to the pion polarisation, and it was found that $\alpha_\pi = (6.8 \pm 1.4) \times 10^{-43} \, \mathrm{cm}^3$. This quantity is of great interest in the study of hadron properties.

As another possibility we mention the study of the production of resonances in the interaction of real photons with the equivalent photons of the Coulomb field. At KEK (N. Sasao et al., Tsukuba, as mentioned in ref. [Ya-87]) the production of axion-like particle is investigated in this manner. On the original suggestion of Primakoff [Pr-51] the π^0-lifetime was measured in the process $\gamma + Z \to \pi^0 + Z$ [Br-74].

4.2. Two-photon collisions

An extensive program of γ–γ physics is going on at high-energy e^+e^- colliders. The dominant graph is shown in fig. 4.4. The charged particles e^+ and e^- emit *virtual* (or *equivalent*) photons which collide to form a neutral system X with charge parity $C = +1$. There exists a vast literature on this subject, the properties of the virtual γ's are calculated in great detail and the cross sections in e^+e^- collisions are directly related to the corresponding γ–γ cross sections (see [Bu-75, Fi-80, and Br-71], where many further references are contained). An early result is due to F.E. Low [Lo-60] where the measurement of the π^0-lifetime by π^0 production in e^+e^- or e^-e^- collisions is proposed. Using a variant of the equivalent photon method, the cross section for the process $e^-e^+ \to e^-e^+X$ is found to be related to the cross section for $\gamma + \gamma \to X$ by (we use the notation of ref. [AB-86])

$$d\sigma_{e^-e^+\to e^-e^+X}(s) = \eta^2 \int d\omega \, f(\omega) \, d\sigma_{\gamma\gamma\to X}(\omega s) \,, \tag{4.2.1}$$

with

$$s = (p_1 + p_2)^2 \,, \qquad \eta = \frac{\alpha}{2\pi} \ln\left(\frac{s}{4m^2}\right) = \frac{\alpha}{\pi} \ln \gamma \,, \tag{4.2.2a}$$

and

$$f(\omega) = (1/\omega)[(2 + \omega)^2 \ln(1/\omega) - 2(1 - \omega)(3 + \omega)] \,. \tag{4.2.2b}$$
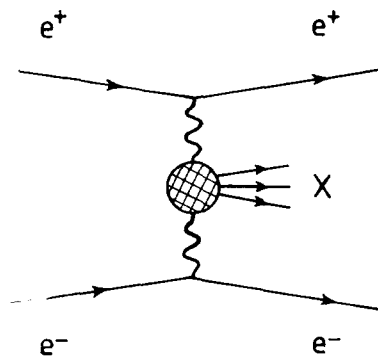

Fig. 4.4. Production of neutral $C = +1$ states X in the collision of two charges particles (e.g., e^+e^-) via the two-photon mechanism.

For a collider, s is given by $s = 4E^2$ where E is the e^+ (e^-)-energy in the laboratory system, m is the electron mass and $\gamma = E/m$. In addition to the situation pertaining to eq. (4.2.1), where the final momenta of e^+ and e^- are not measured (*untagged luminosities*) one can study cases where these momenta are measured (*tagged* or *double-tagged* luminosities, see, e.g., ref. [Fi-80]).

We shall point out the possible usefulness of RHI collisions for the study of $\gamma-\gamma$ collisions (see [Ba-87b]). It is the additional factor $(Z_1 Z_2)^2$, where Z_1 and Z_2 are the charge of the colliding heavy ions, which increases strongly the RHI cross section as compared to the e^+e^- case.

We study the collisions of two equivalent photons in the system where the two heavy ions move with opposite velocities v and $-v$ towards each other (see fig. 4.5). This is equivalent to the collision of two photons with frequency distributions $n_1(\omega_2)$ and $n_2(\omega_2)$ moving in opposite directions. For $\gamma \gg 1$ we can use the expression (see (eq. 1.11a))

$$n_i(\omega_i) = \frac{2}{\pi} Z_i^2 \alpha \ln\left(\frac{\gamma c}{\omega_i R_i}\right),$$ (4.2.3)

where the radius R_i of the ion i determines the minimum impact parameter. The adiabatic cutoff sets in at

$$\omega_i^{\max} = \gamma c / R_i$$ (4.2.4a)

and we put, for simplicity,

$$n_i(\omega_i) = 0 \quad \text{for} \quad \omega_i > \omega_i^{\max}.$$ (4.2.4b)

The Lorentz factor γ is related to the corresponding Lorentz factor γ_p of the projectile (for a fixed target machine) by

$$\gamma_p = 2\gamma^2 - 1.$$ (4.2.5)

The total cross section σ_C for the two-photon process $Z_1 + Z_2 \rightarrow Z_1 + Z_2 + X$ is given by
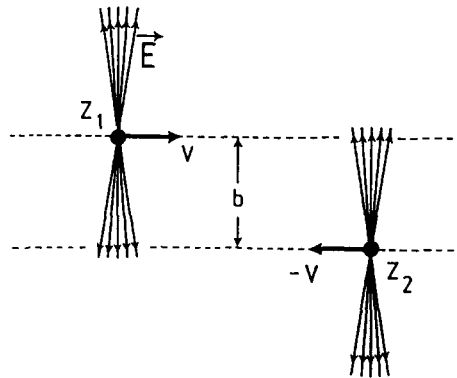

Fig. 4.5. Two relativistic heavy ions collide in a system where they move with opposite velocities v and $-v$ towards each other. This corresponds to the collision of two photons with opposite momenta with photon energy distribution given by $n_1(\omega_1)$ and $n_2(\omega_2)$, according to the equivalent photon method.

$$\sigma_C = \int \frac{d\omega_1}{\omega_1} \int \frac{d\omega_2}{\omega_2} \, n_1(\omega_1) \, n_2(\omega_2) \, \sigma_{\gamma\gamma \to X}(\omega_1 \omega_2) \, . \tag{4.2.6}$$

Introducing the variable $x = \omega_1 \omega_2$ ($4x$ corresponds to the square of the invariant mass of the 2γ-system) one obtains

$$\sigma_C = \left(\frac{Z_1 Z_2 \alpha}{\pi}\right)^2 \int dx \, \sigma_{\gamma\gamma \to X}(x) \, I(x) \, , \tag{4.2.7}$$

where

$$I(x) = \frac{16}{3x} \left(\ln \frac{\gamma c}{\sqrt{x R_1 R_2}}\right)^3 . \tag{4.2.8}$$

There are important differences of this equation as compared with the one used for the $e^+ e^-$ collisions [Lo-60, AB-86]. In the derivation of eqs. (4.2.1) and (4.2.2), it was assumed that $\gamma \gg 1$ (as is appropriate for the $e^+ e^-$ colliders). This means that the adiabatic cutoff, eq. (4.2.4), which is relevant for the RHI collisions, is not important for the $e^+ e^-$ case. The maximum energies of the equivalent photons are determined there by the kinematics of the process (total energy loss for e^+ or e^-, see, e.g., eq. (15) of [Lo-60]). This means that the higher energies will not be easily obtained in RHI collisions.

An important process in γ–γ collisions is the $e^+ e^-$ pair production

$$\gamma + \gamma \to e^+ + e^- \, . \tag{4.2.9}$$

The corresponding $e^+ e^-$ pair production in RHI collisions, being of large importance, will be studied in more detail in section 7. Another purely quantum electrodynamical process is $\gamma + \gamma \to \gamma + \gamma$, the elastic scattering of light on light (see, e.g. [La-86]). Its cross section involves an additional factor α^2 as compared to the pair production; it is, therefore, rather small and it has never been possible to study it directly. On the other hand, the elastic scattering of γ's in the Coulomb field of nuclei has been experimentally investigated (*Delbrück scattering*). In RHI collisions the same processes can also be studied.

It is also possible to form strongly interacting neutral $C = +1$, particles in 2γ-collisions, like $\pi^0, \eta, \eta_c, \ldots$. The π^0 production was originally suggested by Low [Lo-60], the η_c-particle was recently produced at PETRA [Berg-86]. The resonances are usually sufficiently narrow, so that their Breit–Wigner form can well be approximated by a δ-function in the integral, eq. (4.2.7a, b). For example, the π^0 production cross section is given by [Lo-60]

$$\sigma_{\gamma\gamma} = (8\pi^2/\mu\tau) \, \delta(\mu^2 - 4x) \, , \tag{4.2.10}$$

where $\tau = 0.83 \times 10^{-16}$ s and $\mu = 134.9$ MeV are the lifetime and mass of the π^0; respectively [AB-86]. One obtains

$$\sigma_C = \frac{128}{3} \, (Z_1 Z_2 \alpha)^2 \, \frac{1}{\mu^3 \tau} \left(\ln \frac{2\gamma}{\mu \sqrt{R_1 R_2}}\right)^3 . \tag{4.2.11}$$

A similar formula can also be used for the production of other particles, where one has to replace $1/\tau$

by the γ–γ width $\Gamma_{\gamma\gamma}$ of the particular resonance to be studied, and include an appropriate factor for the spin of the particle. One obtains values of the order of some μb for the π^0 production by the two-photon mechanism for the conditions of the present RHI experiments at CERN (60 and 200 GeV/nucleon oxygen beams on Pb targets).

Let us compare the characteristics of the RHI collisions with the e^+e^- collisions. Even in the highest energy RHI experiments, the γ-values achieved are rather low: for $\gamma_p = 60$ or 200, appropriate for the CERN experiments, the corresponding γ-values are rather modest. For a 1 GeV electron, e.g. one has already $\gamma \simeq 2000$. The γ-factor enters, however, only logarithmically in the cross section, whereas the $(Z_1Z_2)^2$ factor enters directly in the cross section formula, giving a distinct advantage for the RHI collisions. The comparatively low value of γ for RHI collisions leads to a limitation of the invariant mass of the 2γ-system.

Finally, let us mention some speculations. Due to the large flux of equivalent photons in the MeV range, RHI collisions would be of interest to look for resonances in the γ–γ system. This could be of special interest at present in the search for an unknown particle which decays into e^+ and e^- (for a recent review on the GSI experiments on positron emission in low energy heavy ion collisions, see [Ki-86]). Various proposals using γ–γ collisions [see, e.g., Za-87, Br-86, and Ts-86] or the Primakoff effect (as mentioned in ref. [Ya-87]) exist in order to look for such an unknown particle. If it is heavier than $2m_ec^2$ then it could decay into e^+e^- pairs and one could look for peaks in the invariant e^+e^- mass spectrum as produced in RHI collisions. This would also complement the search for resonances in the e^+e^- collisions in the MeV region [see, e.g., Wi-87 and Ma-87].

5. Bremsstrahlung

The emission of γ-rays in RHI collisions is an important diagnostic tool for the time development of the nuclear collision (see e.g. [Ka-77] and [Bj-85]). We will first investigate the *bremsstrahlung* process for Coulomb collisions ($b > R_1 + R_2$). This could be a potential source of background to be considered in experiments. A unique feature of this bremsstrahlung effect is the interference of the radiation from the target and projectile. This will be specially important at low values of γ; it leads particularly to the well-known vanishing of the E1 bremsstrahlung for systems with equal charge to mass ratio $Z_1/M_1 = Z_2/M_2$. In contrast to the low energy case, the emission of Coulomb bremsstrahlung at relativistic energies will be predominantly of E1 origin, even for systems with equal charge-to-mass ratio.

In section 5.1 we calculate the spectrum of bremsstrahlung in RHI electromagnetic collisions, and in section 5.2 we compare it to the bremsstrahlung occurring in the violent central collisions.

5.1. Bremsstrahlung in Coulomb collisions

According to eq. (14.67) of the textbook of Jackson [Ja-75], the energy radiated per unit solid angle per unit frequency interval is given classically by

$$\frac{d^2 I}{d\omega \, d\Omega} = \frac{e^2 \omega^2}{4\pi^2 c} |A_1 + A_2|^2 = \frac{e^2 \omega^2}{4\pi^2 c} [|A_1|^2 + |A_2|^2 + 2 \operatorname{Re} A_1 A_2^*], \tag{5.1.1}$$

where $E_\gamma = \hbar\omega$ is now the energy of a real photon and

$$A_i = Z_i \int\limits_{-\infty}^{\infty} \hat{n} \times \left(\hat{n} \times \frac{\boldsymbol{v}_i}{c}\right) e^{i\omega(t - \hat{n}\cdot\boldsymbol{r}_i/c)} \, dt , \tag{5.1.2}$$

where $i = 1$ (2) refers to the projectile (target) labels, $\boldsymbol{r}(\boldsymbol{v}_i)$ are their respective positions (velocities), and $\hat{n}$ is the direction of emission of the photon. By expanding eq. (5.1.1), the first (second) term corresponds to the radiation emitted by the projectile (target) and the third term to the interference between the two previous ones. Let us first discuss the radiation emitted by the target, assumed to be the laboratory system of reference.

The electric fields at the position of the target and at time t, when the projectile passes by with an impact parameter b, are given by eqs. (1.1a, b) of the introduction. In the laboratory system the target has a non-relativistic motion and we can use the dipole approximation [see Ja-75]

$$\left(\frac{d^2 I}{d\omega \, d\Omega}\right)_{(2)} \simeq \frac{Z_2^2 e^2}{4\pi^2 c^3} \left|\int\limits_{-\infty}^{\infty} \hat{n} \times (\hat{n} \times \dot{\boldsymbol{v}}_2) e^{i\omega t}\right|^2$$

$$= \frac{Z_2^2 e^4}{4\pi^2 M_2^2 c^3} \left|\hat{n} \times \hat{n} \times [E_z(\omega) + E_T(\omega)]\right|^2 \tag{5.1.3}$$

where M_2 denotes the target rest mass, $\dot{\boldsymbol{v}}$ is its acceleration, and $E_z(\omega), E_T(\omega)$ are the Fourier transforms of the electric fields of eqs. (1.1). Expanding the triple vector product in eq. (5.1.3) we obtain

$$\left(\frac{d^2 I}{d\omega \, d\Omega}\right)_{(2)} = \frac{Z_1^2 Z_2^4 e^6 x^2}{\pi^2 M_2^2 c^3 b^2 v^2} \left[(1 - \cos^2 \theta) \frac{1}{\gamma^2} K_0^2(x) + (1 - \sin^2\theta \sin^2\phi) K_1^2(x)\right], \tag{5.1.4}$$

where $x = \omega b / \gamma v$, and (θ, ϕ) are the angular coordinates of $\hat{n}$.

The relation between eq. (5.1.4) and the differential cross section for emission of bremsstrahlung radiation is

$$\left(\frac{d\sigma_{br}}{dE_\gamma}\right)_{(2)} = \frac{1}{E_\gamma} \int\limits_{b=R}^{b=\infty} \left(\frac{d^2 I}{dE_\gamma \, d\Omega}\right)_{(2)} d^2 b \, d\Omega . \tag{5.1.5}$$

Both integrations can be done analytically and the final result can be written as

$$\left(\frac{d\sigma_{br}}{dE_\gamma}\right)_{(2)} = \frac{8\pi}{3} \left(\frac{Z_2^2 e^2}{M_2 c^2}\right)^2 \frac{1}{E_\gamma} n_{br}^{(2)}(E_\gamma) , \tag{5.1.6a}$$

where $n_{br}^{(2)}(E_\gamma)$ is equal to the equivalent photon number n_{E1} as given by eq. (1.9) with $Z = Z_1$. The result (5.1.6a) has a very nice interpretation: the emission of bremsstrahlung by the target (or by the projectile) can be viewed as the rescattering of the equivalent photons generated by the projectile (target). The bremsstrahlung cross section is then given by the product of the equivalent photon number per unit energy, given by $n_{E1}(E_\gamma)/E_\gamma$ and the *classical Thomson cross section*

$$\sigma_{\rm T} = (8\pi/3)(Z^2 e^2/Mc^2)^2 \, . \tag{5.1.6b}$$

To calculate the radiation emitted by the projectile we can use eq. (5.1.4) for the radiation emitted in the frame of reference of the projectile by exchanging the indices 1 and 2. Then we make a Lorentz transformation of $d^2 I/d\omega \, d\Omega$, ω and θ to the corresponding variables in the laboratory system (see eqs. (11.30 and 15.5) of Ja-75). We obtain

$$\left(\frac{d^2 I}{d\omega \, d\Omega}\right)_{(1)} = \frac{Z_1^4 Z_2^2 e^6 x^2}{\pi^2 M_1^2 c^3 b^2 v^2} \{[(1 - \beta \cos \theta)^2 - (\cos \theta - \beta)^2]K_0^2(y)$$

$$+ [\cos^2\phi(1 - \beta \cos \theta)^2 + (\cos \theta - \beta)^2]K_1^2(y)\} \, , \tag{5.1.7}$$

where $\beta = v/c$ and $y = \gamma x(1 - \beta \cos \theta)$. Integrating eq. (5.1.7) in the same way as in eq. (5.1.5) one finds

$$\left(\frac{d\sigma_{\rm br}}{dE_\gamma}\right)_{(1)} = \frac{8\pi}{3} \left(\frac{Z_1^2 e^2}{M_1 c^2}\right)^2 \frac{1}{E_\gamma} \, n_{\rm br}^{(1)}(E_\gamma) \, , \tag{5.1.8}$$

where

$$n_{\rm br}^{(1)}(E_\gamma) = \frac{3}{4\pi} \, Z_2^2 \alpha \left(\frac{c}{v}\right)^2 \xi^2$$

$$\times \int_{-1}^{1} du \left\{ \left[1 - \left(\frac{u - \beta}{1 - \beta u}\right)^2\right] \frac{1}{\gamma^2} \, (K_1^2 - K_0^2) + \frac{1}{2} \left[1 + \left(\frac{u - \beta}{1 - \beta u}\right)^2\right](K_0 K_2 - K_1^2) \right\} \, , \tag{5.1.9}$$

with the $K_{\rm N}$ as functions of $\chi = \gamma\xi(1 - \beta u)$, and $u = \cos \theta$. This last integration has to be solved numerically.

The radiation emitted by the projectile interferes with that from the target. To calculate it we have to expand the expression

$$\left(\frac{d^2 I}{d\omega \, d\Omega}\right)_{(3)} = \frac{e^2 \omega^2}{4\pi^2 c} \, (A_1^* \cdot A_2 + A_1 \cdot A_2^*) \, . \tag{5.1.10}$$

To that aim, we rewrite A_1 in the form

$$A_1 \simeq \frac{iZ_1}{\omega} \int_{-\infty}^{\infty} \frac{\hat{n} \times [(\hat{n} - v/c) \times \dot{v}/c]}{(1 - v \cdot \hat{n}/c)^2} \, e^{i\omega t(1 - \beta \cos \theta)} \, dt \, . \tag{5.1.11}$$

We then use $v = v\hat{z}$ in the laboratory system. We also calculate the acceleration $\dot{v}$ in the projectile frame of reference by the action of the fields (1.1). Transforming $\dot{v}$ to the laboratory system, the integration in eq. (5.1.11) can be solved analytically. The amplitude A_2 is simpler to calculate as was already shown in eqs. (5.1.3) and (5.1.4). Inserting A_1 and A_2 obtained in this way in eq. (5.1.10) we find

$$\left(\frac{d^2 I}{d\omega \, d\Omega}\right)_{(3)} = -\frac{2Z_1^3 Z_2^3 e^6 \omega^2}{\pi^2 \gamma^2 M_1 M_2 c^3 v^4} \frac{1}{(1-\beta \cos \theta)} \times \{(1-\cos^2 \theta)\gamma^{-3} K_0(x) K_0(y)$$

$$+ \tfrac{1}{2}(1+\cos^2 \theta - 2\beta \cos \theta) K_1(x) K_1(y)\} \, .$$

(5.1.12)

Integrating eq. (5.1.12) in the same way as in eq. (5.1.5) one finds

$$\left(\frac{d\sigma_{br}}{dE_\gamma}\right)_{(3)} = -\frac{8\pi}{3}\left(\frac{Z_1 Z_2 e^2}{\sqrt{M_2 M_1} c^2}\right)^2 \frac{1}{E_\gamma} n_{br}^{(3)}(E_\gamma) \, ,$$

(5.1.13)

where

$$n_{br}^{(3)}(E_\gamma) = -\frac{3}{\pi} Z_1 Z_2 \alpha \frac{1}{\gamma}\left(\frac{c}{v}\right)^2 \xi \int_{-1}^{1} \frac{du}{[(1-\beta u)^2 - 1/\gamma^2](1-\beta u)}$$

$$\times \left\{\frac{1-u^2}{\gamma^3}\left[(1-\beta u) K_0(\xi) K_1(\chi) - \frac{1}{\gamma} K_1(\xi) K_0(\chi)\right]\right.$$

$$+ \left.\tfrac{1}{2}(1+u^2 - 2\beta u)\left[(1-\beta u) K_1(\xi) K_0(\chi) - \frac{1}{\gamma} K_0(\xi) K_1(\chi)\right]\right\} \, .$$

(5.1.14)

For $Z_1 = Z_2$ and $\gamma \to 1$, we obtain $n_{br}^{(3)} = n_{br}^{(1)} + n_{br}^{(2)}$, which expresses the well-known result of absence of bremsstrahlung dipole radiation for non-relativistic Coulomb collisions of particles with equal charge-to-mass ratio.

In fig. 5.1 we show $n_{br}^{(i)}$ (for $i = 1$ solid line, for $i = 2$ dashed line, and for $i = 3$ dash–dotted line) as a function of the ratio between the nuclear dimension R and the photon wavelength, and for several values of γ. We used $Z_1 = Z_2 = 10$. One observes that $n_{br}^{(3)}$ becomes smaller in comparison to $n_{br}^{(1)}$ and $n_{br}^{(2)}$ as γ increases. In the limit $\gamma \to \infty$, $n_{br}^{(3)} \to 0$. This means that the radiations emitted by the projectile
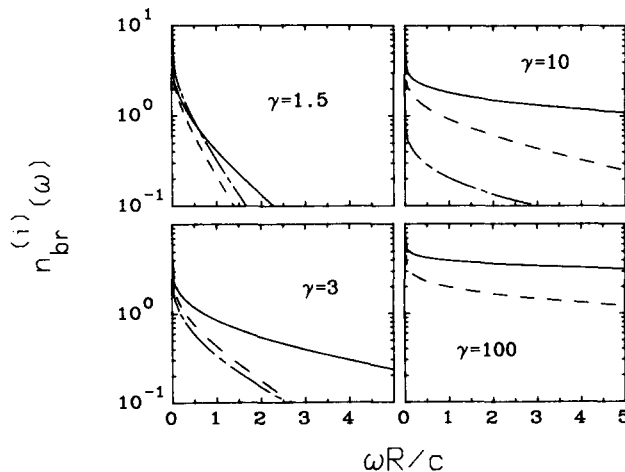

Fig. 5.1. The dimensionless bremsstrahlung strength functions $n_{br}^{(i)}$ (see text) plotted as a function of the ratio between the nuclear dimension R and the photon wavelength for several values of γ.

and by the target do not interfere with each other as $\gamma \to \infty$. It occurs because the recoil of the projectile is not instantaneously preceded by the recoil of the target as in the non-relativistic case. For relativistic energies the recoil of the nuclei is displaced in time by the retardation, which leads to the incoherent emission of radiation. Also, in that limit, the radiation emitted by the projectile is more intense than the one emitted by the target. This is because photons of energy E'_γ in the projectile system of reference, emitted approximately isotropically, appear in the laboratory within a forward cone $\theta_{max} \simeq 1/\gamma$ and with energies of the order of $E_\gamma \simeq \gamma E'_\gamma$, i.e. energetic photons in the laboratory system come from soft photons in the frame of reference of the projectile [see e.g. Ja-75, p. 708].

5.2. Comparison with nuclear bremsstrahlung

A more violent source of bremsstrahlung radiation has its origin in the collisions with $b < R_1 + R_2$ where part of the charges carried by the projectile almost comes into stop. To compare the relevance of these two different mechanisms of producing bremsstrahlung, i.e. the Coulomb and the nuclear one, we use the results of the work of Kapusta [Ka-77], where the nuclear bremsstrahlung in RHI collisions was calculated on the basis of a nuclear *fireball model* which accounts for the possible formation of two fireballs. Integrating eq. (5) of that reference with respect to the solid angle we obtain (for the special case of symmetrical systems, i.e. $Z_1 = Z_2 = Z$)

$$\left(\frac{d\sigma}{dE_\gamma}\right)_{Nbr} = 0.12 \frac{Z^2 \alpha R^2}{E_\gamma} [F(\beta) + F(\beta_{PF}) + F(\beta_{TF})$$
$$- 2\{G(\beta, \beta_{PF}) + G(\beta, \beta_{TF}) - G(\beta_{PF}, \beta_{TF})\}], \tag{5.2.1a}$$

where

$$F(\beta) = \frac{1}{\beta} \ln\left(\frac{1+\beta}{1-\beta}\right) - 2, \tag{5.2.1b}$$

$$G(\beta, \beta_F) = \frac{\beta \beta_F}{2(\beta - \beta_F)} \left[\frac{1-\beta_F^2}{\beta_F} F(\beta_F) - \frac{1-\beta^2}{\beta} F(\beta) + 2(\beta - \beta_F)\right], \tag{5.2.1c}$$

and

$$\beta_{PF} = \frac{\beta[1 + (1-\beta^2)^{1/2}](1+\eta)}{[1 + (1-\beta^2)^{1/2}]^2 + \eta\beta^2}, \qquad \beta_{TF} = \beta_{PF}(\eta \to -\eta), \tag{5.2.2}$$

are, respectively, equal to the projectile and target-fireball velocity. For one-fireball production, $\eta = 0$, so that $\beta_{PF} = \beta_{TF}$, and for two-fireball production, $0 < \eta < 1$. We use the transparency factor η equal to 75%, and define the dimensionless quantity

$$r(\gamma, E_\gamma) = \frac{(d\sigma/dE_\gamma)_{Nbr}}{(d\sigma/dE_\gamma)_{Cbr}}, \tag{5.2.3}$$

where the Coulomb bremsstrahlung cross section $(d\sigma/dE_\gamma)_{Cbr}$ is given by the sum of eqs. (5.1.6), (5.1.8) and (5.1.13). In table 5.1 we show $r(\gamma, E_\gamma)$ for the reaction $^{40}Ca + {}^{40}Ca$ and $E_\gamma = 10\,MeV$. One

Table 5.1

Ratio of nuclear and Coulomb bremsstrahlung cross sections
for the reaction $^{40}Ca + ^{40}Ca$ and $E_\gamma = 10$ MeV; the value of
$E_\gamma(d\sigma/dE_\gamma)_{Nbr}$ is also given

γ	$r(\gamma, E_\gamma = 10$ MeV$)$	$E_\gamma(d\sigma/dE_\gamma)_{Nbr}$ (mb)
1.1	2.6×10^2	5.1×10^{-2}
1.5	5.3×10^5	0.69
10	1.0×10^6	18.5
100	1.5×10^6	27.7

observes that only for low values of γ (in which case Coulomb repulsion corrections to the trajectory must be taken into consideration) the Coulomb bremsstrahlung is relevant. Also, for greater values of E_γ the ratio r increases.

Coulomb bremsstrahlung seems to be of little relevance in RHI collisions. Its role increases for collisions of less massive particles like electron or muon–nucleus scattering, as can be seen directly from eq. (5.1.6a) and, e.g., could be useful for obtaining information on the elastic scattering of photons on unstable particles, like pions. For example, in the process $Z + \pi \to Z + \pi + \gamma$ the scattering of photons on pions has been studied by Antipov et al. [Ant-83, Ant-85], as was already mentioned in section 4. With this method a value of the pion polarisability via the Rayleigh scattering amplitude could be obtained. This Rayleigh contribution increases in importance as compared to the Thomson scattering term (see eq. 5.1.6b) with increasing γ-energy.

6. K-shell ionization

Ionization of K-shell atomic electrons by means of relativistic particles is a subject of increasing theoretical and experimental interest [see e.g. An-87, Me-83, Mo-85]. Opposite to heavy ion scattering at nonrelativistic energies, in the relativistic case *K-shell ionization* is favoured as compared to L, M, etc. ionization of the atoms of a dense target as the ions penetrate it. Among the huge amount of theoretical calculations in this field, we cite Jamnik and Zupancic [Ja-57], Merzbacher and Lewis [Me-58], Davidovic et al. [Da-78], based on PWBA, Bang and Hansteen [Ba-59], Amundsen and Aashamar [Am-81], Becker et al. [Be-85, Va-84, Be-86b], based on semiclassical approaches, and Kolbenstvedt [Ko-67], Komarov [Ko-80], based on the equivalent photon method. Due to its simplicity and the possibility of having an easier insight into the subject we shall here use the same method as the last authors. We compare the final results with the ones obtained in the other approaches.

The method consists in separating the ionization processes into those arising from *close*, $b \leq a_K$, and from *distant*, $b > a_K$, collisions, where the K-shell radius is given by $a_K = \hbar^2/(mZe^2)$.

6.1. Close collisions

The period, T, for an electron in the K-shell is given by

$$T = \frac{2\pi\hbar}{I} = \frac{4\pi\hbar a_K}{Ze^2} = \frac{4\pi\hbar}{mc^2(Z\alpha)^2} , \tag{6.1.1}$$

where $I \simeq (Z\alpha)^2 mc^2/2$ is the ionization energy of the K-shell electron. The ratio of the collision time $t_{col} \simeq b/\gamma v$ in a RHI collision and the period of an electron in the K-shell is

$$\frac{t_{col}}{T} \simeq \frac{1}{4\pi} \frac{Z\alpha}{\gamma\beta} \frac{b}{a_K} .$$ (6.1.2)

When the impact parameter b is smaller than the K-shell radius a_K, we see that the collision time is always smaller than the period of the atomic electron for $\beta \simeq 1$, and that their ratio goes to zero in RHI collisions for which $\gamma \gg 1$. For such collisions the ionizing process can be considered as a collision between the projectile and a *free* electron, with an energy exchange larger than the ionization energy. In a semiclassical sense, we can say that the probability for the ionization of the atom in a collision with impact parameter $b \leq a_K$ is given by

$$P(b \leq a_K) = \int_{-\infty}^{\infty} dz/\Lambda(z) ,$$ (6.1.3)

where

$$\Lambda(z) = [2\rho(b, z)\, \sigma_{BC}(v, b, z)]^{-1}$$ (6.1.4)

is the *mean free path* for the collision between the projectile and the electron in a K-shell. In eq. (6.1.4) the quantity $\rho(b, z)$ is the electronic density in the K-shell at the point with coordinate $r = (b, z)$ with respect to the atomic nucleus, and $\sigma_{BC}(v, b, z)$ is the cross section for the (free) binary collision of the projectile and the electron. The factor two accounts for the presence of two electrons in the K-shell: if the atom contains only one electron in the K-shell, all following results must be divided by a factor two. In the case $\gamma \gg 1$, we can take σ_{BC} outside the integral in eq. (6.1.3), and for the electronic density in the K-shell we use the simplified, non-relativistic, hydrogenic 1s wavefunction, i.e.,

$$\rho(b, z) = |\psi(r)|^2 = (1/\pi a_K^3)\, e^{-2r/a_K} .$$ (6.1.5)

By means of these assumptions, we obtain

$$P(b \leq a_K) = \frac{4\sigma_{BC}}{\pi a_K^3} \int_0^{\infty} \exp\left\{ - \frac{2\sqrt{b^2 + z^2}}{a_K} \right\} dz = 2x\, K_1(x)\, \frac{\sigma_{BC}}{\pi a_K^2} ,$$ (6.1.6)

where $x = 2b/a_K$.
  Since

$$x\, K_1(x) \simeq \begin{cases} 1, & \text{for } x < 1 \\ \sqrt{(\pi x/2)}\, e^{-x}, & \text{for } x > 1, \end{cases}$$ (6.1.7)

the ionization probability, as a function of b, will be approximately constant up to $b \simeq a_K/2$, after which it diminishes exponentially. This behaviour has indeed been found in the more elaborate calculations of Amundsen and Aashamar [Am-81], and later on confirmed by Becker et al. [Be-85], which used first order time-dependent perturbation theory and exact Dirac–Coulomb wave functions for the electrons.

The total cross section due to close collisions is obtained from the integration of eq. (6.1.6) over b. One finds

$$\sigma_{b \leq a_K} \simeq \sigma_{BC} , \tag{6.1.8}$$

i.e., the total cross section for atom ionization in close RHI collisions is about the same as the binary collision cross section σ_{BC}. To calculate σ_{BC}, we observe that, due to Coulomb repulsion, the momentum and energy transferred to the electron, are given by

$$\Delta p = 2\gamma m v \sin(\theta/2) , \quad \text{and} \quad \Delta E = 2m\gamma^2 v^2 \sin^2(\theta/2) . \tag{6.1.9}$$

Now we use the Mott differential cross section for the free binary collision between projectile and electron, i.e.,

$$\frac{d\sigma}{d\Omega} = \frac{Z_1^2 r_e^2}{4} \frac{1 - \beta^2 \sin^2(\theta/2)}{\gamma^2 \beta^4 \sin^4(\theta/2)} , \tag{6.1.10}$$

where $r_e = e^2/mc^2$ is the classical electron radius. Using eq. (6.1.9) we can transform $d\sigma/d\Omega$ into an expression for $d\sigma/d(\Delta E)$, which after integration from $\Delta E_{min} = I$ to $\Delta E_{max} = 2m\gamma^2 v^2$ results in

$$\sigma_{BC} = C \frac{\pi Z_1^2 r_e^2}{\beta^4 \gamma^2} \int_x^1 \frac{1 - \beta^2 \zeta}{\zeta^2} \, d\zeta , \tag{6.1.11}$$

where $x = I/(2m\gamma^2 v^2)$, and C is a factor which accounts for the uncertainties in the integration limits: for example, the energy transferred to the atom can be of order I and be shared by the two electrons, which will not lead to ionization. For $\gamma \gg 1$ this integral gives

$$\sigma_{BC} = 2\pi C Z_1^2 r_e^2 \frac{mc^2}{I} \simeq C \frac{4\pi Z_1^2 r_e^2}{Z_2^2 \alpha^2} . \tag{6.1.12}$$

Inserting this in eq. (6.1.6) we find that the probability for ionizing an atom in a RHI collision with $b \leq a_K$ is approximately given by

$$P(b \leq a_K) \simeq 8C \, (Z_1 \alpha)^2 \, x \, K_1(x) . \tag{6.1.13}$$

Due to eq. (6.1.7), this result means that probability to ionize the atom in a RHI collision with impact parameter smaller than the K-shell radius is approximately constant, independent of the charge of the atom, and proportional to the square of the charge of the projectile. The calculations of Komarov [Ko-80] suggest the value $C = 1$, whereas the most exact calculations of Amundsen and Aashamar [Am-81] and of Becker et al. [Be-85] give $C \simeq 0.45$, that is,

$$P(b \leq a_K/2) \simeq 3.6 (Z_1 \alpha)^2 . \tag{6.1.14}$$

We observe that the simple description above shows remarkably good agreement with the main

features of more precise calculations. Nonetheless, the ionization probability as given by eq. (6.1.14) becomes greater than unity for $Z_1 > 72$ (!). This means that first order perturbation calculations, as those performed by Amundsen and Aashamar and by Becker et al., are not adequate to describe the impact parameter dependence of the ionization probabilities, even for projectiles with intermediate charge values. This can be easily explained by observing that for projectiles with large charges the Coulomb repulsion suffered by electrons in the K-shell will always be large enough to kick them off the orbit, i.e., the ionization probability will be one. Therefore, any perturbation theory will run into trouble in this limit.

For very high energies the contribution of impact parameters larger than the K-shell radius will become larger and larger, as we shall see. Also, for these impact parameters the ionization probability will always be much smaller than one, even for projectiles with very large charges. This means that the violation of the unitarity condition will not have a big influence in the calculation of the *total* ionization cross section.

6.2. Distant collisions

The probability to ionize the atom in a RHI collision with impact parameter larger than the K-shell radius can be calculated in the equivalent photon method by

$$P(b > a_K) = \int_{I/\hbar}^{\infty} N(\omega, b) \, \sigma_\gamma^K(\omega) \, \frac{d\omega}{\omega} \,, \qquad (6.2.1)$$

where $N(\omega, b)$ is the number of equivalent photons incident on the atom per unit area (see section 1), and

$$\sigma_\gamma^K(\omega) = \frac{128\pi}{Z_2^2 \alpha^3} \left(\frac{I}{\hbar\omega}\right)^4 \frac{e^{-4a \, \mathrm{arccot}\, a}}{1 - e^{-2\pi a}} \, \sigma_0 \,, \qquad (6.2.2a)$$

is the photo-electric cross section (see e.g. ref. [He-54] p. 208). In the above equality

$$\sigma_0 = \frac{8\pi}{3} r_e^2 = \frac{8\pi}{3} \frac{e^2}{mc^2} \,, \quad \text{and} \quad a = \sqrt{\frac{I}{\hbar\omega - 1}} \,. \qquad (6.2.2b)$$

The integration in the eq. (6.2.1) can be solved analytically by using the approximation (6.1.7) and by expanding the exponentials in eq. (6.2.2a) around $\hbar\omega \simeq I$, i.e. by putting

$$\sigma_\gamma^K(\omega) \simeq \frac{128\pi}{Z_2^2 \alpha^3} \left(\frac{I}{\hbar\omega}\right)^4 e^{-4} \, \sigma_0 \qquad (6.2.3)$$

in the integrand. We find

$$P(b > a_K) = 0.39 (Z_1 Z_2 \alpha^2)^2 \gamma^{-2} \, K_1^2 (Ib/\gamma\hbar c) \,, \qquad (6.2.4)$$

i.e. $P(b > a_K)$ will decay proportionally to $1/b^2$ until a *cutoff impact parameter* $b \simeq \gamma\hbar c/I$, after which it decays exponentially. For $b = a_K$ we find

$$P(b = a_K) \simeq 1.56(Z_1\alpha)^2 ,$$

which will always be appreciably smaller than one. This means that for these impact parameters one can perform calculations in the first order perturbation theory without problems. The behaviour of the ionization probabilities should not be much different than that given by eq. (6.2.4), what is indeed shown in refs. [Am-81 and Be-85].

Integrating eq. (6.2.4) from $b = a_K$ to $b = \infty$, we find

$$\sigma_{b>a_K} = 4.9 r_e^2 \frac{Z_1^2}{(Z_2\alpha)^2} \xi^2 \left[K_0^2 - K_1^2 + \frac{2}{\xi} K_0 K_1 \right] \simeq 9.8 r_e^2 \frac{Z_1^2}{(Z_2\alpha)^2} \ln\left(\frac{2\gamma}{Z_2\alpha}\right) , \qquad (6.2.5)$$

where $\xi = Ia_K/\gamma\hbar c$.

In fig. 6.1 we show the cross sections for K-shell ionization of lead atoms by means of relativistic argon projectiles as a function of γ. One notes that for great values of γ the contribution of distant collisions $\sigma_{b>a_K}$ is much larger than that from close collisions $\sigma_{b \leq a_K}$ which tends to a constant value for $\gamma \gg 1$.

There exist detailed experimental investigation of inner-shell ionization in electron impact at very high energies. [See, e.g., Ge-82.]

Since the ionization cross sections are large, the relativistic heavy ion ionization could perhaps be used as a variant of the well-known PIXE [see, e.g., Ca-80] technique for the analysis of materials. PIXE means Particle Induced X-ray Emission: one irradiates a target with light particles (mostly protons) and analyses the spectrum of the emitted Röntgen radiation, which originates when the electronic orbital holes of the ionized atoms are filled by electrons of the exterior orbits. This method has already many applications in physics, as well as in chemistry [see, e.g., Jo-76 and Kh-81].

In ref. [An-84] it is mentioned that the K-shell ionization contributes significantly to the stopping power of heavy ions. Therefore, the knowledge of these ionization processes is of interest for possible application of heavy ion bombardment to trigger the deuteron–tritium fusion reaction.
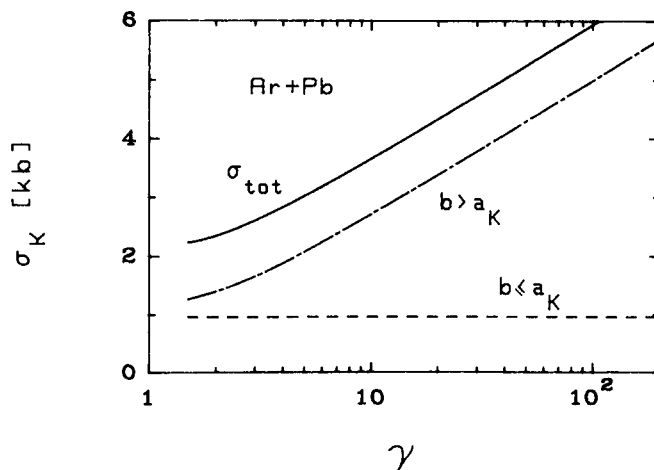

Fig. 6.1. Cross sections for atomic K-shell ionization of lead atoms by means of relativistic argon projectiles, as a function of the Lorentz factor γ. The dashed curve (dash–dotted) corresponds to the contribution of impact parameters smaller (larger) than the K-shell radius. The solid curve is the sum of the two contributions.

7. Lepton pair production in RHI collisions

Soon after the discovery of the positron in 1932, many theoretical works were performed which aimed to evaluate the cross sections for the production of electron–positron pairs in collisions of light (or a fast charged particle) with a nucleus. This was expected to be present in collisions originated by cosmic rays reaching the earth surface and this process would be an experimental check of the validity of the positron theory of Dirac which had just been born. Most of the earlier theoretical works on that subject have been done at about the same time, and in the special case of pair production in the collisions of relativistic charged particles, there were works by Furry and Carlson [Fu-33], Landau and Lifshitz [La-34], Bhabha [Bh-35], Racah [Ra-37], and Nishina, Tomonaga, and Kobayashi [Ni-35]. Except in the work by Furry and Carlson where the final result was shown to be wrong by a missing logarithmic factor, all other works reproduced the same results as that of Landau and Lifshitz [La-34] who studied e^+e^- *production* in a collision of two *fast nuclei* in the Born approximation and treated the projectile motion semiclassically.

It was only recently, with the construction of relativistic heavy ion accelerators, that a new interest in this field appeared [An-87]. The cross sections for pair-production in a collision between two charged particles is roughly proportional to $Z_1^2 Z_2^2$ and for heavy systems like $^{238}U + ^{238}U$ they will be very large, up to many kilobarns. This can be a cause of many difficulties in the study of experiments with relativistic heavy ions (RHI). For example, in RHI colliders they can lead to a beam loss due to the *capture* of slow electrons in an inner orbit of one of the ions [see, e.g., Be-87]; or it could even be useful in order to keep control of the beam luminosity, as was pointed out by Anholt and Gould [An-87].

Among the newest works on this subject [So-80, Ni-82, Be-86a, Ber-86b, Ber-87a, Ba-87a, Be-87], the most exact approach is the one followed by Becker, Grün and Scheid [Be-86a, Be-87] in the semiclassical approximation. They expanded the interaction potential in multipoles and used Coulomb–Dirac wavefunctions for the electron and the positron. In this way, they obtained the impact parameter dependence, as well as the cross sections, for e^+e^- production for any energy of the pair and for RHI beams up to 100 GeV/nucleon. One of the difficulties of the calculation is the evaluation of the multipole sums for beam energies around 100 GeV/nucleons and greater, because it relies strongly on long numerical computing. Another very useful approach is the equivalent photon method, which was used in refs. [So-80, Ber-86b and Ba-87a]. Besides being very simple to calculate, this method provides good quantitative derivation of the total cross sections, although it lacks of a more complete description of the process.

Bertulani and Baur [Ber-87a] have also used the semiclassical approach (which is appropriate for RHI collisions) to deduce the lepton pair (also muon and tau pairs) production probabilities and cross sections in RHI collisions, but instead of using the Coulomb–Dirac wave functions, they used Sommerfeld–Maue wavefunctions for the pair (see e.g. ref. [Be-54] and references therein). These wave functions are equal to the Coulomb–Dirac ones for the spatial region around the nuclei which most contribute to the cross sections. In this way one can avoid the multipole expansion used by Becker, Grün, and Scheid (actually, this had already been suggested by those authors in that paper). Since this process is very similar to the production of pairs by a real photon, we can use many of the integrals that were evaluated by Bethe, Maximon, Davies and Nordsiek [Be-54, Da-54, No-54]. We will show that analytical expressions can be obtained only in special cases of the pair energy. Denoting these energies by ε_+ and ε_-, we will show that we can deduce analytically the pair production probabilities and cross sections when (we use here natural units, with $\hbar = 1$, and $c = 1$)

$$\varepsilon_- , \ \varepsilon_+ \simeq m , \qquad \text{(slow pairs)} \qquad\qquad (7.\text{I}a)$$

$$m \ll \varepsilon_- , \quad \varepsilon_+ \ll \gamma m , \qquad \text{(fast pairs)} \tag{7.Ib}$$

$$\varepsilon_- , \quad \varepsilon_+ \simeq \gamma m , \qquad \text{(ultrafast pairs)} \tag{7.Ic}$$

where γ is the relativistic Lorentz factor associated with the heavy ion beam (see eq. (1.2)).

The results of Landau and Lifshitz are valid when the condition (7.Ib) is valid. Indeed, that is the energy region, which gives the greatest contribution to the total cross section, integrated over the energy of the pair. We show that for heavy ions there will be a correction to their results in a similar way to that found for pair production by a real photon in the field of a large-Z nucleus [Be-54, Da-54, No-54]. Analogous study has also been done by Nikishov and Pichkurov [Ni-82] in the energy region (7.Ib), but slightly different final results were obtained. The energy region inferred by the condition (7.Ic) is easily studied by means of a Lorentz transformation of the results obtained in the energy region (7.Ia), and it is also important since it can originate a cloud of pairs surrounding the projectile in RHI colliders.

In section 7.1 we evaluate the differential probabilities and cross sections for lepton pair production, and we apply it in section 7.2 to the case of slow and ultrafast lepton pairs, and in section 7.3 to fast lepton pairs, which is the most important case for $e^+ e^-$ pairs. In section 7.4 we extend the calculations to include the case for which the target (or the projectile) is not completely naked but still have a part (or all) of its atomic electrons.

Since their masses are much higher, the production of $\mu^+ \mu^-$ and $\tau^+ \tau^-$ pairs depends much more on the energy of the heavy ion beams, as we show in section 7.5. There we show that, if the heavy ion beam energy is not very high ($\gamma \geqslant 16$ for $\mu^+ \mu^-$ production, and $\gamma \geqslant 270$ for $\tau^+ \tau^-$ production), there is a big difference from the results for $e^+ e^-$ production.

In section 7.6 we obtain the cross sections for the pair-production with capture of the electron in an atomic orbit of the projectile, or of the target.

7.1. Probability amplitudes

In the following we shall calculate the electromagnetic production amplitude of lepton pairs in the field of a target nucleus with mass and charge number A_2 and Z_2, respectively, by means of a relativistic projectile with velocity v, impact parameter b, and mass and charge number A_1 and Z_1. The calculation is valid for impact parameters such that $b > R = R_1 + R_2$, where R_1 and R_2 are the respective nuclear radii. We shall consider the target nucleus as fixed, neglecting its recoil, and we place the origin of our coordinate system in its centre of mass.

In the semiclassical approach the projectile is assumed to move in a straight-line and will generate a time-dependent electromagnetic field which will lead to the production of pairs in the field of the target. Since the probability amplitude for pair production is, generally, smaller than unity, we can calculate it in the first order time-dependent perturbation theory (as soon as we take into account the distortion of the wavefunctions of the pair due to the field of the target nucleus). It is given by

$$a_{\ell^+ \ell^-} = \frac{1}{i} \int_{-\infty}^{\infty} dt\, e^{i\omega t} \langle \Psi_{\ell^-} | V(r, t) | \Psi_{\ell^+} \rangle , \tag{7.1.1}$$

where

$$\omega = \varepsilon_+ + \varepsilon_- \tag{7.1.2}$$

and Ψ_{ℓ^+} (Ψ_{ℓ^-}) is the wavefunction of the positive (negative) lepton. The interaction potential $V(r, t)$ is given by eqs. (2.1.3) and (2.1.4).

According to eq. (B.11) from appendix B, we can rewrite (7.1.1) as

$$a_{\ell^+\ell^-} = \frac{Z_1 e}{i\pi v} \int d^2 p_T \frac{H(p')}{p_T^2 + (\omega/\gamma v)^2} e^{ip_T \cdot b} ,$$ (7.1.3)

where

$$p' = (p_T, \omega/v) ,$$ (7.1.4)

and

$$H(p') = \int d^3 r \langle \Psi_{\ell^-} | v_\mu j_\mu(r) e^{ip' \cdot r} | \Psi_{\ell^+} \rangle ,$$ (7.1.5)

with $v_\mu = (1, v)$. The index T means an arbitrary direction, perpendicular to the beam. Using the continuity equation for the transition current and eq. (7.1.4), we can express the above matrix element in terms of the longitudinal and transversal components of the transition current as

$$H(p') = \int d^3 r \langle \Psi_{\ell^-} | \left[\frac{j_z}{v\gamma^2} + \frac{p_T \cdot j_T}{\omega} \right] e^{ip' \cdot r} | \Psi_{\ell^+} \rangle .$$ (7.1.6)

For $\gamma \gg 1$ we can neglect the first term inside brackets in the above equation, as it is done quite generally in the equivalent photon approximation. Then eq. (7.1.3) reduces to

$$a_{\ell^+\ell^-} = \frac{Z_1 e^2}{i\pi\omega v} \int \int d^2 p_T d^3 r \frac{p_T \cdot \langle \Psi_{\ell^-} | \alpha_T e^{ip' \cdot r} | \Psi_{\ell^+} \rangle}{p_T^2 + (\omega/\gamma v)^2} e^{ip_T \cdot b} ,$$ (7.1.7)

where we used $j_T = e\alpha_T$, and α_T is a Dirac matrix with component perpendicular to the beam direction.

For $\Psi_{\ell^\pm}$ we use the Sommerfeld–Maue wave functions which were also used by Davies, Bethe, and Maximon [Be-54, Da-54] (see also [Ak-65], p. 143) to calculate pair production by means of a real photon (see [Be-54] for a complete discussion about these wavefunctions), namely

$$\Psi_{\ell^-} = N_- e^{ik_- \cdot r}[1 - (i/2\varepsilon_-)\alpha \cdot \nabla] u \, F(-ia_-, 1, -ik_- r - ik_- \cdot r) ,$$ (7.1.8a)

and

$$\Psi_{\ell^+} = N_+ e^{-ik_+ \cdot r}[1 + (i/2\varepsilon_+)\alpha \cdot \nabla] w \, F(-ia_+, 1, ik_+ r + ik_+ \cdot r) ,$$ (7.1.8b)

where u and w are the Dirac spinors corresponding to the negative and positive leptons with momenta k_- and k_+, respectively, F is the confluent hypergeometric function and

$$a_\pm = Z_2 e^2/v_\pm , \qquad N_\pm = \exp[\mp \pi a_\pm/2] \, \Gamma(1 + ia_\pm) ,$$ (7.1.8c)

where $v_\pm$ equals the respective velocities of the created pair.

Inserting eq. (7.1.8) in eq. (7.1.7) we find

$$a_{\ell^+\ell^-} = \frac{Z_1 e^2}{\mathrm{i}\pi\omega v} N_+ N_- \sum_{\lambda=1,2} u^* [\alpha^\lambda G_{1\lambda} + \alpha^\lambda(\boldsymbol{\alpha}\cdot\boldsymbol{G}_{2\lambda}) + (\boldsymbol{\alpha}\cdot\boldsymbol{G}_{3\lambda})\alpha^\lambda] w \,, \tag{7.1.9}$$

where $\lambda = 1, 2$ represents the two orthogonal components transverse to the beam. The tensors $G_{1\lambda}$, $G_{2\lambda}$, and $G_{3\lambda}$ are given by

$$[G_{1\lambda}, G_{2\lambda}, G_{3\lambda}] = \int \mathrm{d}^2 p_\mathrm{T} \, \frac{p_\mathrm{T}^\lambda[I_1, I_2, I_3]}{p_\mathrm{T}^2 + (\omega/\gamma v)^2} \, \mathrm{e}^{\mathrm{i}\boldsymbol{p}_\mathrm{T}\cdot\boldsymbol{b}} \,, \tag{7.1.10}$$

where

$$I_1 = \int \mathrm{e}^{\mathrm{i}\boldsymbol{q}\cdot\boldsymbol{r}} F_1 F_2 \, \mathrm{d}^3 r \,, \tag{7.1.11a}$$

$$I_2 = \frac{\mathrm{i}}{2\varepsilon_+} \int \mathrm{e}^{\mathrm{i}\boldsymbol{q}\cdot\boldsymbol{r}} F_1 \nabla F_2 \, \mathrm{d}^3 r \,, \tag{7.1.11b}$$

$$I_3 = \frac{\mathrm{i}}{2\varepsilon_-} \int \mathrm{e}^{\mathrm{i}\boldsymbol{q}\cdot\boldsymbol{r}} F_2 \nabla F_1 \, \mathrm{d}^3 r \,, \tag{7.1.11c}$$

with

$$\boldsymbol{q} = \boldsymbol{p}' - \boldsymbol{k}_+ - \boldsymbol{k}_- \,, \tag{7.1.11d}$$

and

$$F_1 \equiv F(\mathrm{i}a_-, 1, \mathrm{i}k_- r + \mathrm{i}\boldsymbol{k}_- \cdot \boldsymbol{r}) \,, \qquad F_2 \equiv F(-\mathrm{i}a_+, 1, \mathrm{i}k_+ r + \mathrm{i}\boldsymbol{k}_+ \cdot \boldsymbol{r}) \,. \tag{7.1.11e}$$

The integrals (7.1.11) were calculated analytically by Nordsiek, Bethe, and Maximon [Be-54, No-54]. The differential probability for the production of lepton pairs is obtained from eq. (7.1.9) as

$$\mathrm{d}P_{\ell^+\ell^-} = \sum_{\text{spins}} |a_{\ell^+\ell^-}|^2 \rho_\mathrm{f} \,, \tag{7.1.12a}$$

where

$$\rho_\mathrm{f} = \frac{k_+ k_-}{(2\pi)^6} \, \varepsilon_+ \varepsilon_- \, \mathrm{d}\varepsilon_+ \, \mathrm{d}\varepsilon_- \, \mathrm{d}\Omega_+ \, \mathrm{d}\Omega_- \tag{7.1.12b}$$

is the density of final states of the pair.
Using the properties of the Dirac matrices we find

$$
\begin{aligned}
\mathrm{d}P_{\ell^+\ell^-} = \left(\frac{Z_1 e^2}{\pi \omega v}\right)^2 |N_+ N_-|^2 \frac{\rho_f}{\varepsilon_+ \varepsilon_-} \sum_\lambda \{ & [\varepsilon_+ \varepsilon_- - k_{+z} k_{-z} + m^2] |G_{1\lambda}|^2 \\
& + [\varepsilon_+ \varepsilon_- + k_{+z} k_{-z} - m^2][|G_{2\lambda}|^2 + |G_{3\lambda}|^2 - 2(G^*_{3\lambda})_z (G_{2\lambda})_z] - 2(\boldsymbol{k}_- \cdot \boldsymbol{G}^*_{2\lambda})(\boldsymbol{k}^{\mathrm{T}}_+ \cdot \boldsymbol{G}^{\mathrm{T}}_{3\lambda}) \\
& + 2(\boldsymbol{k}^{\mathrm{T}}_+ \cdot \boldsymbol{k}^{\mathrm{T}}_-)[(\boldsymbol{G}^{\mathrm{T}}_{3\lambda})^* \cdot \boldsymbol{G}^{\mathrm{T}}_{2\lambda}] + 2(\boldsymbol{k}_- \cdot \boldsymbol{G}^*_{3\lambda})[\boldsymbol{k}_+ \cdot \boldsymbol{G}_{2\lambda} - k_{+z}(G_{3\lambda})_z] \\
& + 2G^*_{1\lambda}[\varepsilon_- \{\boldsymbol{k}_+ \cdot \boldsymbol{G}_{2\lambda} - k_{+z}(G_{3\lambda})_z\} + \varepsilon_+ \{\boldsymbol{k}_- \cdot \boldsymbol{G}_{3\lambda} - k_{-z}(G_{2\lambda})_z\}] \\
& + 2k_{-z}(G^*_{2\lambda})_z [\boldsymbol{k}_+ \cdot (\boldsymbol{G}_{3\lambda} - \boldsymbol{G}_{2\lambda})] + \text{complex conjugate} \} .
\end{aligned}
\tag{7.1.13}
$$

In the approximations we are going to make, the integrals $[G_{1\lambda}, G_{2\lambda}, G_{3\lambda}]$ will be zero for one of the components, say $\lambda = 2$ if we choose b along the x-axis, and the sum in λ reduces to only one term.

7.2. Slow and ultrafast electron–positron pairs

7.2.1. Slow pairs

We now consider the production of low-energetic lepton pairs obeying the condition (7.Ia). We use the analytic expressions for the integrals (7.1.11) as given by the equations (6.13) of the work of Bethe and Maximon [Be-54] and keep only the terms in lowest order in k_+/m and k_-/m. Since only values of p_T up to $\omega/\gamma v \ll m$ will contribute to the integrals (7.1.11), we also put $p_T = 0$ in the numerators of those expressions. Inserting the obtained results for I_1, I_2, and I_3 in eq. (7.1.10), we find

$$
G_{12}, G_{22}, G_{32} = 0 ,
\tag{7.2.1a}
$$

and

$$
G_{11} = \frac{C}{\omega^3}\left[2(k_{-z} - k_{+z}) - i\omega Z_2 e^2 \frac{(k_+ k_{+z} + k_- k_{-z})}{k_+ k_-} \right] M(b, \omega, \gamma) ,
\tag{7.2.1b}
$$

$$
G_{21} = -\frac{C}{\omega^2}\left[\hat{z} + iZ_2 e^2 \frac{(k_+ k_{+z}\hat{z} - P/2)}{k_+ k_-} \right] M(b, \omega, \gamma) ,
\tag{7.2.1c}
$$

$$
G_{31} = \frac{C}{\omega^2}\left[\hat{z} - iZ_2 e^2 \frac{(k_- k_{-z}\hat{z} + P/2)}{k_+ k_-} \right] M(b, \omega, \gamma) ,
\tag{7.2.1d}
$$

with

$$
\boldsymbol{P} = k_- \boldsymbol{k}_+ - k_+ \boldsymbol{k}_- ,
\tag{7.2.2}
$$

and where $\hat{z}$ is a unit vector in the RHI beam direction. The function $M(b, \omega, \gamma)$ is given by

$$
\begin{aligned}
M(b, \omega, \gamma) &= \omega \int \mathrm{d}^2 p_T \frac{p_T \cos\theta\, e^{ip_T b \cos\theta}}{[p_T^2 + (\omega/\gamma v)^2][p_T^2 + \omega^2]} \\
&= \frac{2\pi i}{1 - 1/\gamma^2 v^2}\left[\frac{1}{\gamma v} K_1\left(\frac{\omega b}{\gamma v}\right) - K_1(\omega b) \right] ,
\end{aligned}
\tag{7.2.3}
$$

where K_1 is the modified Bessel function of first order. Inserting eq. (7.2.1) in eq. (7.1.13) and keeping only the lowest order terms in k_+/m and k_-/m, we find

$$dP_{\ell^+\ell^-}(b) = \frac{8}{(2\pi)^8} Z_1^2 Z_2^2 e^4 \frac{k_+ k_-}{\omega^6 v^2} |N_+ N_- C|^2 |M(b,\omega,\gamma)|^2$$

$$\times \{[k_+^2 \sin^2\theta_+ + k_-^2 \sin^2\theta_-][1-(Z_2 e^2)^2] + 2\varepsilon_+ \varepsilon_- (Z_2 e^2)^2\} \, d\Omega_+ \, d\Omega_- \, d\varepsilon_+ \, d\varepsilon_- \, .$$

$$(7.2.4)$$

The impact parameter dependence of eq. (7.2.4) is imbedded in the function $M(b,\omega,\gamma)$, which we plot in fig. 7.1 as a function of ωb and for $\gamma = 100$. We observe that M tends rapidly to its asymptotic value for $\omega b \gtrsim 1$. This asymptotic value is obtained by neglecting the second term inside brackets in the numerator, and the second term in the denominator of eq. (7.2.3), i.e. we can set

$$M \simeq \frac{2\pi i}{\gamma v} K_1\left(\frac{\omega b}{\gamma v}\right), \quad \text{for} \quad b \gtrsim \frac{1}{m}, \quad\quad (7.2.5)$$

where we used the approximation $\omega \simeq 2m$.

Since the Compton wavelength of the muon (or tau) is much smaller than the nuclear dimensions, this approximation is very good for describing the impact parameter dependence of $\mu^+\mu^-$ and $\tau^+\tau^-$ pair production. Nonetheless, in the case of e^+e^- it will only be appropriate for impact parameters larger than the Compton wavelength of the electron, which is much larger than the nuclear dimensions. As we will soon see, this will have as a consequence that the total cross section, integrated over all impact parameters will depend on the nuclear dimensions in the case of muon and tau pair production, but not in the case of electron pair production. This will lead to very different behaviour of the cross sections in the two cases. Let us therefore study first the case of e^+e^- production and let the study of $\mu^+\mu^-$ and $\tau^+\tau^-$ production to the section 7.5.

In the case of e^+e^- production one can have impact parameters much smaller than the Compton wavelength, for which we see in fig. 7.1 that $M \rightarrow 0$, what seems to be an unrealistic behaviour. In fact, the probability to produce an electron–positron pair should go to a constant value as $b \rightarrow 0$, what was
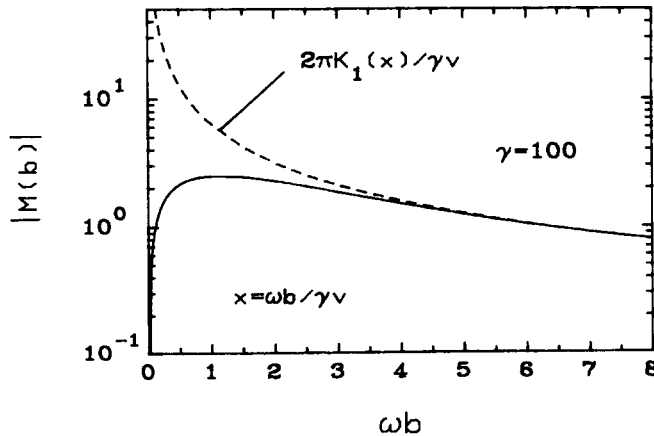

Fig. 7.1. Impact parameter dependence of the production probability of slow electron–positron pairs in RHI collisions expressed in terms of the dimensionesss function $M(b)$ as given by eq. (7.2.3). The dashed line corresponds to its asymptotic limit, as given by eq. (7.2.5).

indeed shown in the calculations of Becker, Grün and Scheid [Be-86a]. We would obtain the same in our calculations if we had not neglected the first term inside the brackets in eq. (7.1.6), which although it does not contribute appreciably to the cross section, has a finite, non-zero contribution for the differential probability as $b \rightarrow 0$. But for $\omega b \gtrsim 1$ the impact parameter dependence is very well reproduced by using the approximation (7.2.5). Moreover, the differential probability decreases very slowly until impact parameters much larger than the Compton wavelength of the electron and the uncertainty about the impact parameter dependence for $b \lesssim 1/m$ is not very important for the total cross section, especially for RHI collisions.

The modified Bessel function of first order has the following property (see eq. 6.1.7):

$$(\omega b / \gamma v) \, K_1(\omega b / yv) \simeq \begin{array}{ll} 1, & \text{for} \quad \omega b / \gamma v < 1, \\ 0, & \text{for} \quad \omega b / \gamma v > 1. \end{array}$$ (7.2.6)

This implies that the pair production probability decays like $1/b^2$ for impact parameter b larger than the Compton wavelength, i.e., for $b > 1/m$, until to a cutoff limit given by $b \simeq \gamma v / \omega$. Above this cutoff limit it will decay exponentially, which will guarantee the convergence of the cross section. Indeed, with these simplifications the differential cross section can be easily obtained by using

$$g(\zeta) = 2\pi \int_{1/m}^{\infty} b \left(\frac{\omega}{\gamma v} \right)^2 K_1^2 \left(\frac{\omega b}{\gamma v} \right) db = \pi \zeta^2 \left[K_0^2 - K_1^2 + \frac{2}{\zeta} K_0 K_1 \right]$$

$$\simeq 2\pi \ln(\delta / \zeta) \quad \text{for} \quad \zeta \ll 1,$$ (7.2.7a)

where the Bessel functions K_N are functions of the parameter

$$\zeta = \omega / \gamma m v,$$ (7.2.7b)

and $\delta = 0.681\ldots$ is a number related to the Euler's constant. We can write the result as (putting $v = 1$)

$$d\sigma_{e^+e^-} = \frac{4}{\pi} (Z_1 Z_2 r_e \alpha)^2 \frac{k_+ k_-}{\omega^6} \frac{a_+ a_-}{(e^{2\pi a_+} - 1)(1 - e^{-2\pi a_-})} \ln \left(\frac{\gamma \delta m}{\omega} \right)$$

$$\times \{ [k_+^2 \sin^2 \theta_+ + k_-^2 \sin^2 \theta_-][1 - (Z_2 \alpha)^2] + 2\varepsilon_+ \varepsilon_-(Z_2 \alpha)^2 \} \, d\Omega_+ \, d\Omega_- \, d\varepsilon_+ \, d\varepsilon_-,$$ (7.2.8)

where $r_e = e^2/mc^2 = 2.817\ldots$ fm is the classical electron radius, $\alpha = e^2/\hbar c \simeq 1/137$ is the fine structure constant, and we used

$$|N_+ N_- C|^2 = \frac{4(2\pi)^4 \alpha^2 a_+ a_-}{(e^{2\pi a_+} - 1)(1 - e^{-2\pi a_-})},$$ (7.2.9)

which can be inferred from the definitions (7.1.8c). From eq. (7.2.8) one can calculate the invariant mass of the e^+e^- pairs for a given experimental setup. We observe that the angular distribution of the slow pairs is symmetric around 90° due to the presence of the sine functions inside brackets of eq. (7.2.8); i.e., slow pairs are created preferentially with respective velocities perpendicular to the beam direction.

The angular integrations can be carried out easily and we get

$$\frac{d^2\sigma_{e^+e^-}}{d\varepsilon_+\,d\varepsilon_-} = \frac{128\pi}{3}\,(Z_1Z_2r_e\alpha)^2\,\frac{a_+a_-}{(e^{2\pi a_+}-1)(1-e^{-2\pi a_-})}\,\frac{\sqrt{(\varepsilon_+-m)(\varepsilon_--m)}}{\omega^4}$$

$$\times\,[(\omega-2m)+(Z_2\alpha)^2(\tfrac{7}{2}m-\omega)]\ln(\gamma\delta m/\omega)\,.\tag{7.2.10}$$

For heavy ions, and for pair energies such that $(\varepsilon_\pm - m) \ll m$, we have in most cases

$$a_\pm = Z_2\alpha\sqrt{m/2(\varepsilon_\pm - m)} \gg 1\,.\tag{7.2.11}$$

Then eq. (7.2.10) simplifies to

$$\frac{d^2\sigma_{e^+e^-}}{d\varepsilon_+\,d\varepsilon_-} = 32\pi Z_1^2 Z_2^6 \alpha^6 r_e^2\,\frac{m^2}{\omega^4}\ln\!\left(\frac{\gamma\delta m}{\omega}\right)e^{-2\pi a_+}\,.\tag{7.2.12}$$

In fig. 7.2 we plot the dimensionless function $(m/r_e)^2(d^2\sigma/d\varepsilon_+\,d\varepsilon_-)$ obtained from eq. (7.2.10) as a function of $(\varepsilon_- - m)/m$ for $(\varepsilon_+ - m)/m = 0.01$, and as a function of $(\varepsilon_+ - m)/m$ for $(\varepsilon_- - m)/m = 0.01$. The dashed lines correspond to the approximation (7.2.12). We observe that, while it increases rapidly as a function of ε_+, it is approximately constant as a function of ε_-. This is a consequence of the different behaviour of the electron and the positron wavefunctions in the Coulomb field of the target. The positrons are very unlikely to be produced with small kinetic energies due to the Coulomb repulsion in the field of the target nucleus. For targets with small charge this effect diminishes because a_+ gets smaller and the energy distribution for positrons and electrons tends to be a symmetric function of ε_+ and ε_- (see eq. 7.2.13).

In the collisions of nuclei with small charge (like e.g. α–α collisions) and for pair energies such that $a_\pm \ll 1$, eq. (7.2.10) becomes

$$\frac{d^2\sigma_{e^+e^-}}{d\varepsilon_+\,d\varepsilon_-} = \frac{32}{3\pi}\,(Z_1Z_2r_e\alpha)^2\sqrt{(\varepsilon_+-m)(\varepsilon_--m)}\,\frac{(\omega-2m)}{\omega^4}\ln\!\left(\frac{\gamma\delta m}{\omega}\right),\tag{7.2.13}$$
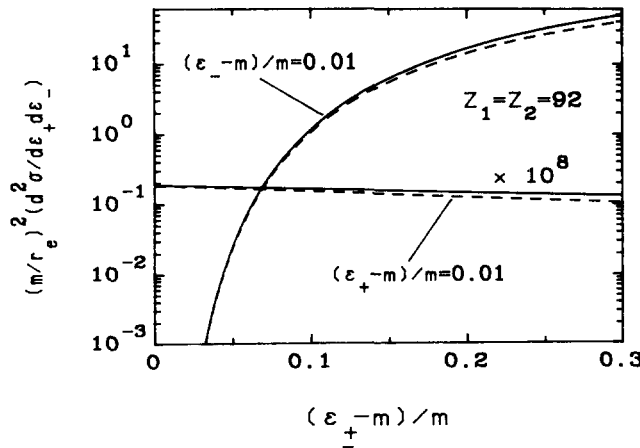
Fig. 7.2. The double differential cross section $d^2\sigma/d\varepsilon_+\,d\varepsilon_-$ in units of r_e^2/m^2, for $Z_1 = Z_2 = 92$, and as a function of $(\varepsilon_+ - m)/m$ for $(\varepsilon_- - m)/m = 0.01$ (increasing curve). Also shown is the dependence of this function with respect to $(\varepsilon_- - m)/m$ for $(\varepsilon_+ - m)/m = 0.01$ (flat curve). This curve is multiplied by 10^8 in order to be shown in the same figure. The dashed lines correspond to the approximation (7.2.12).
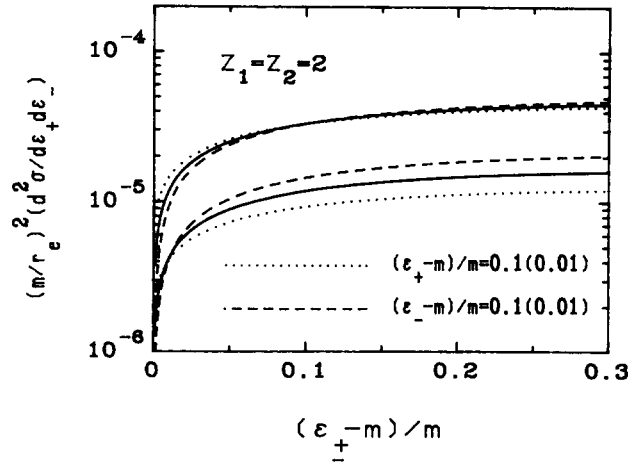
Fig. 7.3. The double differential cross section $d^2\sigma/d\varepsilon_+\,d\varepsilon_-$ in units of r_e^2/m^2 and as a function of $(\varepsilon_+ - m)/m$ for $(\varepsilon_- - m)/m = 0.1$ (upper dashed curve), and 0.01 (lower dashed curve) for $Z_1 = Z_2 = 2$. Also shown is the dependence of this function with respect to $(\varepsilon_- - m)/m$ for $(\varepsilon_+ - m)/m = 0.01$ (upper dotted curve), and 0.01 (lower dotted curve). The solid curves correspond to the approximation (7.2.15).

which is symmetric in ε_+ and ε_-. In fig. 7.3 we plot the same function as in fig. 7.2, but for $Z_1 = Z_2 = 2$. The solid curves correspond to the approximation (7.2.13) for $(\varepsilon_+ - m)/m = 0.1$ (upper curve), and 0.01 (lower curve). The other curves are obtained from eq. (7.1.10) for $\varepsilon_+ = $ constant (dotted curves), and for $\varepsilon_- = $ constant (dashed curves), and show the deviations from the approximation (7.2.13).

As a last remark, we observe that when the relative velocity v_r of the created pair is very small, i.e., when

$$v_r \lesssim \alpha = 1/137,\tag{7.2.14}$$

then one must take into account the Coulomb interaction between these particles. This was considered by Sacharov [Sa-48] in connection with the formation of a bound state of the electron–positron system (positronium). Since the main effect of considering the distortion of the Coulomb field is the presence of the terms containing $a_\pm$ in eq. (7.2.8), we can also make a correction to include the case (7.2.14) by multiplying (7.2.8) by the factor

$$\frac{2\pi\alpha/v_r}{1 - e^{-2\pi\alpha/v_r}}.\tag{7.2.15}$$

This correction will have as a consequence that the momentum of the electron and of the positron will be strongly correlated and that the cross section (7.2.8) will have a sharp maximum when they are approximately equal in magnitude and in direction, i.e., for $k_+ \simeq k_-$ (see also [La-86], p. 387).

7.2.2. Ultrafast pairs

The calculations of the last section can also be used to determine the probabilities and cross sections to produce slow pairs in the frame of reference of the projectile, as soon as we make the exchange $Z_1 \leftrightarrow Z_2$ and evaluate the pair momenta and energies in that frame. However, in the laboratory frame of reference (target frame) these pairs will be very fast, with energies in the region given by eq. (7.Ic).

Since the pairs are seen in the projectile frame moving approximately perpendicular to the beam direction, they will be observed in the laboratory frame moving very forwardly up to a maximum spreading angle of about $m/\varepsilon_\pm \simeq 1/\gamma \ll 1$ (here use the notation $\varepsilon'_\pm$, etc. in the projectile frame, and $\varepsilon_\pm$, etc. in the laboratory frame).

We can deduce the cross section for the production of ultrafast pairs by making a Lorentz transformation of the expression (7.2.8) to the laboratory system. We use that $k_+ k_-\, d\Omega_+\, d\Omega_-\, d\varepsilon_+\, d\varepsilon_-$ is a Lorentz invariant quantity, and that for $\gamma \gg 1$, and $\theta \ll 1$, we have $\varepsilon'_\pm \simeq (\varepsilon_\pm/2\gamma)(1 + \gamma^2\theta^2)$. We also use $k_\pm \simeq \varepsilon_\pm$, and since the average value of $\gamma^2\theta^2$ is of order of unity, we set $\varepsilon'_\pm \simeq \varepsilon_\pm/\gamma$ where possible. Then the angular integration can be performed easily and we obtain

$$\frac{d^2\sigma_{e^+e^-}}{d\varepsilon_+\, d\varepsilon_-} = \frac{64\pi}{5}\,(Z_1 Z_2 r_e \alpha)^2\,\frac{a_+^T a_-^T}{(e^{2\pi a_+^T} - 1)(1 - e^{-2\pi a_-^T})}\,\frac{\varepsilon_+ \varepsilon_-}{\omega^6}$$

$$\times \{(\varepsilon_+^2 + \varepsilon_-^2)[1 - (Z_1\alpha)^2] + 2\varepsilon_+\varepsilon_-(Z_1\alpha)^2\}\,\ln(\gamma^2\delta m/\omega)\,, \tag{7.2.16}$$

where

$$a_\pm^T = Z_1\alpha/v_\pm^T\,, \tag{7.2.17}$$

with $v_\pm^T$ equal to the transverse velocity of the pair. When $a_\pm^T \ll 1$ eq. (7.2.16) simplifies to

$$\frac{d^2\sigma_{e^+e^-}}{d\varepsilon_+\, d\varepsilon_-} = \frac{16}{5\pi}\,(Z_1 Z_2 r_e \alpha)^2\,\frac{\varepsilon_+ \varepsilon_-}{\omega^6}\,(\varepsilon_+^2 + \varepsilon_-^2)\,\ln\!\left(\frac{\gamma^2\delta m}{\omega}\right)\,. \tag{7.2.18}$$

Although this formula is only valid for pair energies $\varepsilon_\pm \simeq \gamma m$, it shows a close resemblance to the results for fast-pairs which we calculate in the next section. Nonetheless, since the energy region where the above equation can be applied is very restricted, most of the pairs will be created with energies obeying the condition (7.Ib), as we shall see in the next section.

7.3. Fast electron–positron pairs

We now consider the production of energetic lepton pairs obeying the condition (7.Ib). We use again the expressions (6.13) given in the work of Bethe and Maximon [Be-54] and disregard terms of order $(m/\varepsilon_\pm)^2$ and higher. We also put $p_T = 0$ in the numerators of those expressions. We find

$$I_1 = 2C\,\frac{\varepsilon_+ \varepsilon_-}{\omega}\,\frac{1}{[m^2 + (p_T - k_+^T)^2][m^2 + (p_T - k_-^T)^2]}$$

$$\times \left\{ V_\pm(x)\,\frac{(k_+^T)^2 - (k_-^T)^2}{[p_T - (k_+^T + k_-^T)]^2} + i\,\frac{Z_2\alpha}{m^2}\,W_\pm(x)\,[m^2 + (k_+^T)^2 + (k_+^T)^2] \right\}\,, \tag{7.3.1a}$$

$$I_2 = C\,\frac{\varepsilon_-}{\omega}\,\frac{1}{[m^2 + (p_T - k_-^T)^2]}$$

$$\times \left\{ V_\pm(x)\,\frac{(k_+^T + k_-^T)}{[p_T - (k_+^T + k_-^T)]^2} + i\,\frac{Z_2\alpha}{m^4}\,W_\pm(x)\,[k_+(k_-^T)^2 - m^2 k_-^T] \right\}\,, \tag{7.3.1b}$$

$$I_3 = C \frac{\varepsilon_+}{\omega} \frac{1}{[m^2 + (p_T - k_+^T)^2]}$$

$$\times \left\{ -V_\pm(x) \frac{(k_+^T + k_-^T)}{[p_T - (k_+^T + k_-^T)]^2} + i \frac{Z_2 \alpha}{m^4} W_\pm(x) [k_-(k_+^T)^2 - m^2 k_+^T] \right\}, \tag{7.3.1c}$$

where

$$V_\pm(x) = F(-ia_+, ia_-; 1; x), \tag{7.3.2a}$$

$$W_\pm(x) = F(1 - ia_+, 1 + ia_-; 2; x), \tag{7.3.2b}$$

and

$$x = 1 - \frac{(k_+^T + k_-^T)^2 [\omega^2 - (k_+ - k_-)^2]}{4\omega^2 (\varepsilon_+ - k_{+z})(\varepsilon_- - k_{-z})}. \tag{7.3.2c}$$

Substituting these equations in the integrals (7.1.10) we will find that they are much more complicated than the ones in the section 7.2 due to the fact that the denominators contain the quantities k_+^T and k_-^T which are not negligible in comparison with m. Indeed, for fast pairs the angular distribution is very forward peaked and their transverse momenta will be of order

$$k_+^T, k_-^T \simeq m. \tag{7.3.3}$$

But this implies that, again for $b \gtrsim 1/m$ we can take those denominators outside of the integrals over p_T by putting $p_T = 0$ in them. This simplifies the calculation enormously, since now we can calculate the integral in p_T analytically as in the case of slow pairs, and we obtain

$$G_{11} = 4\pi C \frac{\varepsilon_+ \varepsilon_-}{\gamma v} K_1\left(\frac{\omega b}{\gamma v}\right) \frac{1}{[m^2 + (k_+^T)^2][m^2 + (k_-^T)^2]}$$

$$\times \left\{ V_\pm(x) \frac{(k_+^T)^2 - (k_-^T)^2}{(k_+^T + k_-^T)^2} + i \frac{Z_2 \alpha}{m^2} W_\pm(x) [m^2 + (k_+^T)^2 + (k_-^T)^2] \right\}, \tag{7.3.4a}$$

$$G_{21} = 2\pi C \frac{\varepsilon_-}{\gamma v} K_1\left(\frac{\omega b}{\gamma v}\right) \frac{1}{[m^2 + (k_-^T)^2]}$$

$$\times \left\{ V_\pm(x) \frac{(k_+^T + k_-^T)}{(k_+^T + k_-^T)^2} + i \frac{Z_2 \alpha}{m^4} W_\pm(x) [k_+(k_-^T)^2 - m^2 k_-^T] \right\}, \tag{7.3.4b}$$

$$G_{31} = 2\pi C \frac{\varepsilon_+}{\gamma v} K_1\left(\frac{\omega b}{\gamma v}\right) \frac{1}{[m^2 + (k_+^T)^2]}$$

$$\times \left\{ -V_\pm(x) \frac{(k_+^T + k_-^T)}{(k_+^T + k_-^T)^2} + i \frac{Z_2 \alpha}{m^4} W_\pm(x) [k_-(k_+^T)^2 - m^2 k_+^T] \right\} \tag{7.3.4c}$$

Inserting this result in eq. (7.1.13) we will find a complicated angular structure for the differential probability. But, this angular distribution is of the same form as that found by Bethe and Maximon [Be-54] for e^+e^--production by a real photon. Therefore, using the same steps as they used for the evaluation of the angular integration, it is straightforward to show that the differential probability for the production of fast pairs is given by

$$\frac{d^2 P_{e^+e^-}}{d\varepsilon_+ \, d\varepsilon_-} = \frac{4}{\pi^2} \, (Z_1 Z_2 \alpha r_e)^2 \, \frac{1}{\gamma^2} \, K_1^2\left(\frac{\omega b}{\gamma}\right) \frac{1}{\omega^2} \, [\varepsilon_+^2 + \varepsilon_-^2 + \tfrac{2}{3}\varepsilon_+\varepsilon_-]\left[\ln\left(\frac{2\varepsilon_+\varepsilon_-}{m\omega}\right) - \tfrac{1}{2} - f(Z_2)\right],$$
(7.3.5)

where

$$f(Z) = Z^2 \alpha^2 \sum_{n=1}^{\infty} \frac{1}{n(n^2 + Z^2 \alpha^2)} \, .$$
(7.3.6)

Here we find already a crucial physical difficulty within this approach. Since the pairs with energies in the range given by eq. (7.Ib) obey the same conditions in the projectile frame of reference, this expression should have the same structure if it was calculated in that frame of reference. But it is not so, because if we had calculated it in the frame of reference of the projectile, it would mean a simple exchange $Z_2 \leftrightarrow Z_1$ in eq. (7.3.5), which would lead to a different result due to the presence of the function $f(Z_1)$ in eq. (7.3.5). This difficulty arises because our approach is not symmetric in the nuclear charges from the very beginning. For example, the wave functions for the electron and positron are determined in the frame of reference of the nucleus at rest, neglecting the influence of the other nucleus on them. A solution to this problem by using a Lorentz covariant theory with Lorentz transformed wave functions for the electron–positron pair is, by no way, simple, and to restore the required symmetry in the nuclear charges we postulate an average of the expressions obtained in the projectile and in the target system of reference as a reasonable result. This amounts in the substitution of the function $f(Z_2)$ by the averaged one

$$\bar{f}(Z_1, Z_2) = [1/(Z_1 + Z_2)][Z_1 \, f(Z_1) + Z_2 \, f(Z_2)] \, .$$
(7.3.7)

When $Z_1 \ll Z_2$ (or $Z_2 \ll Z_1$), this modification is not relevant, since in eq. (7.3.5) it will appear $f(Z_G)$ where Z_G is the greater from (Z_1, Z_2). But, when $Z_1 \simeq Z_2$ the approximation (7.3.7) is rather speculative, because we do not know how the influence of both nuclear charges on the electron–positron wave functions will be. This point may be a source for future investigations.

Integrating eq. (7.3.5) over ε_- we find

$$\frac{dP_{e^+e^-}}{d\varepsilon_+} \simeq \frac{112}{9\pi^2} \, (Z_1 Z_2 \alpha r_e)^2 \, \frac{1}{\gamma^2} \, K_1^2\left(\frac{2\varepsilon_+ b}{\gamma}\right)\varepsilon_+\left[\ln\left(\frac{\varepsilon_+}{m}\right) - \frac{1}{2} - \bar{f}(Z_1, Z_2)\right].$$
(7.3.8)

The same result can be obtained for $dP_{e^+e^-}/d\varepsilon_-$ by exchanging the indices $-$ and $+$ in eq. (7.3.8). The respective expressions for the differential cross sections can be deduced from eqs. (7.3.5) and (7.3.8) by using the integral (7.2.7). For example, the differential cross section $d\sigma/d\varepsilon_+$ is equal to

$$\frac{d\sigma_{e^+e^-}}{d\varepsilon_+} = \frac{56}{9\pi} \, (Z_1 Z_2 \alpha r_e)^2 \, \frac{1}{\varepsilon_+} \left[\ln\left(\frac{\varepsilon_+}{m}\right) - \frac{1}{2} - \bar{f}(Z_1, Z_2)\right]\ln\left(\frac{\gamma \delta m}{2\varepsilon_+}\right).$$
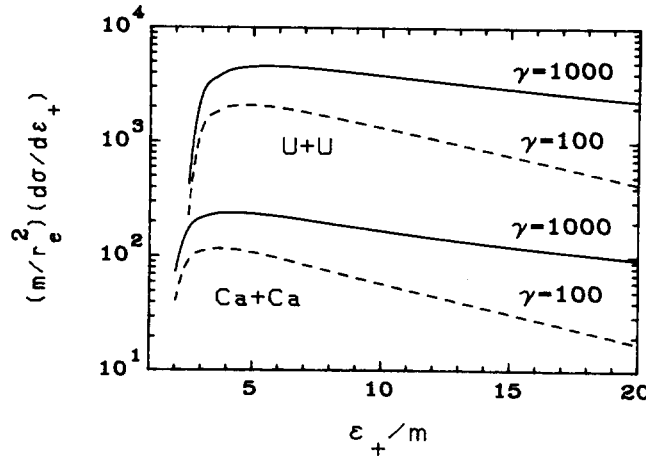(7.3.9)

Fig. 7.4. The differential cross section $d\sigma_{e^+e^-}/d\varepsilon_+$ for production of e^+e^- pairs in uranium–uranium collisions (upper curves) and calcium–calcium collisions (lower curves) as a function of the positron energy ε_+, and for $\gamma = 100$ and 1000.

In fig. 7.4 we plot the differential cross section $d\sigma_{e^+e^-}/d\varepsilon_+$ for production of e^+e^- pairs in uranium–uranium collisions and calcium–calcium collisions as a function of the positron energy ε_+, and for $\gamma = 100$ and 1000. Already here we see that the creation of positrons (and electrons) with small energies is strongly suppressed in comparison with the ones with higher energies and, when γ increases, more and more positrons (and electrons) with higher energies are produced. Indeed, in this figure we see that the dashed curve ($\gamma = 100$) decreases faster with increasing energy of the positrons than the full curve ($\gamma = 1000$).

Now we integrate (7.3.8) over ε_+ and use the approximation (7.2.6), in order to obtain the probability to create a e^+e^- pair in a RHI collision as a function of the impact parameter:

$$P_{e^+e^-}(b) \simeq \frac{14}{9\pi^2} (Z_1 Z_2 \alpha r_e)^2 \frac{1}{b^2} \left[\ln^2\left(\frac{\gamma\delta}{2mb}\right) - [1 + 2\bar{f}(Z_1, Z_2)] \ln\left(\frac{\gamma\delta}{2mb}\right) \right], \tag{7.3.10}$$

valid for $\gamma\delta/m \gtrsim b \gtrsim 1/m$.

In fig. 7.5 we plot the probability to create a e^+e^- pair in uranium–uranium and calcium–calcium collisions as a function of the Lorentz factor γ, and for impact parameter equal to the Compton wavelength $b = 1/m$. We note that for calcium–calcium collisions, $P_{e^+e^-} \ll 1$, even for very large values of γ, which justifies the use of first order perturbation theory. Nonetheless, for uranium–uranium collision, $P_{e^+e^-} > 1$, for $\gamma \gtrsim 500$, which violates the unitarity condition. This means that for extremely high energies, greater than several hundreds of GeV/nucleon, and for very heavy ions, it will be necessary to account for higher order terms in the perturbation theory. In other words, one must consider the probability of creating two or more pairs in a single collision above those energies.

As we mentioned before, $P_{e^+e^-}(b)$ goes to a constant, finite value for $b \lesssim 1/m$, and diminishes very slowly (like $1/b^2$) as a function of b, up to a limit γ/m after which it decays exponentially, and this is the reason why the cross sections for pair production will be very large. In fact, integrating eq. (7.3.10) from $b = 1/m$ to $b = \gamma/m$ we find

$$\sigma_{e^+e^-} = \frac{28}{27\pi} (Z_1 Z_2 \alpha r_e)^2 \left[\ln^3\left(\frac{\gamma\delta}{2}\right) - \tfrac{3}{2}(1 + 2\bar{f}) \ln^2\left(\frac{\gamma\delta}{2}\right) \right]. \tag{7.3.11}$$
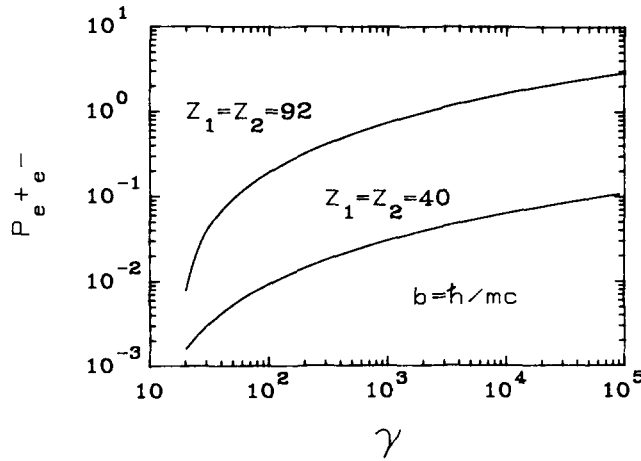
Fig. 7.5. The probability $P_{e^+e^-}$ for production of e^+e^- pairs in uranium–uranium collisions and calcium–calcium collisions as a function of the relativistic Lorentz factor γ, and for impact parameter $b = 1/m$. Observe that for uranium–uranium collisions it becomes greater than one for $\gamma \gtrsim 500$.

Since the integration of eq. (7.3.5) over b can be done analytically by using eq. (7.2.7), a better result can be also found by integrating numerically $d^2\sigma/d\varepsilon_+ \, d\varepsilon_-$ over ε_+ and ε_-. But, for $\gamma \gtrsim 100$ eq. (7.3.11) agrees very well with the numerical calculations. Except for the second term inside brackets and an irrelevant factor in the logarithm which is not important for $\gamma \gg 1$, the above expression agrees with the result found by Landau and Lifshitz [La-34] in the Born approximation. The second term inside brackets is a correction due to the distortion of the electron–positron wavefunctions in the field of the nuclei.

In fig. 7.6 we plot the cross section for production of e^+e^- pairs in relativistic uranium–uranium collisions and calcium–calcium collisions as a function of the Lorentz factor γ, based on eq. (7.3.11). These cross sections are about one to two orders of magnitude smaller than the ones calculated by Bertulani and Baur [Ber-86b], where the equivalent photon method was used. This occurs because there the equivalent photon numbers were integrated from a minimum impact parameter equal to R
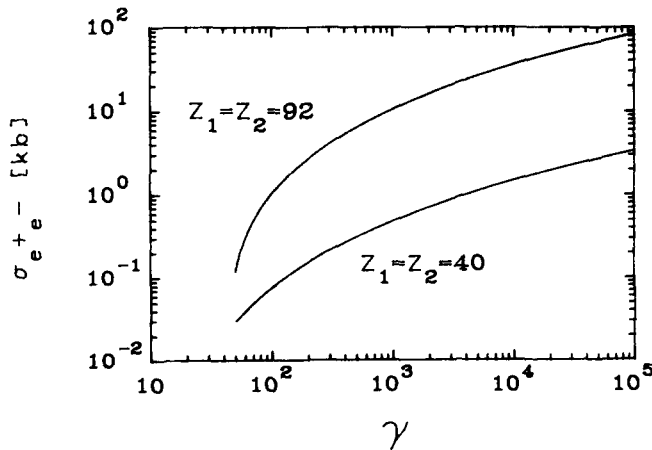

Fig. 7.6. The cross section $\sigma_{e^+e^-}$ for production of e^+e^- pairs in uranium–uranium collisions and calcium–calcium collisions as a function of the relativistic Lorentz factor γ. The ordinate is given in kilobarns.

(sum of the nuclear radii). As we saw, the minimum impact parameter that should be used is equal to the Compton wavelength, below which the contribution to the total cross section for pair production is negligible. That error makes the cross section in ref. [Ber-86b] much bigger than it should be. But the results agree quite well with the ones obtained here if we make the substitution $R \rightarrow 1/m$ in that calculation. In view of our previous discussion about the pair production probability, there must exist some corrections to eq. (7.3.11) for uranium–uranium collisions with $\gamma \gtrsim 500$. There one must take also into account the probability of creating two or more pairs in a single RHI collision. This may change the dependence of the cross section on γ.

From the previous results one observes that the probability for the production of fast e^+e^- pairs in the collision of two fast nuclei in comparison with slow (or ultrafast) ones scales like

$$P_{e^+e^-}^{\text{fast}} / P_{e^+e^-}^{\text{slow}} \simeq \ln^2(\gamma/mb) .$$ (7.3.12a)

and the ratio between the cross sections scales like

$$\sigma_{e^+e^-}^{\text{fast}} / \sigma_{e^+e^-}^{\text{slow}} \simeq \ln^2 \gamma ,$$ (7.3.12b)

which means that for $\gamma \gg 1$, most of the e^+e^- pairs will be fast ones, i.e., will have energies in the range given by eq. (7.Ib). Therefore, we can say that the total probability or cross section for producing e^+e^- pairs in RHI collisions are given accurately enough by eqs. (7.3.10) and (7.3.11), or by the respective numerical integration of (7.3.5).

7.4. Effects of screening

The above cross sections were evaluated under the assumption that the RHI were naked, without their electron cloud. Let us, for simplicity, assume that only one of the ions is screened by the atomic electrons, say the target. Then, the correction to the previous results can be performed in a completely analogous way as in the case of pair production by a real photon [Be-54]. Therefore, we only present the final results, which for partial screening are

$$\frac{d\sigma_{e^+e^-}}{d\varepsilon_+} = \frac{2}{9\pi} (Z_1 Z_2 \alpha r_e)^2 \frac{1}{\varepsilon_+} \left[6\Phi_1(\chi) + \Phi_2(\chi) - \frac{28}{3} \ln Z_2 - 28\bar{f} \right] \ln\left(\frac{\gamma \delta m}{2\varepsilon_+} \right) ,$$ (7.4.1)

where Φ_1 and Φ_2 are the Bethe functions for atomic screening [Be-34] as functions of the parameter (see also [Ak-65], p. 395)

$$\chi = (2m\omega/\varepsilon_+\alpha)Z_2^{-1/3} .$$

In case of complete screening, i.e., when $\varepsilon_\pm/m \gg Z_2^{1/3}\alpha$, then we can use $\Phi_1(0) = 4 \ln 183$ and $\Phi_2(0) = 4 \ln 183 - 2/3$, and eq. (7.4.1) reduces to

$$\frac{d\sigma_{e^+e^-}}{d\varepsilon_+} = \frac{56}{9\pi} (Z_1 Z_2 \alpha r_e)^2 \frac{1}{\varepsilon_+} \left[\ln\left(\frac{183}{Z_2^{1/3}} \right) - \frac{1}{42} - \bar{f} \right] \ln\left(\frac{\gamma \delta m}{2\varepsilon_+} \right) .$$ (7.4.2)

The total cross sections for e^+e^--pair production in RHI when one of the ions is completely screened is obtained by integrating eq. (7.4.2) from $\varepsilon_+ = Z_2^{1/3}\alpha m$ to γm, i.e.,
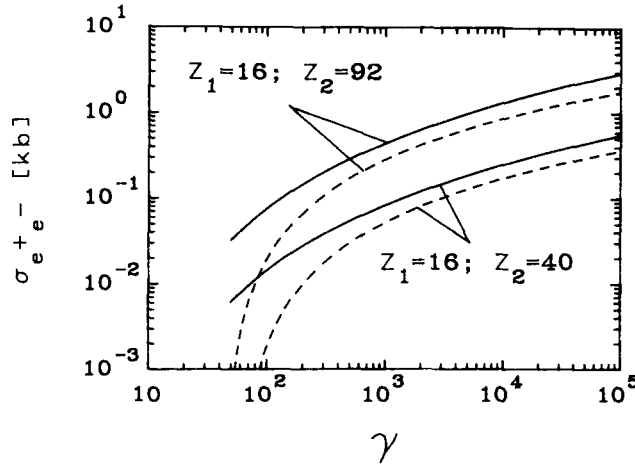
Fig. 7.7. The cross section $\sigma_{e^+e^-}$ for production of e^+e^- pairs in oxygen–uranium collisions and oxygen–calcium collisions as a function of the relativistic Lorentz factor γ. The solid lines refer to completely naked projectile and target and the dashed lines refer to completely naked projectile, but completely screened target.

$$\sigma_{e^+e^-} = \frac{28}{9\pi}\,(Z_1 Z_2 \alpha r_e)^2 \left[\ln\!\left(\frac{183}{Z_2^{1/3}}\right) - \frac{1}{42} - \bar{f}\right]\left[\ln^2(\gamma\delta Z_2^{1/3}\alpha) - \ln^2(\delta/2)\right].$$ (7.4.3)

In the case of partial screening a numerical integration of eq. (7.4.1) will be necessary.

In fig. 7.7 we show the cross section for pair production in oxygen–calcium and oxygen–uranium collisions as a function of the Lorentz factor γ. The solid lines correspond to the case of no-screening of the target and of the projectile, as it could be the situation in a RHI collider. The dashed lines correspond to the case of complete screening of the target. The effect of screening is very important for low energies of the beam and diminishes in importance for very high energies. However, when screening is present the cross sections will always be smaller by at least a factor 2–4, also for very high beam energies.

7.5. Production of heavy leptons

The same previous calculations can be applied for $\mu^+\mu^-$ and $\tau^+\tau^-$-pair production in RHI, but care must be taken on the following facts. First, since the Compton wavelength of these leptons satisfy the condition

$$\hbar/mc \ll R = R_1 + R_2 ,$$ (7.5.1a)

where

$$R_{1,2} \simeq 1.2 A_{1,2}^{1/3} \text{ fm}$$ (7.5.1b)

are the nuclear radii of the ions, the impact parameter dependence of the pair production probabilities are accurately enough described by expressions given in section 7.2, but in the cross sections one must substitute the variable ζ as given in eq. (7.2.7b) by another one given by

$$\xi = \omega R / \gamma v \, . \tag{7.5.2}$$

This means that, for

$$\gamma \gg 16 \, , \quad \text{for } \mu^+ \mu^- \text{ pair production} \, , \tag{7.5.3a}$$

and

$$\gamma \gg 270 \, , \quad \text{for } \tau^+ \tau^- \text{ pair production} \, , \tag{7.5.3b}$$

we can replace the mass of the electron by the mass of the respective lepton and

$$\ln(\gamma \delta m / \omega) \quad \text{by} \quad \ln(\gamma \delta / \omega R) \tag{7.5.4}$$

in the equations for the cross sections given in the previous sections to obtain the respective cross sections for $\mu^+ \mu^-$ and $\tau^+ \tau^-$ production.

The conditions (7.5.3) are quite severe and only for RHI accelerators working at extremely large energies it will be useful, especially for $\tau^+ \tau^-$ production. Therefore, we consider the opposite case, i.e., when $\gamma \lesssim 16$ for $\mu^+ \mu^-$ and $\gamma \lesssim 270$ for $\tau^+ \tau^-$ production. Then the function in eq. (7.2.7a) becomes

$$g(\xi) \simeq \pi^2 e^{-2\xi} \, . \tag{7.5.5}$$

The expressions (7.2.8) and (7.2.10) will be correct if we replace

$$\ln(\gamma \delta m / \omega) \quad \text{by} \quad (\pi / 2) e^{-2\omega R / \gamma} \, . \tag{7.5.6}$$

This means that the double differential cross section for $\mu^+ \mu^-$ and $\tau^+ \tau^-$ production with beam energies satisfying the above condition is

$$\frac{\mathrm{d}^2 \sigma_{\ell^+ \ell^-}}{\mathrm{d}\varepsilon_+ \, \mathrm{d}\varepsilon_-} = \frac{64\pi^2}{3} \, (Z_1 Z_2 r_\ell \alpha)^2 \, \frac{a_+ a_-}{(e^{2\pi a_+} - 1)(1 - e^{-2\pi a_-})} \, \frac{\sqrt{(\varepsilon_+ - m)(\varepsilon_- - m)}}{\omega^4}$$

$$\times \left[(\omega - 2m) + (Z_2 \alpha)^2 (\tfrac{7}{2} m - \omega) \right] e^{-2\omega R / \gamma} \, , \tag{7.5.7}$$

where the subscript $\ell^+ \ell^-$ is used in this section for muon or tau pairs.

When the charges of the ions are small, such that the approximation $a_\pm \ll 1$ can be used, we can integrate eq. (7.5.7) from $\varepsilon_\pm = m$ to $2m$ and obtain

$$\frac{\mathrm{d}\sigma_{\ell^+ \ell^-}}{\mathrm{d}\varepsilon_+} = \tfrac{1}{3}(Z_1 Z_2 \alpha r_\ell)^2 \, \frac{1}{m} \left(\frac{\gamma}{2mR} \right)^{3/2} \left(\frac{\varepsilon_+}{m} - 1 \right)^{3/2} \left[\Gamma(\tfrac{3}{2}) - \Gamma\!\left(\frac{3}{2} ; \frac{2mR}{\gamma} \right) \right] e^{-2(\varepsilon_+ + m)R / \gamma}$$

$$\simeq \frac{\sqrt{\pi}}{6} \, (Z_1 Z_2 \alpha r_\ell)^2 \, \frac{1}{m} \left(\frac{\gamma}{2mR} \right)^{3/2} \left(\frac{\varepsilon_+}{m} - 1 \right)^{3/2} e^{-2(\varepsilon_+ + m)R / \gamma} \, , \tag{7.5.8}$$

where $\Gamma(\lambda; y)$ is the incomplete gamma function (see [Gr-65], p. 940), and the last equality corresponds to the asymptotic limit $mR / \gamma \gg 1$.

We integrate eq. (7.5.8) over ε_+ in order to find the total cross section for muon (or tau) production under the condition that $mR/\gamma \gtrsim 1$, namely

$$\sigma_{\ell^+\ell^-} = \tfrac{1}{48}(Z_1 Z_2 \alpha r_\ell)^2 \left(\frac{\gamma}{mR}\right)^4 \left[\Gamma(\tfrac{3}{2}) - \Gamma\left(\frac{3}{2}; \frac{2mR}{\gamma}\right)\right]\left[\Gamma(\tfrac{5}{2}) - \Gamma\left(\frac{5}{2}; \frac{2mR}{\gamma}\right)\right] e^{-4mR/\gamma}$$

$$\simeq \frac{\pi}{128}(Z_1 Z_2 \alpha r_\ell)^2 \left(\frac{\gamma}{mR}\right)^4 e^{-4mR/\gamma} .$$

(7.5.9)

This result is in good agreement with that of ref. [Ba-87a], where the cross section was calculated by using the equivalent photon method. There the cross section was given in terms of the exponential integral function $Ei(x)$ (see [Gr-65], p. 312) and the asymptotic limit for $mR/\gamma \gg 1$ is exactly the same as the one obtained above (see eq. (10) of that reference). In RHI collisions, for which the above approximations are not valid, a numerical integration of eq. (7.5.7) has to be performed.

Numerical values are plotted in fig. 7.8 for $\sigma_{\ell^+\ell^-}$ in the collision $^{16}O + {}^{16}O$ as a function of the Lorentz factor γ. The cross sections are much smaller than that for e^+e^- production in the same energy regime. This is due to the severe limitation imposed by the adiabatic cutoff in the cross section for projectile energies such that $mR/\gamma \gtrsim 1$, which strongly inhibits the creation of very massive particles when this condition is attained. When the projectile energy is very high, such that the conditions (7.5.3) are valid, then we can use eq. (7.3.11) also for $\mu^+\mu^-$ and $\tau^+\tau^-$ production. But even in that case the cross sections will be smaller by a factor $(m_e/m_\ell)^2$ (i.e., approximately 10^{-4} for $\mu^+\mu^-$ production, and approximately 10^{-7} for $\tau^+\tau^-$ production) in comparison with that for e^+e^- production.
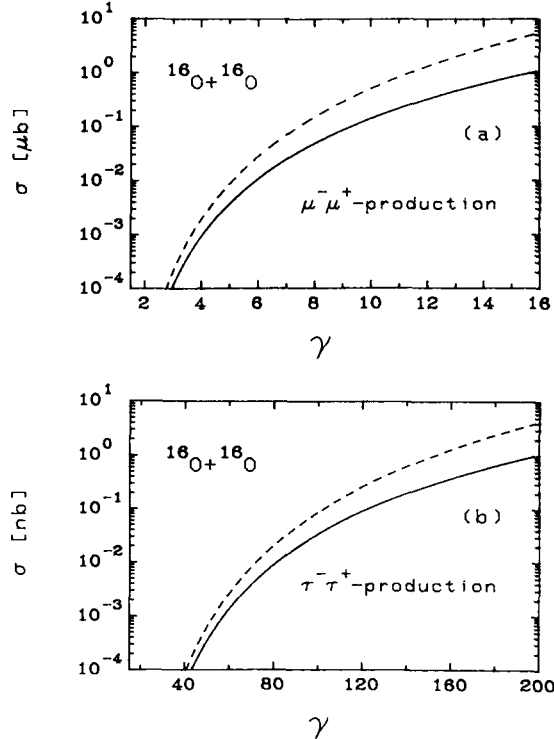

Fig. 7.8. The cross section $\sigma_{\ell^+\ell^-}$ for production of (a) $\mu^+\mu^-$ and (b) $\tau^+\tau^-$ pairs in oxygen–oxygen collisions as a function of the Lorentz factor γ. The solid lines correspond to the eq. (7.5.9) and the dashed lines to its asymptotic limit.

Lepton-pair production is suggested [see e.g. Do-83] as being a potentially efficient probe of quark matter formed in RHI collisions. As we saw in this section, the electromagnetic production of leptons is by no means negligible, and although the multiplicity (i.e. the number of pairs) in a single collision is smaller or about one, the cross sections for it are very high and can be a source of experimental difficulties in the signature of that aspect of the quark–gluon plasma formation.

As a final remark, let us compare the electromagnetic production of leptons in RHI collisions with the corresponding process in relativistic electron colliders. For a detailed theoretical study of that, see [Bu-75]. In such machines, the γ-values achieved are much higher than in the heavy ion case, therefore the cross sections are accurately enough given by eq. (7.3.11). We have astonishingly large e^+e^- production cross sections in RHI collisions, due to the large charge factor $Z_1^2 Z_2^2$, however, heavy leptons pairs ($\mu^+\mu^-, \tau^+\tau^-$ pairs) are practically not produced unless the beam energy is very high ($\gamma \gg 16$ for $\mu^+\mu^-$, and $\gamma \gg 270$ for $\tau^+\tau^-$ pairs). Also the electromagnetic production, in the two-photon mechanism, of quark–antiquark states (like the η_C, which was recently studied with the PLUTO detector at PETRA in high energy e^+e^- collisions [Berg-86]), will be negligible unless the beam energy is extremely large ($\gamma \gg 600$ in case of η_C production).

7.6. Pair production with atomic shell capture

With the obtained large values of the cross sections for production of free electron–positron pairs, it is also of interest to study those pair production processes where the electron is captured in a bound atomic orbit in the projectile, or in the target. The first theoretical work on this subject was carried out by Becker, Grün and Scheid [Be-87]. There they used a partial wave expansion of the electron and the positron in terms of exact Dirac–Coulomb wave functions, and calculated numerically the probabilities and cross sections for the process in the first order semiclassical theory. Bertulani and Baur [Ber-87b] have performed a different calculation to the same process by trying to avoid the partial wave expansion and to obtain analytical formulas for the important cases. This can be accomplished by using approximate wave functions for the final bound state of the electron and for the free positron. We use the same approach as in section 7 on the production of free pairs in the collisions of fast nuclei.

In fig. 7.9 (taken from [Be-86c]) a scheme of the Dirac spectrum, describes the two distinct pair-production situations: (a) pair-production with K-shell capture and (b) production of free pairs.
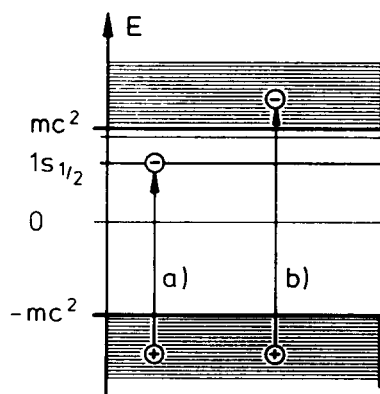

Fig. 7.9. A perturbation of the vacuum leading to (a) pair creation with the capture of the electron in the K-shell and (b) production of free electron–positron pairs.

We show that explicit analytical results can be found for the capture of the created electron in a K-shell of the projectile, or in the target. The cross sections for the capture in higher atomic orbits, being of much less importance, are easily guessed. We also show how the limiting cases can be obtained by using the equivalent photon method.

7.6.1. Pair production with K-shell capture

In the previous sections we have shown that the probability amplitude to create an electron–positron pair, with respective energies equal to ε_+, ε_-, in a RHI collision with $\gamma \gg 1$ is given by eq. (7.1.7). If the electron is created in a K-shell orbit (see fig. 7.9) then, instead of eq. (7.1.2), we must use

$$\omega = \varepsilon_+ + m - I_K , \tag{7.6.1}$$

with I_K equal to the ionization energy of the K-shell electron (in the following we shall use $I_K = 0$, which is appropriate only for small-Z nuclei).

For the positron wave function, Ψ_{e^+}, we use the Sommerfeld–Maue function (7.1.8b), and for the captured electron we use the bound K-shell wavefunction, valid for $Z_2 e^2 \ll 1$,

$$\Psi_{e^-} = N_-[1 + \tfrac{1}{2}iZ_2 e^2 \boldsymbol{\alpha} \cdot \boldsymbol{r}/r] e^{-\eta r} u_0 , \tag{7.6.2a}$$

where

$$u_0^{1/2} = \begin{pmatrix} 1 \\ 0 \\ 0 \\ 0 \end{pmatrix}, \quad u_0^{-1/2} = \begin{pmatrix} 0 \\ 1 \\ 0 \\ 0 \end{pmatrix}, \quad \eta = mZ_2 e^2 , \quad \text{and} \quad N_- = \sqrt{(Z_2 me^2)^3/\pi} . \tag{7.6.2b}$$

The components $u_0^{+1/2}$ and $u_0^{-1/2}$ of the spinor u_0 correspond to the electron with spin up and down, respectively (see [Ak-65], eq. 31.11).

Although, due to the use of these approximate wavefunctions, the following results may be appropriate for RHI collisions for which one (or both) nuclei satisfy the condition $Ze^2 \ll 1$, we expect that even for very heavy nuclei they will be useful, since the main ingredients are contained in the calculations.

Inserting eqs. (7.1.8b) and (7.6.2) in eq. (7.1.7) we find

$$a_{e^+e^-}^K = \frac{Z_1 e^2}{i\pi\omega v} N_+ N_- \sum_{\lambda=1,2} u_0^*[\alpha^\lambda G_{1\lambda} + (\boldsymbol{\alpha} \cdot \boldsymbol{G}_{2\lambda})\alpha^\lambda + \alpha^\lambda(\boldsymbol{\alpha} \cdot \boldsymbol{G}_{3\lambda})]w , \tag{7.6.3}$$

where $\lambda = 1, 2$ represents the two orthogonal components transverse to the beam. As in eq. (7.1.10), the tensors $G_{1\lambda}$, $G_{2\lambda}$, and $G_{3\lambda}$ are given by

$$[G_{1\lambda}, \boldsymbol{G}_{2\lambda}, \boldsymbol{G}_{3\lambda}] = \int d^2 p_T \frac{p_T^\lambda[J_1, \boldsymbol{J}_2, \boldsymbol{J}_3]}{p_T^2 + (\omega/\gamma v)^2} e^{i\boldsymbol{p}_T \cdot \boldsymbol{b}} , \tag{7.6.4}$$

where

$$J_1 = \int e^{iq \cdot r - \eta r} F_2 \, d^3r \,, \tag{7.6.5a}$$

$$J_2 = -\frac{iZ_2 e^2}{2} \int e^{iq \cdot r - \eta r} \frac{r}{r} F_2 \, d^3r \,, \tag{7.6.5b}$$

$$J_3 = \frac{i}{2\varepsilon_+} \int e^{iq \cdot r - \eta r} \nabla F_2 \, d^3r \,, \tag{7.6.5c}$$

$$q = p' - k_+ \,, \tag{7.6.5d}$$

and

$$F_2 \equiv F(-ia_+, 1, ik_+ r + ik_+ \cdot r) \,. \tag{7.6.5e}$$

The integrals (7.6.5) are very similar to the ones involved in the photoelectric effect and can be carried out analytically (see e.g. [Ak-65], pp. 435 and 436).

Since only values of p_T up to $\omega/\gamma v \ll m$ will contribute to the integrals (7.6.4), we put $p_T = 0$ in eq. (7.6.5), which amounts to use $q = (\omega/v)\hat{z} - k_+$ in them, where $\hat{z}$ is equal to a unit vector in the beam direction. In this way, the integral in p_T of eq. (7.6.4) can be done exactly in terms of the modified Bessel function of first order. As we have shown in the preceding section, this approximation is good for RHI collisions with impact parameters larger than the Compton wavelength of the electron, i.e., for $b \gtrsim 1/m$, which are the impact parameters which most contribute to the total cross sections. Indeed, for $b \lesssim 1/m$ the probability amplitude for pair production tends to a constant value (see the exact numerical calculations of Becker, Grün and Scheid [Be-87]), while for $b \gtrsim 1/m$ it decays proportionally to $1/b^2$, up to a cutoff limit given by $b \simeq \gamma/\omega$. This has as a consequence that the contribution of impact parameters $b \gtrsim 1/m$ to the total cross sections increases logarithmically with the RHI-beam energy, while the contribution from smaller impact parameters gives a constant and small quantity.

With these approximations the integrals (7.6.4) can be solved analytically and we obtain (we choose b along the x-axis)

$$G_{12}, G_{22}, G_{32} = 0 \,, \tag{7.6.6a}$$

and

$$G_{11} = -i \frac{4\pi^2 Z_2 e^2}{\gamma v} \frac{k_+(k_+ - \varepsilon_+ \cos \theta_+)}{\varepsilon_+(\varepsilon_+ + m)(\varepsilon_+ - k_+ \cos \theta_+)^2} K_1\left(\frac{\omega b}{\gamma v}\right) \,, \tag{7.6.6b}$$

$$G_{21} = i \frac{2\pi^2 Z_2 e^2}{\gamma v^2} \frac{\omega \hat{z} - v k_+}{(\varepsilon_+ + m)(\varepsilon_+ - k_+ \cos \theta_+)^2} K_1\left(\frac{\omega b}{\gamma v}\right) \,, \tag{7.6.6c}$$

$$G_{31} = i \frac{2\pi^2 Z_2 e^2}{\gamma v^2} \frac{\omega \hat{z} - v k_+}{m(\varepsilon_+ + m)(\varepsilon_+ - k_+ \cos \theta_+)} K_1\left(\frac{\omega b}{\gamma v}\right) \,, \tag{7.6.6d}$$

where K_1 represents the modified Bessel function of first order, and ϕ_+ and θ_+ are, respectively, the azimuthal and the polar angles of emission of the created positron with respect to the beam direction.

The differential probability for pair production with K-shell capture is obtained from eq. (7.6.3) as

$$dP^K_{e^+e^-} = \sum_{spins} |a^K_{e^+e^-}|^2 \frac{k_+ \varepsilon_+}{(2\pi)^3} d\varepsilon_+ d\Omega_+ , \qquad (7.6.7)$$

where the summation is taken over different spin orientations of the electron and the positron. Using the properties of the Dirac matrices we find

$$dP^K_{e^+e^-} = \left(\frac{Z_1 e^2}{\pi \omega v}\right)^2 |N_+ N_-|^2 \frac{k_+}{(2\pi)^3} \{(\varepsilon_+ + m)|G_{11}|^2 + 2G^*_{11}[k_+ \cdot (G_{21} - G_{31}) - 2k^T_+ \cdot G^T_{21}]$$

$$+ (\varepsilon_+ - m)[|G_{21}|^2 + |G_{31}|^2 + 2(2G^T_{21} \cdot G^T_{31} - G_{21} \cdot G_{31})]\} d\varepsilon_+ d\Omega_+ , \qquad (7.6.8)$$

where $k^T_+(G^T_{\mu\lambda})$ denotes the transverse component of $k_+(G_{\mu\lambda})$.

Now we insert the expressions (7.6.6) in (7.6.8), putting $v \simeq c = 1$ overall, and we find

$$dP^K_{e^+e^-} = \frac{2}{\pi} Z^2_1 Z^6_2 \alpha^8 \frac{1}{(e^{2\pi a_+} - 1)} \frac{m^3}{\varepsilon_+(\varepsilon_+ + m)^3} \frac{\sin^2\theta_+}{(1 - (k_+/\varepsilon_+)\cos\theta_+)^4}$$

$$\times [\chi(\chi^3 + \chi^2 - \chi - 1) + (4 - 6\chi + 2\chi^3)\cos^2\phi_+ - (1 + \chi + 2\cos^2\phi_+)$$

$$\times (\chi^2 - 1)^{3/2}\cos\theta_+] \frac{1}{\gamma^2} K^2_1\left(\frac{\omega b}{\gamma}\right) d\varepsilon_+ d\Omega_+ , \qquad (7.6.9)$$

where $\chi = \varepsilon_+/m$, and $\alpha = e^2/\hbar c \simeq 1/137$ is the fine structure constant.

The angular distribution for the direction of emission of the created positron may be expressed in terms of the dimensionless function

$$W^K_{e^+e^-} = \frac{2\pi \sin^2\theta_+}{(1 - (k_+/\varepsilon_+)\cos\theta_+)^4} [2 - 4\chi - \chi^2 + 2\chi^3 + \chi^4 - (2 + \chi)(\chi^2 - 1)^{3/2}\cos\theta_+] , \qquad (7.6.10a)$$

which is obtained by integration of the angular part of eq. (7.6.9) over the azimuthal angle ϕ_+.

When $(\varepsilon_+ - m) \ll m$, then

$$W^K_{e^+e^-} \simeq 4\pi(k^2_+/m^2)\sin^2\theta_+ , \qquad (7.6.10b)$$

which means that low-energetic positrons will be emitted preferentially in the direction perpendicular to the RHI-beam. For $\varepsilon_+ \gg m$, the angular distribution is approximately

$$W^K_{e^+e^-} \simeq 4\pi\left(\frac{\varepsilon_+}{m}\right)^4 \frac{\sin^2\theta_+}{(1 - (k_+/\varepsilon_+)\cos\theta_+)^4} \simeq 64\pi\left(\frac{\varepsilon_+}{m}\right)^4 \frac{\theta^2_+}{[(m/\varepsilon_+)^2 + \theta^2_+]^4} , \qquad (7.6.10c)$$

which implies that highly energetic positrons will be created with their momenta directed very forwardly, up to a maximum angle $\theta^{max}_+ \simeq m/\varepsilon_+$.

Integrating eq. (7.6.9) over the angular distribution of the positrons we find

$$\frac{dP^K_{e^+e^-}}{d\varepsilon_+} = 8Z_1^2Z_2^6\alpha^8 \frac{1}{(e^{2\pi a_+}-1)} \frac{k_+m}{(\varepsilon_++m)^3} \frac{1}{\gamma^2} K_1^2\left(\frac{\omega b}{\gamma}\right)$$

$$\times \left[\frac{4}{3} + \frac{2\varepsilon_+}{3m} + \left(\frac{\varepsilon_+}{m}\right)^2 - \frac{\varepsilon_++2m}{k_+} \ln\left(\frac{\varepsilon_++k_+}{m}\right)\right]. \tag{7.6.11}$$

The modified Bessel function of first order has the property given by eq. (7.2.6), which implies that the pair production probability decays like $1/b^2$ for impact parameter b larger than the Compton wavelength, i.e. for $b > 1/m$, until to a cutoff limit given by $b \simeq \gamma/\omega$. Above this cutoff limit it will decay exponentially, which will guarantee the convergence of the cross section. Indeed, with these simplifications the differential cross section can be easily obtained by using eq. (7.2.7). We can write the result as

$$\frac{d\sigma^K_{e^+e^-}}{d\varepsilon_+} = 8Z_1^2Z_2^6\alpha^6r_e^2 \frac{1}{(e^{2\pi a_+}-1)} \frac{k_+m^3}{(\varepsilon_++m)^5} g(\zeta)$$

$$\times \left[\frac{4}{3} + \frac{2\varepsilon_+}{3m} + \left(\frac{\varepsilon_+}{m}\right)^2 - \frac{\varepsilon_++2m}{k_+} \ln\left(\frac{\varepsilon_++k_+}{m}\right)\right], \tag{7.6.12}$$

where $r_e = e^2/mc^2 = 2.817 \ldots$ fm is the classical electron radius.
For $\varepsilon_+ \simeq m$,

$$\frac{d\sigma^K_{e^+e^-}}{d\varepsilon_+} \simeq \frac{2\pi}{3} Z_1^2Z_2^6\alpha^6r_e^2 \frac{k_+^3}{m^4} e^{-2\pi a_+} \ln\left(\frac{\gamma\delta}{2}\right). \tag{7.6.13}$$

For $\varepsilon_+ \gg m$,

$$\frac{d\sigma^K_{e^+e^-}}{d\varepsilon_+} \simeq 16\pi Z_1^2Z_2^6\alpha^6r_e^2 \frac{m}{\varepsilon_+^2} \frac{1}{e^{2\pi Z_2\alpha}-1} \ln\left(\frac{\gamma\delta m}{\varepsilon_+}\right). \tag{7.6.14}$$

In fig. 7.10 we plot eq. (7.6.12), in units of r_e^2/m, as a function of ε_+/m, and for $Z_1 = Z_2 = 8$ and $\gamma = 100$. Also shown are the low (dashed line) and high (dotted line) positron energy approximation. We observe that the spectrum is strongly suppressed for $\varepsilon_+/m \simeq 1$, which is due to the Coulomb repulsion in the field of the nucleus, which prevents creation of low energy positrons. It has a maximum around $\varepsilon_+ \simeq 2m$, and decays like eq. (7.6.14) after that. Since, as a function of ε_+, the differential cross section for production of free pairs decays proportionally to $1/\varepsilon_+$, the total cross section (integrated over ε_+) for pair production with capture, besides of an extra factor $(Z_2\alpha)^3$, will increase more slowly as a function of γ than that for production of free pairs.

If we integrate numerically eq. (7.6.12) over the positron energy we obtain the solid curve as shown in fig. 7.11, for $Z_1 = Z_2 = 8$ and as a function of γ. Also shown (dashed line) in that figure is the approximate expression

$$\sigma^K_{e^+e^-} \simeq \frac{33\pi}{10} Z_1^2Z_2^6\alpha^6r_e^2 \frac{1}{e^{2\pi Z_2\alpha}-1}\left[\ln\left(\frac{\gamma\delta}{2}\right) - \frac{5}{3}\right], \tag{7.6.15}$$
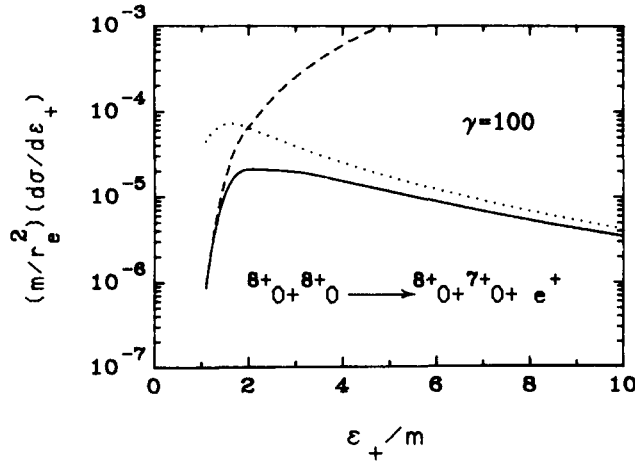
Fig. 7.10. The differential cross section $d\sigma_{e^+e^-}^K/d\varepsilon_+$ in units of r_e^2/m, for $Z_1 = Z_2 = 8$ (naked oxygen ions), $\gamma = 100$, and as a function of ε_+/m. The dashed curve corresponds to the approximation (7.6.13) for low-energy positrons. The dotted curve corresponds to the high energy approximation (7.6.14).
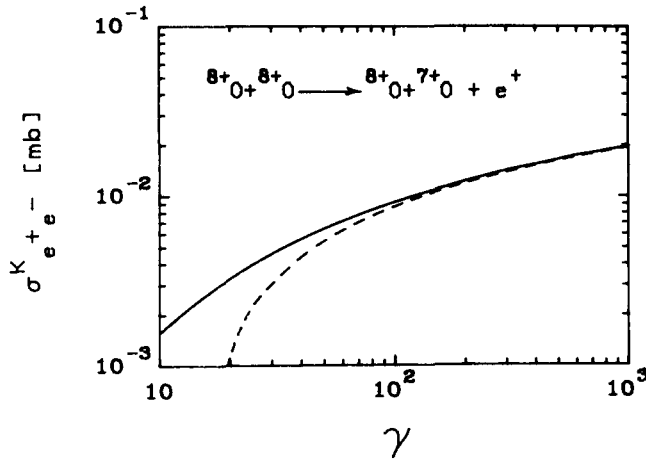

Fig. 7.11. The cross section $\sigma_{e^+e^-}^K$, for pair production with simultaneous capture of the electron in the K-shell of one of the nucleus, in a RHI collision with $Z_1 = Z_2 = 8$ (naked oxygen ions), and as a function of γ.

which can be obtained by setting $k_+ = \varepsilon_+$ overall in eq. (7.6.12) and integrating it from $\varepsilon_+ = 2m$ to ∞. It will be a good approximation for the numerical integration of eq. (7.6.12) with $\gamma \gtrsim 50$.

The ratio of the total cross section for the production of free pairs (see eq. (7.3.11)) and that for which the electron is captured in a K-shell atomic orbit (which give the biggest contribution, as we shall see in the next section) is approximately given by

$$\frac{\sigma_{e^+e^-}^{capt}}{\sigma_{e^+e^-}^{free}} \simeq \frac{33\pi}{20} (Z_2\alpha)^3 \left[\ln\left(\frac{\gamma\delta}{2}\right)\right]^{-2}. \tag{7.6.16}$$

This means that, compared with the production of free pairs, pair production with capture will be more important for ions with larger charges and for lower energies. For $Z_2 = 8$ and $\gamma = 100$, we find $\sigma^{capt}/\sigma^{free} \simeq 10^{-4}$.

7.6.2. Contribution from higher orbits

In principle, it is possible to calculate the cross sections for capture of the electron to higher atomic orbits in a way similar to the K-shell capture. However, since the calculations become more cumbersome and the contributions are much smaller than that for capture in the K-shell, we prefer to use another method which is based on the previous works for the one-photon annihilation of positrons with atomically bound electrons [Fe-33, Ni-34, Ak-65].

First we mention how some of the results of the previous section can be obtained with the equivalent photon method. In this approach one needs the cross section for the photoproduction process

$$\gamma + Z_2 \rightarrow e^+ + (Z_2' + e^-)_{K,L,\ldots} .$$ (7.6.17)

By time reversal, this process is related to the one-photon annihilation process

$$e^+ + (Z_2 + e^-)_{K,L,\ldots} \rightarrow \gamma + Z_2 ,$$ (7.6.18)

the theoretical cross sections for which are known since the thirties, like e.g. in the calculations of Fermi and Uhlenbeck [Fe-33], Nishina, Tomonaga and Tamaki [Ni-34], and others (see e.g. [Ak-65], p. 463, and references therein). In the extreme relativistic (E.R.), $\varepsilon_+ \gg m$, and non-relativistic (N.R.), $\varepsilon_+ \simeq m$, cases we have [Ni-34]

$$\sigma^{ann} = 8\pi^2 Z_2^6 \alpha^5 r_e^2 \begin{cases} \dfrac{k_+}{3m} \dfrac{1}{e^{2\pi a_+} - 1} & (\text{N.R.}) , \\[3mm] \dfrac{m}{\varepsilon_+} \dfrac{1}{e^{2\pi Z_2 \alpha} - 1} & (\text{E.R.}) . \end{cases}$$ (7.6.19)

By means of the detailed balance theorem, these cross sections are related to the photoproduction cross sections by

$$\sigma_\gamma^{prod} = 8\pi^2 Z_2^6 \alpha^5 r_e^2 \begin{cases} \dfrac{k_+^3}{12m^3} \dfrac{1}{e^{2\pi a_+} - 1} & (\text{N.R.}) , \\[3mm] \dfrac{m}{\varepsilon_+} \dfrac{1}{e^{2\pi Z_2 \alpha} - 1} & (\text{E.R.}) . \end{cases}$$ (7.6.20)

In the equivalent photon method it is assumed that the processes originated by the time-varying electromagnetic field generated by a relativistic charge are the same as those caused by a plane wave pulse of light containing $n(\omega)/\omega$ photons per unit energy. In this way, the cross sections for any electromagnetic process in RHI collisions can be related to that for the same process originated by a real photon σ_γ by means of the expression (see section 1)

$$\frac{d\sigma^{RHI}}{d\omega} = \frac{n(\omega)}{\omega} \sigma_\gamma^{prod} .$$ (7.6.21)

In the case of pair production $d\omega = d\varepsilon_+$ and (see eq. (1.11a))

$$n(\omega) \simeq \frac{2}{\pi} Z_1^2 \alpha \ln\left(\frac{\gamma \delta m}{\omega}\right) .$$ (7.6.22)

Now it is a simple matter to show that by inserting eq. (7.6.20) in eq. (7.6.21) and using eq. (7.6.22) we reproduce the eqs. (7.6.13) and (7.6.14).

In ref. [Ni-34] the one-photon annihilation of L-shell electrons and positrons was also considered. It was found that the dominant contribution comes from the L_1-subshell and that the cross section is given by 1/8 of the K-shell cross section. This is related to a general scaling law, which also appears in the photo-electric effect (see e.g. [Be-77], p. 303), given by

$$\sigma_{ns} = \sigma_{1s}/n^3 ,$$ (7.6.23)

where the index ns denotes the spherically symmetric atomic subshells of order n. This relation reflects the behaviour of the bound state wave functions in momentum space at large momenta. Assuming that this behaviour is valid for contribution of all atomic shells, one would obtain an increase of the total capture cross section (into s-orbits, which are the most important), as compared to that for capture in the K-shell, by a factor

$$\sum_{n=1}^{\infty} 1/n^3 = \xi(3) = 1.202 ,$$ (7.6.24)

where ξ is the Riemann ξ-function. This means that eqs. (7.6.12) and (7.6.15) should be multiplied by eq. (7.6.24) if we want to have the contribution of all atomic orbits, which implies in a correction of about 20% for the total cross section.

The capture process in RHI collisions could well be crucial for future relativistic colliders: the electron capture process changes the charge state of the circulating ions and leads to a beam-loss in further turns [An-87]. In a 100 GeV/nucleon uranium collider with a luminosity of 10^{27} cm^{-2} s^{-1} one can easily estimate the number of electron captures per second: this energy corresponds to an equivalent laboratory energy of 20 400 GeV/nucleon, i.e., a value of $\gamma \simeq 2 \times 10^4$. From eq. (7.3.11) we find that the total cross section for the production of free pairs is approximately $\sigma \simeq 60$ kb. This means that approximately 10^8 pairs are produced per second. From eq. (7.6.15) we find that approximately 10^5 electrons per second will be captured in atomic orbits of the ions in the interaction region of the same beam. As pointed out by Anholt and Gould [An-87] this may limit to an upper value the beam energy to be obtained in a RHI collider, or may even be used to control the beam luminosity by measuring the total amount of positrons created per unit time. The capture cross section should also be put into relation with other characteristic cross sections. For example, the nuclear geometric cross section is of order of one barn, i.e. they are a small fraction of the atomic capture cross section.

In principle, it is also possible to produce heavy lepton pairs [see Mo-87], like $\mu^+\mu^-$ and $\tau^+\tau^-$ with the capture of a negative lepton. But, due to the much higher masses of these leptons, the corresponding cross sections are much smaller and expected to be of minor importance.

Also interesting in this context is the possibility of formation of π^--atoms by means of the strong interactions in RHI. For an experimental proposal in this direction see ref. [HK-87].

8. Conclusions

Electromagnetic effects in relativistic nuclear collisions are very important and interesting. Since the electromagnetic interaction is well known, reliable theoretical predictions are possible. This makes, e.g., the electron an ideal probe to investigate nuclear structure. Since there is only the electromagnetic interaction between the electron and the target nucleus, a detailed study of electromagnetic form-factors is possible, which allows an extensive determination of nuclear transition densities. With nuclear scattering below the Coulomb barrier, it is possible to avoid the strong nuclear interaction between them and obtain very interesting and useful information about nuclear electromagnetic matrix-elements (transition matrix-elements, as well as static moments, like quadrupole moments of excited states). Especially with heavy ions, it becomes possible to achieve multiple excitation of nuclear levels (e.g., rotational bands).

We have presented a study of the electromagnetic effects (Coulomb excitation, particle production, etc.) in relativistic heavy ion collisions. The method of equivalent photons has proven to be a very powerful and transparent tool to study these effects. It allows a clear separation into a purely kinematical aspect (equivalent photon numbers) and the cross sections for a process induced by real photons. Since with an increasing value of the relativistic parameter γ the hardness of the equivalent photons is increased, many new possibilities open up. We have studied these new possibilities in a way as simple as possible.

In the case of relativistic Coulomb excitation, a comparison between detailed calculations in the semiclassical and in the plane wave Born approximation was useful in obtaining a new insight into this subject. In both approaches it is possible to develop the interaction potential in terms of different multipolarities, which enables the study of the contribution of each multipolarity to a particular nuclear reaction. The PWBA cross section integrated over angles is shown to be equal to the semiclassical one integrated over impact parameters. By factorizing the cross section integrated over the excitation energy, we reach an expression for the number of equivalent photons for different multipolarities and frequencies of the electromagnetic interaction. A comparison with the results derived by other methods was useful to clarify some points in this matter.

Rather simple classical and quantal considerations show the importance of giant resonance excitations in peripheral RHI collisions. The present experimental status can be compared to theoretical calculations using a sum rule approach to the nuclear states, and a completely satisfactory agreement is found. Fragmentation can also be of practical importance, like, e.g., the production of new and interesting isotopes (like ^{19}Ne). In view of recently proposed detailed experimental studies of extreme peripheral collisions, the possibility of multiphonon giant dipole oscillations is discussed. Such a possibility does not seem to exist in electron scattering due to the much smaller charge as compared to a heavy ion. Using a harmonic oscillator model, absolute values for total cross sections can be obtained with simple formulas. The cross sections are found to be quite appreciable. Whereas the cross sections for heavy projectile excitation are larger than those for light projectile excitation, such as ^{16}O or ^{32}S, the separation amplitude of neutrons and protons will be larger for lighter projectiles. This could prove to be a means of producing new and exotic nuclei, perhaps, e.g., polyneutrons. We can also include – in a phenomenological way – the effects of damping of the giant dipole collective motion in the theory. A theoretical study indicates quite safely the possibility of excitation of such states with appreciable values for the cross sections. A beautiful application of the theory of relativistic Coulomb excitation was illustrated by the experiment for the $\Lambda\Sigma^0$ conversion in the field of a nucleus with large charge. Besides allowing a test to the theory, it showed that the theory can be a basis for powerful studies of

electromagnetic properties of hadrons. In the special case of that experiment it was used to extract the lifetime of the Σ^0 particle, which agreed with the theoretical values predicted by the SU(3) theory for the hadrons.

With increasing collision energy, pion production due to electromagnetic processes will become important: it can be quantitatively calculated based on our knowledge of pion production in photonuclear interactions. Bremsstrahlung, the elastic scattering of the equivalent photons on charged particles, is relatively unimportant for the heavy ions, although interesting effects are also to be observed in this field. Atomic ionization by means of relativistic projectiles is of large importance, due to the enormous values for the ionization cross sections. Lepton pair production, especially e^+e^- pairs, is also of great interest due to its large cross sections. We found tractable analytical results for the relevant kinematical situations in this process: there are slow pairs produced around the target and the projectile (what we called ultrafast pairs) charges, respectively, and dominantly, an intermediate energy region. In addition, we saw that an analysis of the impact parameter dependence of this process points directly to the limitation of first order perturbation theory for extremely relativistic heavy ion collisions. The capture of the created electrons in an orbit of the projectile will tend to reduce the beam luminosity due to the charge change.

The *central* and *peripheral* collisions of relativistic heavy ions may be compared to the case of two potential lovers walking on the same side of the street, but in opposite directions. If they do not care, they can collide frontally, which could not be bad at all. It may be a good opportunity for the beginning of *strong interactions* between them. A third observer will easily notice this situation, or the consequences of it. On the other hand, if they pass far from each other, they can still exchange glances (just *electromagnetic* interaction!), which can even lead to their *excitation*. But for the observer this will not be so easily noticed. He must be very interested in this situation to be able to detect something. He can surprisingly discover that the effects of these *peripheral* collisions are sometimes more interesting than the violent frontal ones.

Acknowledgements

9. Appendices

A. The relativistic Winther–Alder functions

In this appendix we make a resumé of the relativistic kinematic functions $G_{\pi lm}$, introduced in section 2, eq. (2.1.15), and first calculated by Winther and Alder [Wi-79].

The functions $G_{\pi lm}(x)$, where $x = c/v$, are given in terms of the Legendre polynomials $P_l^m(x)$, calculated for $x > 1$. For $m \geq 0$ they are

$$G_{Elm}(x) = i^{l+m} \frac{\sqrt{16\pi}}{l(2l+1)!!} \left[\frac{(l-m)!}{(l+m)!}\right]^{1/2} (x^2 - 1)^{-1/2}$$

$$\times \left\{ \frac{(l+1)(l+m)}{2l+1} P_{l-1}^m(x) - \frac{l(l-m+1)}{2l+1} P_{l+1}^m(x) \right\} \tag{A.1a}$$

$$G_{Mlm}(x) = i^{l+m+1} \frac{\sqrt{16\pi}}{l(2l+1)!!} \left[\frac{(l-m)!}{(l+m)!}\right]^{1/2} (x^2 - 1)^{-1/2} m\, P_l^m(x) , \tag{A.1b}$$

while for $m < 0$ one can use

$$G_{El,-m}(x) = (-1)^m\, G_{Elm}(x) , \tag{A.1c}$$

$$G_{Ml,-m}(x) = (-1)^{m+1}\, G_{Mlm}(x) . \tag{A.1d}$$

In the non-relativistic limit, $x = c/v \gg 1$, we find from the above definitions

$$G_{Elm}(c/v) = i^{l+m} \frac{\sqrt{16\pi}}{2l+1} \frac{(c/v)^l}{[(l+m)!(l-m)!]^{1/2}} , \tag{A.2a}$$

and

$$G_{Mlm}(c/v) = i^{l+m+1} \frac{m}{l} \frac{\sqrt{16\pi}}{2l+1} \frac{(c/v)^{l-1}}{[(l+m)!(l-m)!]^{1/2}} . \tag{A.2b}$$

In the extreme relativistic limit, $\gamma \gg 1$, we obtain

$$G_{Elm}(c/v) = iG_{Mlm}(c/v) = i^{l+m} \frac{m}{l} \frac{\sqrt{4\pi}}{m!(2l+1)!!} \left[\frac{(l+m)!}{(l-m)!}\right]^{1/2} (2\gamma)^{1-m} , \tag{A.3a}$$

while

$$G_{El0}(c/v) = i^l \frac{(l+1)\sqrt{4\pi}}{(2l+1)!!} \frac{1}{\gamma} \quad \text{and} \quad G_{Ml0}(c/v) = 0 . \tag{A.3b}$$

From the general expressions (A.1) we find the values of $G_{\pi lm}$ for $l \leq 3$:

$$G_{E11}(x) = \tfrac{1}{3}\sqrt{8\pi}x , \qquad G_{E10}(x) = -i\tfrac{4}{3}\sqrt{\pi(x^2 - 1)} ; \tag{A.4a}$$

$$G_{M11}(x) = -i\tfrac{1}{3}\sqrt{8\pi} , \qquad G_{M10}(x) = 0 ; \tag{A.4b}$$

$$G_{E22}(x) = -\tfrac{2}{5}x\sqrt{\pi(x^2 - 1)/6} , \qquad G_{E21}(x) = i\tfrac{2}{5}\sqrt{\pi/6}(2x^2 - 1) , \qquad G_{E20}(x) = \tfrac{2}{5}x\sqrt{\pi(x^2 - 1)} ; \tag{A.4c}$$

$$G_{M22}(x) = i\tfrac{2}{5}\sqrt{\pi(x^2-1)/6}\,, \qquad G_{M21}(x) = \tfrac{2}{5}x\sqrt{\pi/6}\,, \qquad G_{M20}(x) = 0\,; \tag{A.4d}$$

$$G_{E33}(x) = \tfrac{1}{21}\sqrt{\pi/5}\,x(x^2-1)\,, \qquad G_{E32}(x) = -i\tfrac{1}{21}\sqrt{2\pi(x^2-1)/15}(3x^2-1)\,,$$

$$G_{E31}(x) = -\tfrac{1}{105}x\sqrt{\pi/3}(15x^2-11)\,, \qquad G_{E30}(x) = i\tfrac{2}{105}\sqrt{\pi(x^2-1)}(5x^2-1)\,. \tag{A.4e}$$

To obtain the other components one can use eqs. (A.1c) and (A.1d).

B. The total cross sections in the PWBA and in the semiclassical approximation

We shall prove that the PWBA and semiclassical total cross sections are the same for the inelastic electromagnetic collision of relativistic spin-zero particles with an atomic or a nuclear system. The proof was given by Bertulani and Baur [Ber-85] and is similar to the one for the nonrelativistic case found in the textbook of Bethe and Jackiw [Be-68].

Using the integral representation

$$\frac{e^{ik|r-r'|}}{|r-r'|} = \frac{1}{2\pi^2}\int \frac{e^{ip\cdot(r-r')}}{p^2-k^2}\,d^3p \tag{B.1}$$

we can write eq. (2.3.1) as

$$T_{fi} = \frac{Z_1 e}{2\pi^2}\int\int d^3p\, d^3r'\, \frac{e^{i(q-p)\cdot r'}}{p^2-k^2}\,F(p)\,, \tag{B.2}$$

where

$$q = (q_x, q_y, q_z) \equiv (q_T, \omega/v)\,, \tag{B.3}$$

$$F(p) = \int d^3r\, \langle f|(v_\mu/c^2)\, j_\mu(r)\, e^{ip\cdot r}|i\rangle\,. \tag{B.4}$$

Integrating over r' we obtain

$$T_{fi} = 4\pi Z_1 e\, F(q)/(q^2-k^2)\,. \tag{B.5}$$

According to the relations (2.4.1) and (2.4.7) the total cross section is

$$\sigma_{\text{PWBA}} = 8\pi\left(\frac{Z_1 e}{\hbar v}\right)^2 \sum_{\text{spins}} \int_0^{q_T^{\max}} \frac{|F(q)|^2}{[q_T^2 + (\omega/\gamma v)^2]^2}\, q_T\, dq_T\,, \tag{B.6}$$

where we used

$$q^2 - k^2 = q_T^2 - (\omega/\gamma v)^2\,. \tag{B.7}$$

In the semiclassical calculations the excitation amplitude is given by

$$a_{fi} = \frac{1}{i\hbar} \int dt \, e^{i\omega t} \langle f|(v_\mu/c^2) \, j_\mu(r) \, \Phi(r, t)|i\rangle \,, \tag{B.8}$$

where $\Phi(r, t)$ is the Lienard–Wiechart potential given by eq. (2.1.4). We can also write it in the integral representation

$$\Phi(r, t) = \frac{Z_1 e}{2\pi^2} \int d^3p \, e^{ip\cdot[R-R'(t)]}/p^2 \,, \tag{B.9}$$

where

$$R = (x, y, \gamma z) \,, \qquad R' = (b_x, b_y, \gamma v t) \,. \tag{B.10}$$

Inserting this in eq. (B.8), the integral in t yields

$$(2\pi/\gamma v) \, \delta(p_z - \omega/\gamma v) \,,$$

and therefore,

$$a_{fi} = \frac{Z_1 e}{i\pi\hbar v} \int d^2 p_T \, \frac{F(p')}{p_T^2 + (\omega/\gamma v)^2} \, e^{ip_T \cdot b} \,, \tag{B.11}$$

where

$$p' = (p_T, \omega/v) \,. \tag{B.12}$$

The total cross section is obtained by integrating the above squared expression over all possible impact parameters:

$$\sigma_{s.c.} = \sum_{spins} \int |a_{fi}|^2 \, d^2b = 8\pi \left(\frac{Z_1 e}{\hbar v}\right)^2 \sum_{spins} \int_0^\infty \frac{|F(p')|^2}{[p_T^2 + (\omega/\gamma v)^2]^2} \, p_T \, dp_T \,. \tag{B.13}$$

Comparing eqs. (B.6) and (B.13), we observe that the equality between the semiclassical and the PWBA cross section is guaranteed if we are allowed to replace q_T^{max} by infinity in eq. (B.6), which is generally the case, as soon as the form factor $F(q)$ is a rapidly decreasing function of q_T.

C. Useful handy formulas

In the following we give some approximate formulas, useful for the fast calculation of a given electromagnetic process in ultrarelativistic heavy ion collisions (i.e., for $\gamma \gg 1$). For more details see the corresponding sections of this review.

Equivalent photon method

For *one-photon* processes:

$$\sigma = \int n(\omega) \, \sigma_{\gamma N}(\omega) \, \frac{\mathrm{d}\omega}{\omega} \, , \tag{C.1}$$

where

$$n(\omega) = \frac{2}{\pi} Z_P^2 \alpha \, \ln\!\left(\frac{\gamma c}{\omega R}\right) , \tag{C.2}$$

$\sigma_{\gamma N}$ is the photo-nuclear cross section for photon energy $\hbar\omega$, $R = 1.2(A_P^{1/3} + A_T^{1/3})$ is the sum of the nuclear radii, and α is the fine-structure constant. The indices P and T denote the projectile and the target parameters, respectively.

For *two-photon* processes:

$$\sigma = \int I(x) \, \sigma_{\gamma\gamma}(x) \, \frac{\mathrm{d}x}{x} \, , \tag{C.3}$$

where

$$I(x) = \frac{16}{3} \left(\frac{Z_P Z_T \alpha}{\pi}\right)^2 \ln^3\!\left(\frac{\gamma \hbar c}{\sqrt{x R_P R_T}}\right) , \tag{C.4}$$

$\sigma_{\gamma\gamma}$ is the photon–photon cross section, and $4x$ is the square of the invariant mass of the 2γ-system.

Excitation of giant dipole resonances in RHI collisions

Direct electromagnetic excitation of GDR's on a nuclear target by means of RHI's:

$$\sigma = 2\pi S \, \ln\!\left(\frac{2\gamma A_T^{1/3}}{A_P^{1/3} + A_T^{1/3}}\right) , \tag{C.5}$$

where

$$S = 5.45 \times 10^{-4} \, \frac{Z_P^2 Z_T N_T}{A_T^{2/3}} \; \mathrm{mb} \, . \tag{C.6}$$

Multiple electromagnetic excitation of GDR's on a nuclear target by means of RHI's:

$$\sigma^{(N>1)} = \frac{\pi S}{N!(N-1)} \left(\frac{S}{R^2}\right)^{N-1} . \tag{C.7}$$

Ionization of K-shell atomic electrons

$$\sigma = 9.8 r_e^2 \, \frac{Z_P^2}{(Z_T \alpha)^2} \, \ln\!\left(\frac{2\gamma}{Z_T \alpha}\right) , \tag{C.8}$$

where $r_e = e^2/mc^2$ is the classical electron radius.

Production of lepton pairs
Production of e^+e^--pairs:

$$\sigma = \frac{28}{27\pi} (Z_P Z_T \alpha r_e)^2 \ln^3\left(\frac{\gamma}{2}\right).$$ (C.9)

Production of $\mu^+\mu^-$- and of $\tau^+\tau^-$-pairs. Here we have to distinguish between two cases: (a) if $\gamma \gg 16$ for muon-pair production, or $\gamma \gg 200$ for tau-pair production, then we can use the previous formula with r_ℓ ($\ell = \mu$ or τ) in place of r_e, (b) if the Lorentz factor does not satisfy the above conditions, then we have the following formula

$$\sigma = \frac{\pi}{128} (Z_P Z_T \alpha r_\ell)^2 \left(\frac{\gamma\hbar}{m_\ell cR}\right)^4 e^{-4m_\ell cR/\gamma\hbar}.$$ (C.10)

Electron-pair production with capture of the electron in an atomic K-shell orbit:

$$\sigma = \frac{33}{20} Z_P^2 Z_T^5 \alpha^5 r_e^2 \ln\left(\frac{\gamma}{2}\right).$$ (C.11)

Production of a neutral resonance particle with mass m and positive charge conjugation parity

$$\sigma = \frac{128}{3} (Z_P Z_T \alpha)^2 \frac{\hbar^3 \Gamma_{\gamma\gamma}}{m^3 c^4} (2J+1) \ln^3\left(\frac{2\gamma\hbar}{mc\sqrt{R_P R_T}}\right).$$ (C.12)

where $\Gamma_{\gamma\gamma}$ is the branching ratio for $\gamma\gamma$-decay, and J the spin of the resonance.

References

[Ab-64]   M. Abramowitz and I.A. Stegun, Handbook of Mathematical Functions (National Bureau of Standards, Washington, DC, 1964).
[AB-86]   M. Aguilar-Benitez et al., Phys. Lett. B170 (1986) 1.
[Ak-57]   A.I. Akhiezer and A.G. Sitenko, Phys. Rev. 106 (1957) 1236.
[Ak-65]   A.I. Akhiezer and V.B. Berestetskii, Quantum Electrodynamics (Interscience, New York, 1965).
[Al-66]   K. Alder and A. Winther, Coulomb Excitation (Academic Press, New York, 1966).
[Al-75]   K. Alder and A. Winther, Electromagnetic Excitation (North-Holland, Amsterdam, 1975).
[Am-81]   P.A. Amundsen and K. Aashamar, J. Phys. B 14 (1981) 4047.
[An-84]   R. Anholt et al., Phys. Rev. A 30 (1984) 2234.
[An-87]   R. Anholt and H. Gould, preprint LBL-20661, to be published as a chapter in: Advances in Atomic and Molecular Physics, ed. B. Bederson (Academic Press, Orlando, 1987);
          H. Gould, Atomic Physics Aspects of a Relativistic Nuclear Collider (Lawrence Berkeley Laboratory, Berkeley) Preprint LBL 18593 UC-28;
          V. Metag, P. Kienle and H. Ahrens, eds., Bericht vom Arbeitstreffen über Experimente am geplanten Experimentier Speicherring ESR der GSI (25–26 October 1984).
[Ant-83]   Yu.M. Antipov et al., Phys. Lett. B 121 (1983) 445.
[Ant-85]   Yu.M. Antipov et al., Z. Phys. C 26 (1985) 495.
[Ant-87]   Yu.M. Antipov et al., Phys. Rev. D 36 (1987) 21.
[Ar-72]   T.A. Armstrong et al., Phys. Rev. D 5 (1972) 1640.
[Art-72]   X. Artru and G.B. Yodh, Phys. Lett. B 40 (1972) 43.
[Ba-59]   J. Bang and J.M. Hansteen, K. Dan. Vidensk. Selsk. Mat. Fys. Medd. 31 (1959) no. 13.
[Ba-72]   V.K. Balasubrahmanyan, C.J. Crannell, F.A. Hagen, J.F. Ormes and M.J. Ryan, in: Proc. 12th Int. Conf. on Cosmic Rays (Hobart, Tasmania, 1972).

[Ba-84a] G. Baur, F. Rösel, D. Trautmann and R. Shyam, Phys. Rep. 111 (1984) 333.
[Ba-84b] G. Baur, B. Hoffmann, F. Rösel, D. Trautmann and R. Shyam, in: Proc. Workshop COPECOS (Bad Honnef, 1984) (World Scientific, Singapore, 1984) p. 538.
[Ba-85]   G. Baur, F. Rösel, D. Trautmann and R. Shyam, in: Proc. 6th Int. Symp. on Polarization Phenomena in Nuclear Physics (Osaka 1985) p. 105.
[Ba-86a] G. Baur and C.A. Bertulani, Phys. Lett. B 174 (1986) 23.
[Ba-86b] G. Baur and C.A. Bertulani, Phys. Rev. C 34 (1986) 1654.
[Ba-86c] G. Baur, C.A. Bertulani and H. Rebel, Nucl. Phys. A 458 (1986) 188.
[Ba-86d] G. Baur, C.A. Bertulani and H. Rebel, in: Proc. Int. Symp. on Weak and Electromagnetic Interactions in Nuclei (1–5 July 1986, Heidelberg, Germany) ed. H.V. Klapdor (Springer, Berlin) p. 980.
[Ba-86e] G. Baur and C.A. Bertulani, in: Proc. Int. School of Heavy Ion Physics (12–22 October 1986, Erice, Italy) ed. R.A. Broglia (Plenum, New York).
[Ba-86f] G. Baur, Phys. Lett. B 178 (1986) 135.
[Ba-87a] G. Baur and C.A. Bertulani, Phys. Rev. C 35 (1987) 836.
[Ba-87b] G. Baur and C.A. Bertulani, Z. Phys. A, in press.
[Bay-86] G. Baym, in: Proc. of the Int. School of Heavy Ion Physics (Erice, Italy, 12–22 October 1986) ed. R.A. Broglia (Plenum, New York).
[Be-34]   H.A. Bethe, Proc. Cambridge Philos. Soc. 30 (1934) 524.
[Be-54]   H.A. Bethe and L.C. Maximon, Phys. Rev. 93 (1954) 768.
[Be-68]   H.A. Bethe and R.W. Jackiw, Intermediate Quantum Mechanics (Benjamin, New York, 1968) p. 326.
[Be-77]   H.A. Bethe and E.E. Salpeter, Quantum Mechanics of One- and Two-electron Atoms (Plenum, New York, 1977).
[Be-85]   U. Becker, N. Grün and W. Scheid, J. Phys. B (At. Mol. Phys.) 18 (1985) 4589.
[Be-86a] U. Becker, N. Grün and W. Scheid, J. Phys. B (At. Mol. Phys.) 19 (1986) 1347.
[Be-86b] U. Becker, N. Grün, W. Scheid and G. Soff, Phys. Rev. Lett. 56 (1986) 2016.
[Be-86c] U. Becker, Ph.D. thesis (Giessen University, 1986) unpublished.
[Be-87]   U. Becker, N. Grün and W. Scheid, J. Phys. B20 (1987) 2075.
[Ber-85] C.A. Bertulani and G. Baur, Nucl. Phys. A 442 (1985) 739.
[Ber-86a] C.A. Bertulani and G. Baur, Phys. Rev. C 33 (1986) 910.
[Ber-86b] C.A. Bertulani and G. Baur, Nucl. Phys. A 458 (1986) 725.
[Ber-86c] C.A. Bertulani, Revista Brasileira de Física 16 (1986) 380.
[Ber-86d] C.A. Bertulani, in: Proc. Workshop on Gross Properties of Nuclei and Nuclear Excitations, (Hirschegg, Austria, January 1986) ed. H. Feldmeier.
[Ber-87a] C.A. Bertulani and G. Baur, Jülich preprint (1987).
[Ber-87b] C.A. Bertulani and G. Baur, Jülich preprint (1987).
[Ber-87c] C.A. Bertulani and G. Baur, submitted for publication to Nucl. Phys. A.
[Berg-86] Ch. Berger et al., Phys. Lett. B 167 (1986) 120.
[Bh-35]   H.J. Bhabha, Proc. R. Soc. London Ser. A 152 (1935) 559.
[Bj-85]   J.D. Bjorken and L. McLerran, Phys. Rev. D 31 (1985) 63.
[Bo-75]   A.G. Bohr and B. Mottelson, Nuclear Structure Vol. II (Benjamin, Reading, MA, 1975).
[Br-50]   H.L. Bradt and B. Peters, Phys. Rev. 77 (1950) 54.
[Br-71]   S.J. Brodsky, T. Kinoshita and H. Terazawa, Phys. Rev. D 4 (1971) 1532.
[Br-74]   A. Browman, J. Dewire, B. Gittelman, K.M. Hanson, D. Larson, E. Loh and R. Lewis, Phys. Rev. Lett. 33 (1974) 1400.
[Br-85]   P. Braun-Munzinger et al., Proposal 814 submitted to the AGS Program Committee, SUNY at Stony Brook, accepted 1985 (unpublished).
[Br-86]   S.J. Brodsky et al., Phys. Rev. Lett. 56 (1986) 1763.
[Bu-75]   V.M. Budnev, I.F. Ginzburg, G.V. Medelin and V.G. Serbo, Phys. Rep. 15 (1975) 181.
[Ca-80]   T.A. Cahill, Annu. Rev. Nucl. Part. Sci. 30 (1980) 211.
[Ca-87]   L.F. Canto, R. Donangelo, L.F. Oliveira and J.O. Rasmussen, Phys. Rev. C 35 (1987) 2175.
[Co-61]   S. Coleman and S.L. Glashow, Phys. Rev. Lett. 6 (1961) 423.
[Da-54]   H. Davies, H.A. Bethe and L.C. Maximon, Phys. Rev. 93 (1954) 788.
[Da-78]   D.M. Davidovic, B.L. Moisewitch and P.H. Norrington, J. Phys. B 11 (1978) 847.
[Do-83]   G. Domokos, Phys. Rev. D 28 (1983) 123.
[Dr-62]   J. Dreitlein and H. Primakoff, Phys. Rev. 125 (1962) 1671.
[Dy-77]   F. Dydak, F.L. Navarria, O.E. Overseth, P. Steffen, J. Steinberger, H. Wahl, E.G. Williams, F. Eisele, C. Geweniger, K. Kleinknecht, H. Taureg and G. Zech, Nucl. Phys. B 118 (1977) 1.
[Ei-70]   J.M. Eisenberg and W. Greiner, Excitation Mechanisms of the Nucleus (North-Holland, Amsterdam, 1970).
[Em-87]   H. Emling et al., Proposal to the SIS Program Committee (GSI-Darmstadt, Germany, February 1987).
[Ev-86a] M.V. Evlanov and A.M. Sokolov, Nucl. Phys. A 452 (1986) 477.
[Ev-86b] M.V. Evlanov and A.M. Sokolov, Sov. J. Nucl. Phys. 44 (1986) 773.
[Fä-70a] G. Fäldt, Phys. Rev. D 2 (1970) 846.

[Fä-70b]   G. Fäldt and H. Pilkuhn, Ann. Phys. (USA) 58 (1970) 454.
[Fä-74]   G. Fäldt, H. Pilkuhn and H.G. Schlaile, Ann. Phys. (USA) 82 (1974) 326.
[Fe-24]   E. Fermi, Z. Phys. 29 (1924) 315.
[Fe-33]   E. Fermi and G.E. Uhlenbeck, Phys. Rev. 44 (1933) 510.
[Fe-55]   E.L. Feinberg, Zh. Eksp. Theor. Fiz. 29 (1955) 115.
[Fi-80]   J.H. Field, Nucl. Phys. B 168 (1980) 582.
[Fi-87]   R.D. Fischer et al., in: Proc. Workshop on Experiments and Experimental Facilities at SIS/ESR (March 30–April 1, 1987, GSI
            Darmstadt).
[Fo-84]   W.A. Fowler, Rev. Mod. Phys. 56 (1984) 149.
[Fr-83]   E.M. Friedlander, H.H. Heckman and Y. Karant, Phys. Rev. C 27 (1983) 2436.
[Fu-33]   W.H. Furry and J.F. Carlson, Phys. Rev. 44 (1933) 238.
[FW-66]   T. de Forest and J.D. Walecka, Adv. Phys. 15 (1966) 57.
[Ga-87]   D. Galetti, T. Kodama and M.C. Nemes, Ann. Phys. (USA) 177 (1987) 229.
[Ge-82]   H. Genz et al., Z. Phys. A 305 (1982) 9.
[Ge-87]   H. Geissel et al., Accepted proposal to the SIS-ESR Experimental Program (GSI-Darmstadt, February 1987).
[Gl-55]   R.J. Glauber, Phys. Rev. 99 (1955) 115.
[Gl-59]   R.J. Glauber, in: Lectures in Theoretical Physics, Vol. I, ed. W.E. Britin (Interscience, New York, 1959) p. 315.
[Go-84]   A. Goldberg, Nucl. Phys. A 420 (1984) 636.
[Gr-65]   I.S. Gradshteyn and I.M. Ryzhik, Table of Integrals, Series, and Products (Academic Press, New York, 1965).
[Gr-85]   D.E. Greiner, H. Crawford, P.J. Lindstrom, J.M. Kidd, D.L. Olson, W. Schimmerling and T.J. Symons, Phys. Rev. C 31 (1985) 416.
[Ha-87]   P.G. Hansen and B. Jonson, Europhys. Lett. 4 (1987) 409.
[He-54]   W. Heitler, The Quantum Theory of Radiation (Oxford, 1954).
[He-76]   H.H. Heckman and P.J. Lindstrom, Phys. Rev. Lett. 37 (1976) 56.
[Hi-87]   D. Hilscher et al., in: Proc. Workshop on Experiments and Experimental Facilities at SIS/ESR, GSI-Report, April 1987.
[HK-87]   S. Hirenzaki, T. Kajino, K.-I. Kubo, H. Toki and I. Tanihata, Phys. Lett. B 194 (1987) 20.
[Ho-84]   B. Hoffman and G. Baur, Phys. Rev. C 30 (1984) 247.
[Hu-85]   M.S. Hussein and K.W. McWoy, Nucl. Phys. A 445 (1985) 124.
[Hü-81]   J. Hüfner and M.C. Nemes, Phys. Rev. C 23 (1981) 2538.
[Ja-57]   D. Jamnik and C. Zupancic, K. Dan. Vidensk. Selsk. Mat. Fys. Medd. 31 (1957) no. 1.
[Ja-59]   M. Jacob and G.C. Wick, Ann. Phys. (USA) 7 (1959) 404.
[Ja-75]   J.D. Jackson, Classical Electrodynamics (Wiley, New York, 1975).
[Ja-84]   P.L. Jain, M.M. Aggarwal, M.S. El-Nagdy and A.Z.M. Ismail, Phys. Rev. Lett. 52 (1984) 1763.
[Jä-75]   R. Jäckle and H. Pilkuhn, Nucl. Phys. A 247 (1975) 521.
[Jo-74]   C.J. Joachain and C. Quigg, Rev. Mod. Phys. 46 (1974) 279.
[Jo-76]   S.A.E. Johansson and T.B. Johansson, Nucl. Instrum. Methods 137 (1976) 473.
[Ka-77]   J.I. Kapusta, Phys. Rev. C 15 (1977) 1580.
[Ka-84]   T. Kajino and A. Arima, Phys. Rev. Lett. 52 (1984) 739.
[Ke-82]   K.U. Kettner, H.W. Becker, L. Buchmann, J. Görres, H. Kräwinkel, C. Rolfs, P. Schmalbrock, H.P. Trautvetter and A. Vlieks, Z.
            Phys. A 308 (1982) 73.
[Kh-81]   R. Khan and D. Crumpton, Crit. Rev. Anal. Chem. 11 (1981) 103.
[Ki-86]   P. Kienle, Annu. Rev. Nucl. Part. Sci. 36 (1986) 605.
[Ko-67]   H. Kolbenstvedt, J. Appl. Phys. 38 (1967) 4785.
[Ko-80]   F. Komarov, Radiat. Eff. 46 (1980) 39.
[Ko-87]   T. Kobayashi et al., in: Abstract Book of the 11th Int. Conf. on Particles and Nuclei (Kyoto, April 20–24, 1987) p. 476.
[La-34]   L.D. Landau and E.M. Lifshitz, Phys. Zs. Sowjet. 6 (1934) 244.
[La-85]   K. Langanke and S.E. Koonin, Nucl. Phys. A 439 (1985) 384.
[La-86]   L.D. Landau and E.M. Lifschitz, Lehrbuch der Theoretischen Physik, Vol. IV (Akademie-Verlag, Berlin, 1986).
[Li-81]   H. Lipkin, Phys. Rev. D 24 (1981) 1437.
[Lo-60]   F.E. Low, Phys. Rev. 120 (1960) 582.
[Lu-84]   T.W. Ludlam and H.E. Wegner, eds., Proc. 3rd Int. Conf. on Ultra-relativistic Nucleus–Nucleus Collisions (Brookhaven National
            Laboratory, September 1983) Nucl. Phys. A 418 (1984).
[Ma-87]   K. Maier et al., Z. Phys. A 326 (1987) 527.
[Me-58]   R. Merzbacher and H.W. Lewis, Handbook of Physics, Vol. 14 (Springer, Berlin, 1958) p. 166.
[Me-70]   E. Merzbacher, Quantum Mechanics, 2nd Ed. (Wiley, New York, 1970).
[Me-83]   W.E. Meyerhof, Workshop on Atomic Physics with Fast Heavy Ion Beams (Argonne National Laboratory, January 1983).
[Me-84]   M.T. Mercier, J.C. Hill, F.K. Wohn and A.R. Smith, Phys. Rev. Lett. 52 (1984) 898.
[Me-86]   M.T. Mercier, J.C. Hill, F.K. Wohn, C.M. McCullough, M.E. Nieland, J.A. Winger, C.B. Howard, S. Renwick, D.K. Matheis and
            A.R. Smith, Phys. Rev. C 33 (1986) 1655.
[Mi-72]   A.B. Migdal, Yad. Fiz. 16 (1972) 427 [English translation: Sov. J. Nucl. Phys. 16 (1973) 238].

[Mo-85] B.L. Moisevitsch, Phys. Rep. 118 (1985) 133.
[Mo-87] K. Momberger, N. Grün, W. Scheid, U. Becker and G. Soff, J. Phys. B 20 (1987) 281.
[Na-69] K. Nagatani, M.R. Dwarakanath and D. Ashery, Nucl. Phys. A 218 (1969) 325.
[Ni-34] Y. Nishina, S. Tomonaga and H. Tamaki, Sci. Pap. Phys. Math. Res. Jpn 24 (1934) 137.
[Ni-35] Y. Nishina, S. Tomonaga and M. Kobayashi, Sci. Pap. Inst. Phys. Chem. Res. 27 (1935) 137.
[Ni-82] A.I. Nikishov and N.V. Pichkurov, Sov. J. Nucl. Phys. 35 (1982) 561.
[No-54] A. Nordsiek, Phys. Rev. 93 (1954) 785.
[Ol-81] D.L. Olson, B.L. Berman, D.E. Greiner, H.H. Heckman, P.J. Lindstrom, G.D. Westfall and H.J. Crawford, Phys. Rev. C 24 (1981)
         1529.
[Os-82] J.L. Osborne, C.A. Barnes, R.W. Kavanagh, R.M. Kremer, G.J. Mathews, J.L. Zyskind, P.D. Parker and A.J. Howard, Phys. Rev.
         Lett. 48 (1982) 1664.
[Os-84] J.L. Osborne, C.A. Barnes, R.W. Kavanagh, R.M. Kremer, G.J. Mathews, J.L. Zyskind, P.D. Parker and A.J. Howard, Nucl. Phys. A
         419 (1984) 115.
[Pe-85] P.C. Petersen, Ph.D. thesis (Rutgers University, 1985) unpublished.
[Pe-86] P.C. Petersen et al., Phys. Rev. Lett. 57 (1986) 949.
[Pi-80] Y.L. Pivovarov, V.G. Khlabutin and S.A. Vorobiev, Phys. Lett. A 76 (1980) 338.
[Pi-83] Y.L. Pivovarov and A.A. Shirokov, Yad. Fiz. 37 (1983) 1101.
[Po-61] I.Y. Pomeranchuck and I.M. Shmushkevich, Nucl. Phys. 23 (1961) 452.
[Pr-51] H. Primakoff, Phys. Rev. 31 (1951) 899.
[Ra-37] G. Racah, Nuovo Cimento 14 (1937) 93.
[Ra-86] J.O. Rasmussen, L.F. Canto and X.-J. Qiu, Phys. Rev. C 33 (1986) 2033.
[Re-85] H. Rebel, Workshop on Nuclear Reaction Cross Sections of Astrophysical Interest (Kernforschungszentrum Karlsruhe, February 1985)
         unpublished report.
[Re-86] H. Rebel, in: Proc. Int. Summer School Symmetries and Semiclassical Features of Nuclear Dynamics (Poiana Brasov, Romania, 1–13
         September 1986) KfK-report 4158 (1986).
[Re-87] H. Rebel, in: Proc. Workshop on Break-up Phenomena in Nuclear Physics (Bhabha Atomic Research Center, Calcutta, 9–11 February
         1987).
[Ro-78] C. Rolfs and H.P. Trautvetter, Annu. Rev. Nucl. Sci. 28 (1978) 115.
[Sa-48] A.D. Sacharov, 1948, as quoted in: L.D. Landau and E.M. Lifshitz, Lehrbuch der Theoretischen Physik, Vol. IV (Akademic-Verlag,
         Berlin, 1986) p. 387.
[So-80] G. Soff, in: Proc. 18th Winter School (Bielsko-Biala, Poland, 1980) eds. A. Balanda and Z. Stachura, p. 201.
[Ta-85a] I. Tanihata et al., Phys. Lett. B 160 (1985) 380.
[Ta-85b] I. Tanihata et al., Phys. Rev. Lett. 55 (1985) 2676.
[Te-52] K.A. Ter-Martirosyan, Zh. Eksp. Teor. Fiz. 22 (1952) 284, reprinted in: K. Alder and A. Winther, Coulomb Excitation (Academic
         Press, New York, 1966).
[Th-52] J.A. Thie, C.J. Mullin and E. Guth, Phys. Rev. 87 (1952) 962.
[Ts-86] Y.S. Tsai, Phys. Rev. D 34 (1986) 1326.
[Va-84] S.R. Valluri, U. Becker, N. Grün and W. Scheid, J. Phys. B 17 (1984) 4359.
[Wa-58] G.N. Watson, Theory of Bessel Functions, 2nd Ed. (Cambridge Univ. Press, New York, 1958).
[We-34] C.F. Weizsäcker, Z. Phys. 88 (1934) 612.
[We-71] H.A. Weidenmüller and A. Winther, Ann. Phys. (USA) 66 (1971) 218.
[We-79] G.D. Westfall, L.W. Wilson, P.J. Lindstrom, H.J. Crawford, D.E. Greiner and H.H. Heckman, Phys. Rev. C 19 (1979) 1309.
[Wi-34] E.J. Williams, Phys. Rev. 45 (1934) 729.
[Wi-35] E.J. Williams, K. Dan. Vidensk. Selsk. Mat.-Fys. Medd. 13 (1935) no. 4.
[Wi-79] A. Winther and K. Alder, Nucl. Phys. A 319 (1979) 518.
[Wi-87] U. von Wimmersperg et al., Phys. Rev. Lett. 59 (1987) 266.
[Ya-87] Y. Yamaguchi and H. Sato, Phys. Rev. C 35 (1987) 2156.
[Za-87] M.S. Zahir, Phys. Rev. D 35 (1987) 3338.